



**CALIBRATION OF THE AEDC-PWT 16-FT
TRANSONIC TUNNEL WITH THE PROPULSION
TEST SECTION AT VARIOUS REYNOLDS NUMBERS**

**F. M. Jackson
ARO, Inc., a Sverdrup Corporation Company**

**PROPULSION WIND TUNNEL FACILITY
ARNOLD ENGINEERING DEVELOPMENT CENTER
AIR FORCE SYSTEMS COMMAND
ARNOLD AIR FORCE STATION, TENNESSEE 37389**

August 1978

Final Report for Period October 1974 — June 1975

Approved for public release; distribution unlimited.

Prepared for

**ARNOLD ENGINEERING DEVELOPMENT CENTER/DO
ARNOLD AIR FORCE STATION, TENNESSEE 37389**

NOTICES

When U. S. Government drawings, specifications, or other data are used for any purpose other than a definitely related Government procurement operation, the Government thereby incurs no responsibility nor any obligation whatsoever, and the fact that the Government may have formulated, furnished, or in any way supplied the said drawings, specifications, or other data, is not to be regarded by implication or otherwise, or in any manner licensing the holder or any other person or corporation, or conveying any rights or permission to manufacture, use, or sell any patented invention that may in any way be related thereto.

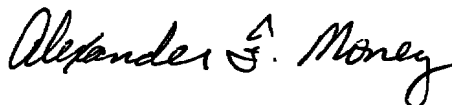
Qualified users may obtain copies of this report from the Defense Documentation Center.

References to named commercial products in this report are not to be considered in any sense as an indorsement of the product by the United States Air Force or the Government.

This report has been reviewed by the Information Office (OI) and is releasable to the National Technical Information Service (NTIS). At NTIS, it will be available to the general public, including foreign nations.

APPROVAL STATEMENT

This report has been reviewed and approved.



ALEXANDER F. MONEY
Project Manager, Research Division
Directorate of Test Engineering

Approved for publication:

FOR THE COMMANDER



ROBERT W. CROSSLEY, Lt Colonel, USAF
Acting Director of Test Engineering
Deputy for Operations

UNCLASSIFIED

REPORT DOCUMENTATION PAGE		READ INSTRUCTIONS BEFORE COMPLETING FORM
1 REPORT NUMBER AEDC-TR-77-121	2 GOVT ACCESSION NO.	3 RECIPIENT'S CATALOG NUMBER
4 TITLE (and Subtitle) CALIBRATION OF THE AEDC-PWT 16-FT TRANSONIC TUNNEL WITH THE PROPULSION TEST SECTION AT VARIOUS REYNOLDS NUMBERS	5 TYPE OF REPORT & PERIOD COVERED Final Report - October 1974 - June 1975	
	6 PERFORMING ORG REPORT NUMBER	
7 AUTHOR(s) F. M. Jackson, ARO, Inc., a Sverdrup Corporation Company	8 CONTRACT OR GRANT NUMBER(s)	
9 PERFORMING ORGANIZATION NAME AND ADDRESS Arnold Engineering Development Center/DO Air Force Systems Command Arnold Air Force Station, Tennessee 37389	10 PROGRAM ELEMENT, PROJECT, TASK AREA & WORK UNIT NUMBERS Program Element 65807F	
11 CONTROLLING OFFICE NAME AND ADDRESS Arnold Engineering Development Center/DOS Air Force Systems Command Arnold Air Force Station, Tennessee 37389	12 REPORT DATE August 1978	
	13 NUMBER OF PAGES 101	
14 MONITORING AGENCY NAME & ADDRESS (if different from Controlling Office)	15 SECURITY CLASS (of this report) UNCLASSIFIED	
	15a DECLASSIFICATION/DOWNGRADING SCHEDULE N/A	
16 DISTRIBUTION STATEMENT (of this Report) Approved for public release; distribution unlimited.		
17 DISTRIBUTION STATEMENT (of the abstract entered in Block 20, if different from Report)		
18 SUPPLEMENTARY NOTES Available in DDC		
19 KEY WORDS (Continue on reverse side if necessary and identify by block number) transonic wind tunnels calibration Reynolds number Mach number		
20 ABSTRACT (Continue on reverse side if necessary and identify by block number) Tests were conducted in the AEDC Propulsion Wind Tunnel (16T) to determine the tunnel test section Mach number distributions and calibration at various Reynolds numbers. The calibration was conducted at Mach numbers from 0.2 to 1.6 and at Reynolds numbers from $0.4 \times 10^6/\text{ft}$ to $6.4 \times 10^6/\text{ft}$. The calibration was conducted using the propulsion test section (Test Section 1) and centerline pipe and wall pressure orifices to define the Mach number distributions. A quantitative evaluation of the effects of tunnel pressure ratio, test section wall angle, and Reynolds number on the centerline Mach number distributions was		

UNCLASSIFIED

UNCLASSIFIED

20. ABSTRACT (Concluded)

determined by analysis of the local Mach number deviations. The results indicate that Mach number distributions of good quality are obtained for both zero and the optimum wall angle schedule. For complete generality, the Tunnel 16T calibration must be defined as a function of test section wall angle, Reynolds number, and Mach number. Comparison of this calibration with previous calibration results indicates that a revision in the tunnel calibration utilized for operations is desirable. Analytical expressions which adequately represent the tunnel calibration at various test conditions were developed. Application of the current calibration to test data demonstrated the validity of considering the effects of Reynolds number on the tunnel calibration.

UNCLASSIFIED

PREFACE

The work reported herein was conducted by the Arnold Engineering Development Center (AEDC), Air Force Systems Command (AFSC), at the request of the AEDC Test and Technology Divisions under Program Element 65807F. The Air Force Project Manager was A. F. Money. The results of the test were obtained by ARO, Inc., AEDC Division (a Sverdrup Corporation Company), operating contractor of AEDC, AFSC, Arnold Air Force Station, Tennessee. The testing was done under ARO Project No. P41S-04A. The manuscript was completed (under ARO Project No. P32A-G1A) in September 1977 and submitted for publication on November 18, 1977.

CONTENTS

	<u>Page</u>
1.0 INTRODUCTION	7
2.0 APPARATUS	
2.1 Test Facility	8
2.2 Calibration Equipment	8
3.0 PROCEDURE	
3.1 Calibration Discussion	9
3.2 Data Reduction and Uncertainty	10
3.3 Flow Quality	11
4.0 RESULTS AND DISCUSSION	
4.1 Mach Number Distributions	12
4.2 Tunnel Calibration	15
5.0 CONCLUSIONS	22
REFERENCES	23

ILLUSTRATIONS

Figure

1. Tunnel 16T Centerline Pipe Installation	25
2. Variation of Tunnel Pressure Ratio	28
3. Variation of Test Section Wall Angle	29
4. Tunnel 16T Centerline Mach Number Distributions at $M_\infty = 0.2$ to 0.5 with $\lambda = \lambda^*$, $\theta = 0$, and $P_t \cong 1,200$ psfa	30
5. Tunnel 16T Centerline Mach Number Distributions with $\lambda = \lambda^*$, $\theta = 0$, and $P_t \cong 1,600$ psfa	31
6. Tunnel 16T Wall Mach Number Distributions with $\lambda = \lambda^*$, $\theta = 0$, and $P_t \cong 1,600$ psfa	33
7. Effect of Mach Number on the Mach Number Deviations with $\lambda = \lambda^*$, $\theta = 0$, and $P_t \cong 1,600$ psfa	35
8. Effect of Boundary-Layer Rakes on Centerline Mach Number Distributions with $\theta = 0$, $\lambda = \lambda^*$, and $P_t = 1,600$ psfa	37
9. Tunnel 16T Centerline Mach Number Distributions for Various Tunnel Pressure Ratios with $\theta = 0$ and $P_t = 1,600$ psfa	42
10. Effect of Tunnel Pressure Ratio Variation on the 2- σ Mach Number Deviations for Tunnel Stations 8 to 28 with $\theta = 0$ and $P_t = 1,600$ psfa	48

<u>Figure</u>	<u>Page</u>
11. Effect of Pressure Ratio Variation on Auxiliary Flow Requirements with $\theta = 0$ and $P_t = 1,600$ psfa	49
12. Effect of Pressure Ratio Variation on Tunnel Total Power Requirements with $\theta = 0$ and $P_t = 1,600$ psfa	50
13. Effect of Auxiliary Flow Utilization at $M_\infty = 0.75$, $\theta = 0$, and $P_t = 1,600$ psfa	51
14. Tunnel 16T Centerline Mach Number Distributions for Various Test Section Wall Angles with $\lambda = \lambda^*$ and $P_t = 1,600$ psfa	52
15. Effect of Wall Angle Variations on the $2\text{-}\sigma$ Mach Number Deviations for Tunnel Stations 8 to 28 with $\lambda = \lambda^*$ and $P_t = 1,600$ psfa	58
16. Effect of Wall Angle Variation on Auxiliary Flow Requirements with $\lambda = \lambda^*$ and $P_t = 1,600$ psfa	61
17. Effect of Wall Angle Variation on Tunnel Total Power Requirements with $\lambda = \lambda^*$ and $P_t = 1,600$ psfa	62
18. Tunnel 16T Centerline Mach Number Distributions for Various Reynolds Numbers with $\theta = 0$ and $\lambda = \lambda^*$	63
19. Effect of Reynolds Number Variation on the $2\text{-}\sigma$ Mach Number Deviations for Tunnel Stations 8 to 28 at $\lambda = \lambda^*$ and $\theta = 0$	69
20. Effect of Reynolds Number Variations on the Auxiliary Flow Requirements with $\theta = 0$ and $\lambda = \lambda^*$	71
21. Effect of Reynolds Number Variation on Tunnel Total Power Requirements with $\theta = 0$ and $\lambda = \lambda^*$	72
22. Effect of Orifice Selection on the Tunnel 16T Mach Number Calibration with $\lambda = \lambda^*$, $\theta = 0$, and $P_t = 1,600$ psfa	73
23. Effect of Test Section Region on the Tunnel 16T Mach Number Calibration at $\theta = 0$, $\lambda = \lambda^*$, and $P_t = 1,600$ psfa	75
24. Comparison of Tunnel 16T Calibration with $\lambda = \lambda^*$, $\theta = 0$, and $P_t = 1,600$ psfa to Previous Results	76
25. Effect of Pressure Ratio Variation on the Tunnel 16T Calibration with $\theta = 0$ and $P_t = 1,600$ psfa	78
26. Tunnel 16T Calibration with $\lambda = \lambda^*$, $\theta = 0$, and $P_t = 1,600$ psfa	79
27. Tunnel 16T Mach Number Calibration for Various Test Section Wall Angles at $\lambda = \lambda^*$ and $P_t = 1,600$ psfa	80
28. Tunnel 16T Mach Number Calibration for Various Reynolds Numbers with $\lambda = \lambda^*$ and $\theta = 0$	81

<u>Figure</u>	<u>Page</u>
29. Tunnel 16T Mach Number Calibration for Various Reynolds Numbers with $\lambda = \lambda^*$ and $\theta = \theta^*$	82
30. Effect of Reynolds Number Corrections on the Centerline Pipe Average Pressure Coefficient for Tunnel Stations 8 to 28 with $\theta = 0$ and $\lambda = \lambda^*$	83
31. Slopes of Reynolds Number Correction Curves	85
32. Effect of Wall Angle on the Tunnel 16T Reynolds Number Calibration at Subsonic Mach Numbers	87

TABLES

1. Coefficients of the Tunnel 16T Calibration Curve Fit for $\theta = 0$ and $P_t = 1,600$ psfa	89
2. Coefficients of the Tunnel 16T Calibration Surface Fit for Variable Test Section Wall Angle	90
3. Coefficients of the Tunnel 16T Calibration for Specific Mach Numbers at Various Reynolds Numbers with $\theta = \theta^*$ and $P_t \geq 1,000$ psfa	91
4. Coefficients of the Tunnel 16T Calibration for Specific Mach Numbers at Various Reynolds Numbers with $\theta = \theta^*$ and $P_t < 1,000$ psfa	92
5. Coefficients of the Slopes for the Tunnel 16T Reynolds Number Corrections with $\theta = 0$	93
6. Coefficients of the Slopes for the Tunnel 16T Reynolds Number Corrections for Variable Test Section Wall Angle	94

APPENDIX

A. TYPICAL DATA CORRECTIONS	95
NOMENCLATURE	101

1.0 INTRODUCTION

The determination of engine inlet and nozzle performance is an integral part of the development program for modern weapons systems. In recent years several wind tunnel tests have been conducted at AEDC to determine nozzle afterbody pressure drag for various systems. A comprehensive program was also conducted at the AEDC to investigate various aspects of problems associated with nozzle/afterbody (NAB) testing in the transonic flow regime. A particular objective of this program was to evaluate the effect of Reynolds number on nozzle afterbody pressure drag.

To support the program for improving NAB test techniques, tests were conducted in the AEDC Propulsion Wind Tunnel (16T) to determine the tunnel calibration and centerline Mach number distributions at various test section wall porosities. Limited data were obtained to provide an indication of the effects of Reynolds number on the tunnel calibration. Early calibration experience in Tunnel 16T indicated that Reynolds number did not have a significant effect on the Mach number distributions. As a consequence, stagnation pressure has usually not been selected as a variable during tunnel calibration. The results of the porosity calibration are presented in Ref. 1. Those results indicated that at Mach numbers of 0.6 and 0.8 the calibrated Mach number varied slightly (less than 0.001 per million) with increasing Reynolds number. For six-percent porosity and at all Reynolds numbers, however, the Ref. 1 calibrated Mach number agreed within ± 0.002 with the calibration reported in Ref. 2. Considering the small effects of Reynolds number and in lieu of a complete calibration, the use of the Ref. 2 calibration for tunnel operation was continued.

Following the conduct of the Ref. 1 calibration, data presented in Ref. 3 precipitated a more indepth analysis of the effects of Reynolds number on the tunnel calibration. This analysis revealed that a 0.2-percent error in static pressure attributed to use of the Ref. 2 calibration, which neglects the effects of Reynolds number, could cause a 70-drag-count (based on model maximum cross-sectional area) error in nozzle afterbody drag at $M_\infty = 0.6$ and $Re = 5.0 \times 10^6/\text{ft}$. As a consequence of these results, a test was conducted to determine more accurately the effects of Reynolds number variation on the Tunnel 16T calibration.

During the Reynolds number calibration, centerline Mach number distributions were obtained at Mach numbers from 0.2 to 1.6 and for Reynolds numbers from about 0.4 to $6.4 \times 10^6/\text{ft}$. The effects of tunnel pressure ratio and test section wall angle on the tunnel calibration and power consumption were also determined. The results of this calibration are presented in this report. The results of the Reynolds number calibration were utilized to correct previous AEDC nozzle afterbody test data.

Typical data corrections are illustrated in Appendix A. The results of the Reynolds number calibration were also incorporated into a computer program for utilization during Tunnel 16T operation.

2.0 APPARATUS

2.1 TEST FACILITY

The PWT 16-ft Transonic Wind Tunnel (Propulsion Wind Tunnel (16T)) is a continuous flow, closed-circuit tunnel which can be operated at Mach numbers from 0.2 to 1.6. The tunnel has a test section 40 ft long and 16 ft square with six-percent porosity walls. The test section sidewalls can be either converged or diverged 1 deg.

Tunnel 16T is a variable density tunnel which can be operated within a stagnation pressure range of 120 psfa to a maximum of 4,000 psfa, depending upon the Mach number. The stagnation temperature can be varied from a minimum of about 80°F, dependent upon available cooling water temperature, to a maximum of 160°F.

The Tunnel 16T main compressor is a three-stage, axial-flow compressor with variable stator blades. The compressor drive system consists of four motors with a power rating of 216,000 hp. To prevent tunnel choking in the transonic range, test section flow removal (auxiliary flow) is accomplished with a plenum evacuation system (PES). The PES consists of ten compressors which are driven by motors with a total power rating of 179,00 hp. The PES is also utilized for tunnel pressure level control.

Various Mach numbers in Tunnel 16T are established by regulation of pressure ratio, plenum pressure, and the contour of a flexible, two-dimensional Laval nozzle. Mach numbers below 0.55 are obtained by operating the compressor drive motors subsynchronously. Test section flow removal is utilized at Mach numbers above 0.75, and supersonic nozzle contours are utilized at $M_{\infty} \geq 1.05$.

Two 40-ft-long test sections are available for testing in Tunnel 16T. Test Section 1 is generally used for propulsion testing. Test Section 2, which is equipped with a sting support system, is primarily used for aerodynamic testing. This calibration was conducted utilizing the propulsion test section. The general arrangement of the test section and the perforated wall geometry is shown in Fig. 1. Additional details with regard to Tunnel 16T and its capabilities are presented in Ref. 4.

2.2 CALIBRATION EQUIPMENT

A 6.5-in.-diam static pressure pipe was used to obtain the centerline static pressure distribution from tunnel station -5.8 to 48.2. Results from Ref. 1 indicated that this pipe

installation provides a satisfactory measure of both subsonic and supersonic Mach number distributions. The calibration rig, however, does generate some disturbances at the high supersonic Mach numbers.

The rear end of the calibration pipe protruded through a cone tip on the 16T scavenging scoop and was attached internally to a mechanism which provided a restoring moment to counteract the weight of the pipe. A total of four cables, swept rearward at 30 deg to the tunnel centerline and spaced to produce a moment to also aid in removing pipe sag, provided pipe support. The pipe, which encompassed an ogive tip, was subject to a tensile load through the use of a cable which extended far upstream into the tunnel nozzle and connected to a streamlined forebody and cable support system.

The centerline pipe included a total of 75 static orifices. The orifices were spaced at 1-ft intervals from tunnel station -5.8 to 0.2, at 0.5-ft intervals from tunnel station 0.2 to 24.2, at 1-ft intervals from tunnel station 24.2 to 40.2, and 2-ft intervals from tunnel station 40.2 to 48.2. A schematic and photographs of the pipe installation are shown in Fig. 1.

Twenty-six static pressure orifices near the test section floor centerline were used to obtain wall static pressure distributions from station 1.0 to 32. The orifices were installed in the tunnel perforated wall liners; however, the four perforations adjacent to the orifices were filled with plaster as illustrated in Fig. 1.

The pipe orifices and wall pressure orifices were connected to differential pressure transducers which were referenced to the tunnel plenum chamber pressure. The tunnel plenum chamber pressure was determined by measurement from a self-balancing precision manometer. The tunnel stagnation pressure was determined by averaging measurements from two self-balancing precision manometers.

3.0 PROCEDURE

3.1 CALIBRATION DISCUSSION

The calibration was conducted over the Mach number range from 0.2 to 1.6, and data were obtained for Reynolds numbers from 0.4 to $6.4 \times 10^6/\text{ft}$. Primary emphasis was placed upon investigation at Mach numbers from 0.6 to 1.5, which is the principal range of interest for most tests in Tunnel 16T.

The centerline Mach number distributions were defined at tunnel stagnation pressures from 400 to 4,000 psfa (or near the tunnel maximum) in 600-psf increments. The effects of pressure ratio and wall angle variation were defined at a stagnation pressure of 1,600 psfa. This stagnation pressure level was chosen as a baseline since the

Ref. 1 calibration was conducted at 1,600 psfa. The tunnel stagnation temperature was maintained at 110°F for Mach numbers of 0.6 and above and at about 80°F for Mach numbers below 0.6.

Based on data presented in Ref. 1 and results from this test, a nominal pressure ratio schedule was defined for utilization during variations of test section wall angle and Reynolds number. At subsonic Mach numbers the pressure ratio was selected as that associated with generally "flat" Mach number distributions. At supersonic Mach numbers a pressure ratio sufficient to keep the tunnel shock wave system downstream of the model support strut was selected. The nominal pressure ratio, λ^* , schedule is shown in Fig. 2. To determine the effects of pressure ratio on the distributions, the pressure ratio was also varied up to 25 percent above and below the nominal schedule.

Test section wall angle was varied from 0.50 to -1.0 deg. Positive wall angles correspond to wall divergence from the tunnel centerline. The Tunnel 16T optimum wall angle schedule and the range of wall angles investigated during this test are shown in Fig. 3. The optimum wall angle schedule was defined in Ref. 5 as that which provided the "best" pressure distribution on long slender bodies of revolution with a test section blockage of one percent. The optimum wall angle schedule is used during AEDC NAB tests.

3.2 DATA REDUCTION AND UNCERTAINTY

The distribution of local Mach number in the test section was obtained from reduction of the centerline pipe and wall static pressure data to Mach number, assuming isentropic flow through the nozzle. The average Mach number and the 2- σ Mach number deviation for two test section regions were computed. These regions include tunnel stations 8 to 28, which encompass the region in which most AEDC NAB models are installed, and tunnel stations 1 to 20, which is the test region used for the Ref. 2 calibration and most sting-supported test models.

The statistical parameter σ , the standard deviation, is approximately a root-mean-square quantity which is a measure of the deviation of the local Mach numbers from the average. Assuming a normal distribution, 95.4 percent of the local Mach numbers will fall within a distribution band of $\pm 2 \sigma$.

The calibration of Tunnel 16T is based on the measured pressure differential between the test section and the plenum chamber at various operating conditions. As a matter of procedure, a plenum chamber Mach number equivalent was determined from plenum chamber and stagnation pressure measurements using the isentropic relationship. A calibration parameter is defined as the difference between the free-stream and plenum chamber Mach numbers. This parameter ($M_\infty - M_c$) is utilized to express the tunnel calibration for various operating conditions.

A Taylor series method of error propagation was utilized to estimate the uncertainty in the data which could be attributed to instrumentation errors and data acquisition techniques. For a confidence level of 95.4 percent, the maximum errors are as follows:

$\Delta\lambda$	± 0.002
$\Delta\theta$	± 0.04
ΔM_∞	± 0.0004
ΔRe	$\pm 0.02 \times 10^{-6}$
$\Delta(M_\infty - M_c)$	± 0.0019

3.3 FLOW QUALITY

One of the primary objectives of a tunnel calibration is to ascertain whether adequate flow quality exists for acquisition of test data for various locations of test models and various combinations of tunnel conditions. Tunnel flow quality encompasses several parameters, such as flow angularity and turbulence levels, which were not investigated during this calibration. Data presented in Ref. 6 indicate that undesirable pressure gradients do not exist in Tunnel 16T for normal operating conditions. This report, therefore, will deal only with the uniformity of the centerline Mach number distribution. A quantitative evaluation of the uniformity of a Mach number distribution, when no pressure gradients exist, for a particular test section can be obtained by analysis of the 2- σ Mach number deviation.

The author is unaware of any industry "standard" which exists for values of the 2- σ Mach number deviations which are indicative of good Mach number distributions. For purposes of this report, 2- σ Mach number deviations of 0.005 M_∞ and 0.01 M_∞ for subsonic and supersonic Mach numbers, respectively, will be considered indicative of "good" distributions.

The 2- σ Mach number deviation can also be utilized to evaluate the effects of various test parameters on the centerline Mach number distributions. The minimum Mach number deviation for a particular test section length and set of tunnel conditions is, of course, indicative of the "best" distribution. The 2- σ parameter, however, is very sensitive to small changes in the distributions and to moderate changes in local conditions. To facilitate judgement with regard to the effects of various test parameters, a variation in the 2- σ Mach number deviation less than 10 percent of the nominal 2- σ level will be considered insignificant.

4.0 RESULTS AND DISCUSSION

4.1 MACH NUMBER DISTRIBUTIONS

4.1.1 General

Tunnel 16T centerline and wall Mach number distributions were obtained at a variety of test conditions during the calibration. A complete and detailed presentation of all the results is considered unnecessary. Accordingly, only selected data, sufficient to indicate various data trends as well as important results, are presented herein. Typical centerline and wall Mach number distributions obtained at Mach numbers from 0.2 to 1.6 with $\theta = 0$ and $\lambda = \lambda^*$ are presented in Figs. 4, 5, and 6.

Effects of Mach number on the $2\text{-}\sigma$ Mach number deviations for the centerline and wall distributions over the two model test regions are presented in Fig. 7, along with comparisons with previous calibrations. The data indicate that, with some exceptions, the deviations for the distributions over both test regions are better than required for "good" Mach number distributions. Exceptions are the centerline distributions at $M_\infty > 1.2$ for tunnel stations 1 to 20. The data also indicate that the centerline and wall distributions compare reasonably well with the results from Refs. 1 and 2, respectively. The results in Ref. 2 were obtained using orifices mounted in a 2-ft-wide solid plate in the test section floor.

Comparison of the centerline and wall Mach number deviations presented in Fig. 7 indicates that, in general, the centerline distributions are better at subsonic Mach numbers, but the wall distributions are better at supersonic Mach numbers. According to Ref. 1, the centerline Mach number distributions at supersonic Mach numbers are believed to be affected by disturbances which emanate from the calibration rig. Data presented in Figs. 5b and 6b tend to verify this possibility. The pipe disturbance, however, primarily affects only the forward portion of the distributions. Consequently, the Mach number deviations for tunnel stations 1 to 20 are more sensitive to the pipe disturbances than are the deviations for tunnel stations 8 to 28. For this reason and because the latter test region is more applicable for tests in the propulsion test section (particularly the AEDC NAB tests), the remaining data analysis presented will generally be restricted to that for the test region from tunnel stations 8 to 28. In addition, the centerline distributions will be utilized since they are considered superior to the wall distributions at subsonic Mach numbers.

Some test data were obtained with a boundary-layer rake installed on each tunnel wall at tunnel station 32. During the first supersonic Mach number runs, a disturbance from the rakes was observed at the tunnel centerline. As a consequence, the boundary-layer rakes were removed for the remainder of the tests. Repeat runs were

made to evaluate the effects of the rakes on the test data. The effects of the rakes on the centerline Mach number distributions are presented in Fig. 8. These data indicate that the rakes primarily affect the distributions downstream of tunnel station 30. In addition, there is essentially no effect at $M_\infty < 0.8$. Further analysis of these data indicated that for $M_\infty \leq 1.0$ the effect of the rakes on the $2\text{-}\sigma$ Mach number deviations and the tunnel calibrated Mach number was less than ± 0.0002 . At supersonic Mach numbers, the effect on these parameters was less than ± 0.0008 . The data also indicated that the rakes had a small effect on the tunnel pressure ratio, auxiliary weight flow, and power requirements. This could be expected since these parameters are known to vary with test section blockage. Since all the remaining supersonic data presented herein were obtained with the rakes removed, the effect of the rakes was restricted to data for Mach numbers between 0.8 and 1.0. Since the effect of the rakes at these Mach numbers was not considered significant, no attempt was made to distinguish between data with and without the boundary-layer rakes.

4.1.2 Effects of Tunnel Pressure Ratio

Centerline Mach number distributions for various tunnel pressure ratios at Mach numbers from 0.8 to 1.5 for $\theta = 0$ and $P_t = 1,600$ psfa are presented in Fig. 9. These data indicate that the effects of pressure ratio variation are primarily restricted to the rear portion (usually downstream of tunnel station 32) of the distributions. Similar data trends were obtained when the pressure ratio was varied at other Reynolds numbers. Most test models are installed well upstream of tunnel station 32.

The effects of pressure ratio variation on the $2\text{-}\sigma$ Mach number deviations for stations 8 to 28 are presented in Fig. 10. The nominal pressure ratios, λ^* , are also illustrated. The data presented in Fig. 10 indicate that, except for the lower pressure ratios at $M_\infty \leq 0.9$, pressure ratio variation does not significantly affect the Mach number deviations. The lowest pressure ratios at $M_\infty = 0.8$ and 0.9 are not considered indicative of normal operating conditions in Tunnel 16T.

Data presented in Figs. 9 and 10 indicate that acceptable Mach number distributions can be obtained for various pressure ratios. The nominal pressure ratios are noted in Fig. 10. The effect of pressure ratio variation on the auxiliary weight flow requirements is shown in Fig. 11. These data indicate that reducing pressure ratio (to decrease main drive power) significantly increases the auxiliary flow requirements (and therefore the auxiliary power).

An optimum pressure ratio may be defined as that associated with minimum total power requirements and acceptable Mach number distributions. Typical effects of pressure ratio variation on total power consumption are illustrated in Fig. 12. The power

factor is the total power divided by the tunnel stagnation pressure. These data have been corrected for the power of standby compressors and for flow bypassed through the Mach number control valve. The data presented in Fig. 12 indicate that for subsonic Mach numbers the optimum pressure ratios (minimum power) coincide with the nominal pressure ratios. At supersonic Mach numbers, the data indicate that minimum power occurs at the lowest tunnel pressure ratio. These results appear generally consistent with those reported in Ref. 7.

As previously indicated, the normal model of operation in Tunnel 16T is not to utilize plenum suction at the low subsonic Mach numbers. The effects of using auxiliary flow on the distributions at $M_{\infty} = 0.75$ is illustrated in Fig. 13. These data indicate that using auxiliary flow does not affect the distributions upstream of about tunnel station 30. Other data, not presented, indicate that the tunnel calibration is also not affected by using auxiliary flow at $M_{\infty} = 0.75$. The total power required to operate the tunnel, however, was reduced by about six percent. These data indicate that power consumption could possibly be reduced by using auxiliary flow at other Mach numbers below 0.75. No data, however, were obtained during this test to evaluate adequately the effects of auxiliary flow on the Mach number distributions and the tunnel calibration at the lower Mach numbers.

4.1.3 Effects of Wall Angle

Centerline Mach number distributions for various test section wall angles at Mach numbers from 0.6 to 1.5 with $\lambda = \lambda^*$ and $P_t = 1,600$ psfa are presented in Fig. 14. These data indicate that for subsonic Mach numbers, wall divergence decelerates the flow in the aft end of the test section. At supersonic Mach numbers, however, the effects of wall angle variation are not as definitive although they are primarily restricted to the forward portion of the distribution.

The effects of wall angle variation on the 2σ Mach number deviations for tunnel stations 8 to 28 are presented in Fig. 15. The test section wall angles associated with the optimum wall angle schedule, θ^* (Fig. 3), are also noted. The data presented in Fig. 15 indicate that the effects of wall angle variation can be significant. Acceptable Mach number distributions were obtained, however, at almost all wall angles tested. At most Mach numbers, the "best" distributions were obtained near zero wall angle. This result is consistent with that obtained in Ref. 1. Similar data trends were obtained when the wall angle was varied at other Reynolds numbers.

Typical effects of wall angle variation on the tunnel auxiliary flow and total power requirements are presented in Figs. 16 and 17. These data indicate that generally the minimum auxiliary flow and power requirements occur at either $\theta = 0$ or 0.25. In addition, wall convergence significantly increases power requirements at all Mach

numbers. The only occasions that the tunnel is routinely run with converged wall angles is when the optimum wall angle schedule is utilized at Mach numbers between 1.00 to 1.25. Wall angles associated with the optimum wall angle schedule are noted in Figs. 16 and 17. The data in Fig. 17 indicate that at $M_\infty = 1.1$, use of the optimum wall angle rather than $\theta = 0$ increases the power requirements by about 25 percent.

The result that the optimum wall angle schedule does not provide the best Mach number distributions and power utilization at all Mach numbers is a source of confusion. Some discussion of this matter, including the Ref. 5 results, is presented in Ref. 1. In view of the advantages of $\theta = 0$, a test in Tunnel 16T to re-evaluate the optimum wall angle schedule (considering tunnel Mach number distributions, power consumption, and model pressure distributions) is recommended.

4.1.4 Effects of Reynolds Number

Centerline Mach number distributions at various unit Reynolds numbers for Mach numbers from 0.6 to 1.6 with $\theta = 0$ and $\lambda = \lambda^*$ are presented in Fig. 18. These data indicate that variation of Reynolds number has only a small effect on the distributions.

The effect of Reynolds number on the $2\text{-}\sigma$ Mach number deviations for tunnel stations 8 to 28 is presented in Fig. 19. These data indicate that except for $M_\infty = 1.4$ and 1.5, Reynolds number variations have an insignificant effect on the $2\text{-}\sigma$ Mach number deviations. By the criteria previously indicated (Section 3.3), the distributions for all Mach numbers and Reynolds numbers are deemed to be of good quality.

The effects of Reynolds number variation on the tunnel auxiliary flow and power requirements are illustrated in Figs. 20 and 21. The data presented in Fig. 20 indicate that the auxiliary flow requirements slightly increase with increasing Reynolds number. The data presented in Fig. 21 indicate that below $Re = 2.5 \times 10^6/\text{ft}$ the tunnel total power factor increases significantly with decreasing Reynolds number. The tunnel main drive power is proportional to stagnation pressure; however, the auxiliary power is not. This accounts for the variations in power factor shown in Fig. 21.

4.2 TUNNEL CALIBRATION

4.2.1 General

The effect of using either the centerline pipe or wall pressures to define the tunnel calibration with $\theta = 0$, $\lambda = \lambda^*$, and $P_t = 1,600$ psfa is presented in Fig. 22 for the two test regions of interest. These data indicate that, with some exceptions, the calibration based on wall pressures is consistently below that for the pipe pressures. The exceptions

are for the data at $M_\infty \geq 1.5$ for tunnel stations 1 to 20 for which, as previously indicated, the centerline data are affected by disturbances from the calibration pipe. For tunnel stations 8 to 28 the calibrations from the two sets of orifices agree within 0.0012. For tunnel stations 1 to 20 the agreement is within 0.0004 except for $M_\infty > 1.5$. Such agreement is considered quite satisfactory. Consequently, no attempt will be made to explain the consistent differences in the results obtained with the two sets of orifices.

As previously indicated, the centerline pipe data are considered superior to the wall data and will therefore be utilized to define the tunnel calibration. Another factor which influenced this decision is that when the test section wall angle was varied, the data from the wall orifices were affected. Similar results were obtained in Ref. 2 with orifices in the perforated plates.

The comparison between the tunnel calibrations for the two test regions is more explicitly shown in Fig. 23. These data indicate that the calibrations for the two test regions agree within 0.0006. The results for tunnel stations 1 to 20, however, are consistently below the results for tunnel stations 8 to 28. A close analysis of the Mach number distributions presented in Fig. 9 indicates the existence of a flow deceleration, both subsonically and supersonically, in the forward portion of the test section near tunnel station 2. Between stations 8 to 28, the distributions at $\lambda = \lambda^*$ are essentially flat. As a consequence, in the test region from tunnel stations 1 to 20 several "low" local Mach numbers are included in the Mach number averaging that are not within the region between stations 8 to 28. This is believed to account for most of the differences between the calibrations for the two test regions. As previously indicated, however, the test region from tunnel stations 8 to 28 will be utilized to define the calibration for the propulsion test section.

Appropriate comparisons of the current results with the results from Refs. 1 and 2 are presented in Fig. 24. For tunnel stations 8 to 28, the current calibration agrees with the Ref. 1 results within 0.0008 except at $M_\infty = 0.6$. At $M_\infty = 0.6$ the agreement is within 0.0012. For tunnel stations 1 to 20, the current calibration agrees with the Ref. 1 results within 0.0008 except at $M_\infty < 0.7$ and $M_\infty > 1.4$. Comparison of the data in Figs. 22 and 24 indicates that the agreement of the current calibration with the results from Ref. 2 is within ± 0.0015 for both test regions. In addition, the wall data do not provide any better agreement with Ref. 2. The disagreements between the various sets of data are all within the data uncertainty. Normally such agreement would not warrant a change in the tunnel calibration. However, because of the effect that such small differences can have on nozzle afterbody test results, a closer evaluation of the effects of various parameters on the tunnel calibration is desirable.

The consistent differences between the current calibration and Ref. 1, although small, were unexpected and not easily explained. The data were obtained in the same test section with the same centerline pipe installation. The current and Ref. 1 data shown in Fig. 24 were obtained at the same test conditions except for insignificant differences in pressure ratio. Slightly higher tunnel pressure ratios were required for this test because of the installation of a new screen in the wind tunnel diffuser. The instrumentation used and the data reduction procedures for the two tests were essentially the same. There were some differences, however, in the number of instrument channels and the instrumentation setup and calibration procedures.

During Tunnel 16T test installations, some of the test section perforated liner plates are frequently exchanged. Although the same test section was used for this test and Ref. 1, there could have been a slight change in the overall pressure drop characteristics of the liner plate installation. Another factor to consider is the condition of the calibration pipe. The calibration pipe was fabricated for the Ref. 1 test. It was stored for about 14 months and then cleaned up (removal of rust) to be used for the current test. Data from both test programs have indicated that a slight orifice imperfection can produce a significant (10-psfa) error in any individual measurement. It is certain that some small differences in the pipe orifices and finish existed between the two test programs. For example, the disturbance near tunnel station 1.5 for subsonic Mach numbers (see Fig. 9) did not occur during the Ref. 1 test.

In summary, the differences between the current and Ref. 1 calibrations are attributed to changes in instrumentation procedures, liner plate characteristics, and calibration pipe condition. Considering the nature of these factors, it is impossible to determine, without some reservations, which test provides the "best" calibration data. It is therefore concluded that either set of data could probably be utilized to define the Tunnel 16T calibration.

Analytic expressions of the Mach number calibration parameter ($M_\infty - M_c$) are incorporated into facility computer programs for test operations. For the Ref. 2 calibration, which was used for the AEDC NAB tests, linear equations with test section wall angle as a variable were utilized. For the current and Ref. 1 calibrations, analytic expressions of the Mach number calibration parameter were determined using a least-squares, multiple-regression, data-fitting program. Several data fits were required to specify the tunnel calibration at various test conditions.

4.2.2 Effects of Pressure Ratio

The effects of tunnel pressure ratio variation on the Tunnel 16T calibration with $\theta = 0$ and $P_t = 1,600$ psfa are presented in Fig. 25. These data indicate that for the normal

tunnel operating range ($\lambda > 1.16$) pressure ratio variation has an insignificant effect on the tunnel calibration. As a consequence, the calibration is defined independent of the tunnel pressure ratio.

4.2.3 Effects of Wall Angle

The Tunnel 16T calibration at $\theta = 0$ and $P_t = 1,600$ psfa for Mach numbers from 0.2 to 1.6 is presented in Fig. 26. The curves shown result from calculations using polynomial curve fits of the respective data. The results presented at $M_\infty < 0.6$ were extrapolated from data obtained at other pressure levels.

The data presented in Fig. 26 indicate that the Ref. 1 curve fit does not satisfactorily fit the current results, particularly at $M_\infty < 0.8$. As a consequence, it is recommended that the current data be utilized for the tunnel calibration at $\theta = 0$ and $P_t = 1,600$ psfa. The coefficients associated with this curve fit are presented in Table 1. The maximum residual (the difference between the actual and computed value) which results from the curve fit is 0.0007. However, 95 percent of the data have residuals within 0.0004.

The effects of test section wall angle variation on the Tunnel 16T calibration with $\lambda = \lambda^*$ and $P_t = 1,600$ psfa are illustrated in Fig. 27. These data indicate that the calibration is significantly affected by wall angle variation. Calibration data fits are therefore required as a function of wall angle.

A comparison with the Ref. 1 results is also presented in Fig. 27. The curves shown in Fig. 27 depict the analytic surfaces which correspond to the results of the data-fitting program. Results from the current test agree with the Ref. 1 surface fits within ± 0.002 at all test conditions. Wall angles other than zero and those associated with the optimum wall angle schedule are rarely run in Tunnel 16T. For $1.1 \leq M_\infty \leq 1.4$, and the optimum wall angle schedule, which is depicted in Fig. 27, the agreement between this test and that reported in Ref. 1 is within 0.0006. Such agreement is better than that obtained at $\theta = 0$ and is considered satisfactory. To be consistent, however, it is also recommended that the current calibration data be utilized at $\theta \neq 0$ as well as $\theta = 0$. The coefficients associated with the current data surface fit for various wall angles are presented in Table 2. This surface fit results in maximum residuals for 95 percent of the data within 0.0008. Data at $M_\infty = 1.6$ and the optimum wall angle schedule (not shown in Fig. 27), however, were excluded from the data-fitting process as they did not fit the current data trends or those trends exhibited in either Refs. 1 or 2.

4.2.4 Effect of Reynolds Number

Early calibration experience in Tunnel 16T indicated that Reynolds number did not have a significant effect on the tunnel calibration. As a consequence stagnation pressure has usually not been selected as a variable during tunnel calibration. The Ref. 2 calibration was conducted at 1,000 psfa. The Ref. 6 calibration was conducted at a constant Reynolds number of $3.0 \times 10^6/\text{ft}$, which corresponded to a stagnation pressure variation from about 1,500 to 2,000 psf. The data presented in Ref. 6 indicated that the calibrated Mach number was consistently above but within 0.001 of that given in Ref. 2 at most test conditions, and such differences were considered negligible.

The effect of Reynolds number on the Tunnel 16T calibration at $\theta = 0$ and $\theta = \theta^*$ are illustrated in Figs. 28 and 29. These data indicate that except for $M_\infty > 1.4$ and low Reynolds numbers, the tunnel calibrated Mach number increases slightly with increasing Reynolds number. This data trend is the same as that observed at $M_\infty = 0.6$ and 0.8 for the Ref. 1 calibration as illustrated in Fig. 28. At low Reynolds numbers, a "bucket" and change in curve slope was consistently obtained. Based on the results from Ref. 1, such a trend was not expected. The validity of the current low Reynolds number data are therefore subject to question. It was considered particularly coincidental that the "bucket" occurred consistently at $P_t = 1,000$ psfa. Although pressure system lag time is a particular problem at the low Reynolds numbers, no evidence has been found to date to prove the low pressure data trends invalid. The data presented in Fig. 29 also illustrate, as previously noted, that the data for $M_\infty = 1.6$ and $\theta = \theta^*$ do not follow the indicated data trends with regard to the magnitude of the calibration parameter.

For most test conditions the Mach number varies by less than ± 0.003 for variation of Reynolds number over the available range. Such a variation is small compared to data uncertainty and can justifiably be neglected for many types of tunnel test programs. For nozzle afterbody tests, however, such errors can be significant. Because the trends with Reynolds numbers are consistent and repeatable, a correction to the tunnel calibration for Reynolds number effects is possible.

The data presented in Figs. 28 and 29 were utilized to correct nozzle afterbody test data for Reynolds number effects on the calibration. For the correction program, the data were divided into two pressure ranges, with the dividing point at $P_t = 1,000$ psfa. Third-order curve fits of the data at $P_t < 1,000$ psfa and second-order curve fits at $P_t \geq 1,000$ psfa were utilized in the correction program. Coefficients for these two sets of curve fits for specific Mach numbers with $\theta = \theta^*$ are presented in Tables 3 and 4. The calibration parameter was expressed as a function of stagnation pressure, rather than Reynolds number, because pressure is an independent variable.

Utilization of the Reynolds number correction program proved satisfactory. Typical nozzle afterbody data corrections are presented in Appendix A. The correction program was also applied to the current set of calibration data which had been run using the Ref. 2 calibration. It was suggested in Ref. 3 that a possible criterion for Reynolds number corrections is to maintain the average pressure coefficient at the wall as zero. Clearly, this occurs if the static pressure from the tunnel calibrated Mach number is equal to the average static pressure over the test region of interest. This possible criterion was investigated for the centerline pipe data. Typical average pressure coefficients over the test region from tunnel stations 8 to 28, before and after application of the Reynolds number correction program, are presented in Fig. 30. These data indicate that utilization of the Reynolds number corrections produced a zero average pressure coefficient. These results demonstrate the validity of the correction routine. In addition, $\bar{C}_p = 0$ is possibly a satisfactory criterion for data correction in lieu of a tunnel calibration at various Reynolds numbers. Other effects, such as model size and pressure gradients, need to be evaluated, however, before such corrections are recommended.

Although the Reynolds number correction program previously discussed provided good results, it is not suitable for general application in Tunnel 16T because of its limitations with regard to Mach number and wall angle. The tunnel calibration for Tunnel 16T must be expressed for all potential Mach numbers, wall angles, and Reynolds numbers. Based on information in Ref. 1 such a data set can probably not be satisfactorily fit with a hypersurface. Consequently, more than one set of data fits and coefficients are utilized.

By selecting a primary calibration pressure level of 1,600 psfa, analytical expressions and coefficients presented in Tables 1 and 2 can be utilized to compute the tunnel Mach number at all wall angles for $P_t = 1,600$ psfa. The correction for Reynolds number can then be applied by accounting for the differences in the calibration from $P_t = 1,600$ psfa.

Utilization of two sets of coefficients as shown in Tables 3 and 4 and use of a family of third-order curve fits for the Reynolds number corrections is not computationally efficient. Consequently, the data presented in Figs. 28 and 29 were fit to a family of linear curves which pass through the calculated data (Tables 1 and 2) at $P_t = 1,600$ psfa. Errors in Mach number of up to 0.002 at $P_t \leq 1,000$ psfa, but usually less than 0.0005 at $P_t > 1,000$ psfa, result from this practice. Data at low pressures are rarely obtained and considering data uncertainty and pressure lag time should probably never be obtained in Tunnel 16T. As a consequence, the Mach number errors resulting from this simplification of the data reduction program is considered acceptable.

Changes in the calibration parameter ($M_\infty - M_c$) as a linear function of stagnation pressure were used to obtain a family of curve slopes for use in the correction routine. Variation of the slopes ($\Delta(M_\infty - M_c)/\text{psf}$) as a function of Mach number and wall angle (for $M_\infty > 1.0$) are presented in Fig. 31. Although the magnitudes of the data at $M_\infty = 1.6$ and $\theta = \theta^*$ were suspect, the slope for these data was utilized in Fig. 31.

The data presented in Fig. 31 indicate that at supersonic Mach numbers the Reynolds number effect changes with variation in wall angle. The effect of wall angle, however, is amplified by the sensitivity of the slope function. For example, for a slope change of $\pm 1.0 \times 10^6/\text{psf}$ the effect on Mach number is only $\pm 0.001/1,000$ psf. At supersonic Mach numbers, a $\pm 1,000$ -psf variation in stagnation pressure from 1,600 psf completely encompasses the normal tunnel operating range. For most test programs, therefore, the effect of wall angle variation on the Reynolds number corrections at supersonic Mach numbers may be neglected. To diminish the effect of this approach, the supersonic Mach number slope data shown in Fig. 31 for $\theta = 0$ and $\theta = \theta^*$ should be averaged.

Insufficient data were obtained during this test to define the effect of wall angle on the Reynolds number corrections at subsonic Mach numbers. Limited unreported data were obtained, however, during the Ref. 1 calibration at various Reynolds numbers and wall angles. These data are presented in Fig. 32. The data shown illustrate that wall angle also affects the Reynolds number calibration at subsonic Mach numbers. When linear curves of the same slope as that at $\theta = 0$ are fit through the data at a pressure of 1,600 psfa for $\theta \neq 0$, a fair data fit is obtained. Since the worst discrepancy is small and occurs at the lowest pressure levels, the data fit is considered satisfactory. As a consequence, to simplify the data correction program, the effects of wall angle on the Reynolds number correction will be neglected at subsonic Mach numbers. Since wall angle is rarely varied (from $\theta = 0$) at subsonic Mach numbers this procedure is considered acceptable.

To allow the Reynolds number correction routine to be used for any tunnel test condition, the slopes of the linear curves were fit by various polynomials. The coefficients for various slope data fits and the equations for correcting Mach number for Reynolds number effects are presented in Tables 5 and 6. The fairings shown in Fig. 31 result from computations using the slope data fits. The best results were obtained when the range of slope data to be fitted was limited by Mach number and/or wall angle. For simplification of the tunnel conditions computational routine, it is recommended that the slopes be determined using the polynomial which neglects (averages) wall angle and covers the entire Mach number range (Table 6).

5.0 CONCLUSIONS

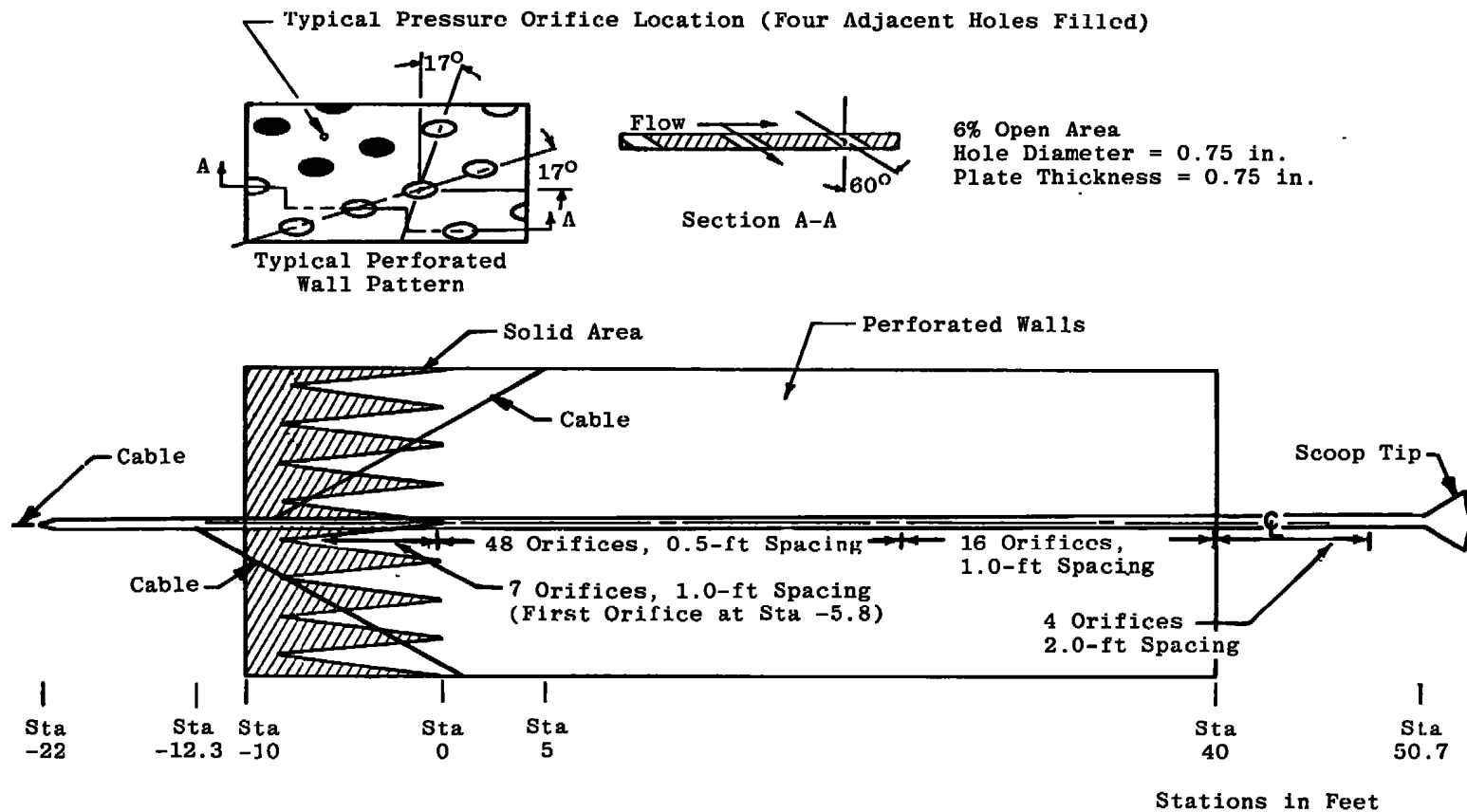
Based on the results from this test to define the effects of Reynolds number variation on the Tunnel 16T test section Mach number distributions and calibration, the following conclusions are made:

1. For the test region from tunnel stations 8 to 28, centerline Mach number distributions of good quality are obtained for Mach numbers from 0.2 to 1.6 for both zero and optimum wall angles.
2. Variation of tunnel pressure ratio over a normal operating range has an insignificant effect on both the Mach number distributions and the tunnel calibration.
3. Variation of tunnel pressure ratio can have a significant effect on tunnel total power requirements. Generally, the minimum power requirements correspond to the minimum pressure ratio which provides "flat" Mach number distributions to tunnel station 40.
4. Variation of test section wall angle can have a significant effect on both the Mach number distributions and the tunnel calibration.
5. Variation of test section wall angle can have a significant effect on the tunnel total power requirements. Generally, the minimum power requirements were obtained at wall angles of either zero or 0.25 deg.
6. Variation of Reynolds number has a negligible effect on the Mach number distributions for Mach numbers less than 1.4.
7. Variation of Reynolds number has a small but definable effect on the Tunnel 16T calibration. The effect should not be neglected during tests for which very small errors in static pressure may be significant.
8. For most test conditions, the current tunnel calibration parameter agrees with the Ref. 1 results within 0.0008 and with the Ref. 2 results within ± 0.0015 . Although such agreement is generally considered good, some changes in the tunnel calibration are desirable.
9. For completeness, the Tunnel 16T calibration must be defined as a function of test section wall angle, Reynolds number, and Mach number. Analytical expressions which adequately represent the tunnel calibration at various test conditions were developed.

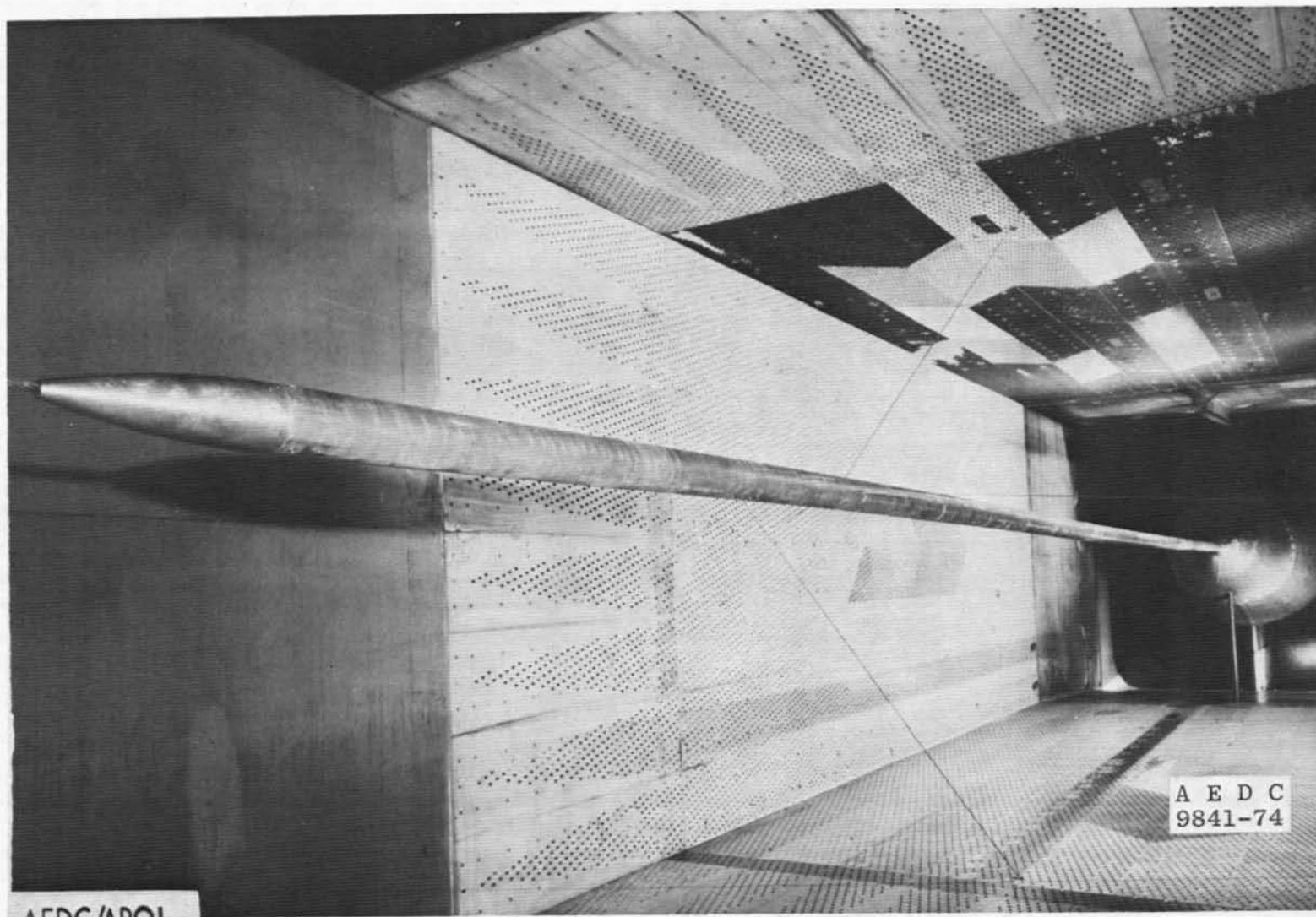
10. The optimum wall angle schedule, which was selected based on typical model pressure distributions, does not provide the best centerline Mach number distributions and power utilization at all Mach numbers. A test to re-evaluate the optimum wall angle schedule is recommended.

REFERENCES

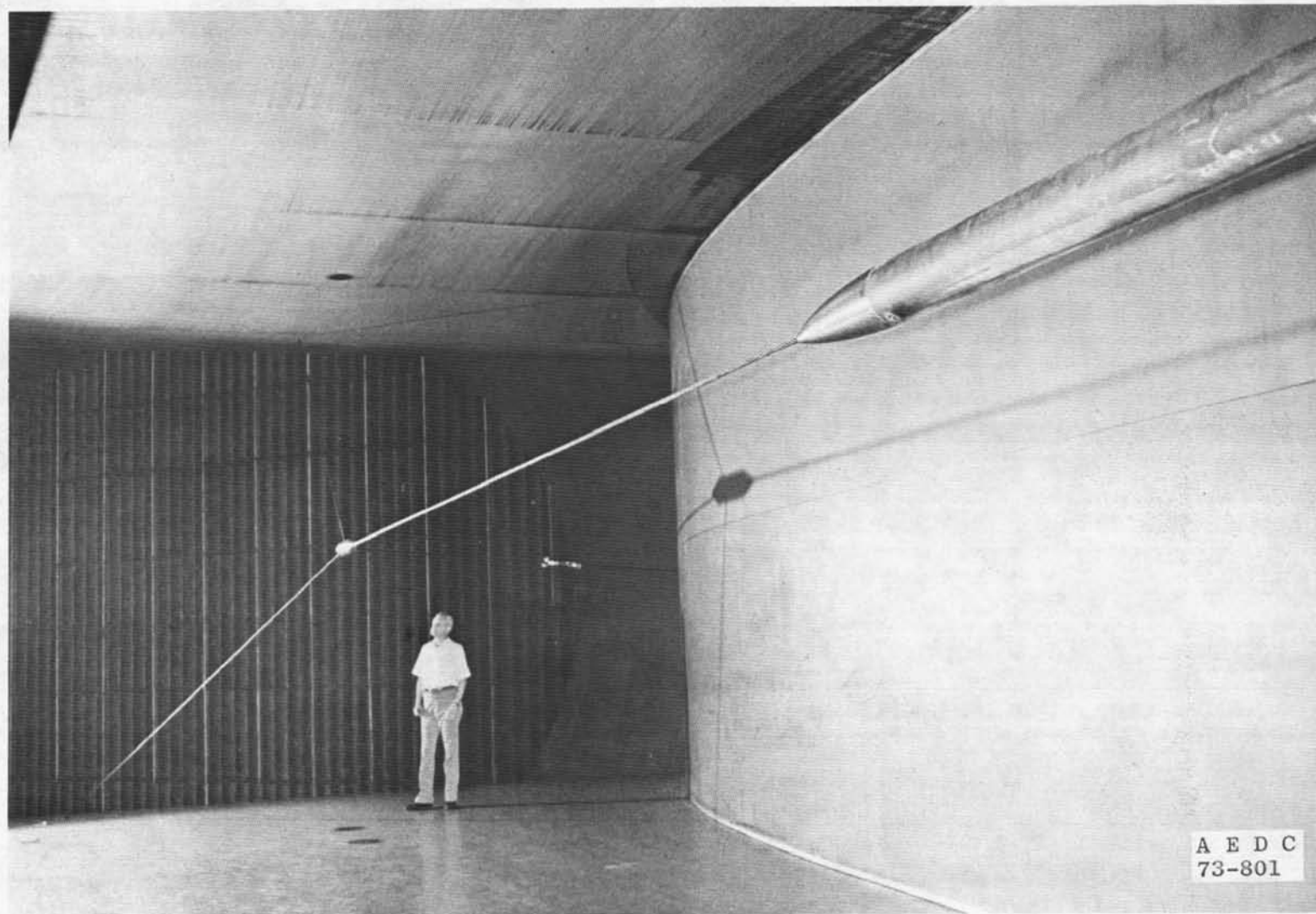
1. Jackson, F. M. "Calibration of the AEDC-PWT 16-Ft Transonic Tunnel at Test Section Wall Porosities of Two, Four, and Six Percent." AEDC-TR-76-13 (AD-B008985L), January 1976.
2. Gunn, J. A. "Check Calibration of the AEDC 16-Ft Transonic Tunnel." AEDC-TR-66-80 (AD633277), May 1966.
3. Aulehla, F. and Besigk, G. "Reynolds Number Effects on Fore- and Aft-Body Pressure Drag, II." AGAR-CPP-150 (Paper No. 12 for FDP/PEP Symposium at Rome). September 1974.
4. Test Facilities Handbook (Tenth Edition). "Propulsion Wind Tunnel Facility, Vol. 4." Arnold Engineering Development Center, Arnold Air Force Station, Tennessee, May 1974.
5. Nichols, James H. "Determination of Optimum Operating Parameters for the PWT 16-Ft Transonic Circuit Utilizing One-Percent Bodies of Revolution." AEDC-TN-59-100 (AD225362), September 1959.
6. Jackson, F. M. "Supplemental Calibration Results for the AEDC Propulsion Wind Tunnel (16T)." AEDC-TR-70-163 (AD872475), August 1970.
7. Dick, R. S. "Calibration of the 16-Ft Transonic Circuit of the Propulsion Wind Tunnel with an Aerodynamic Test Cart Having 6-percent-Open Inclined-Hole Walls." AEDC-TN-58-90 (AD204846), November 1958.



a. Schematic of test installation
Figure 1. Tunnel 16T centerline pipe installation.



b. Pipe, main supporting cables, and rear mount
Figure 1. Continued.



c. Pipe and forward cable system
Figure 1. Concluded.

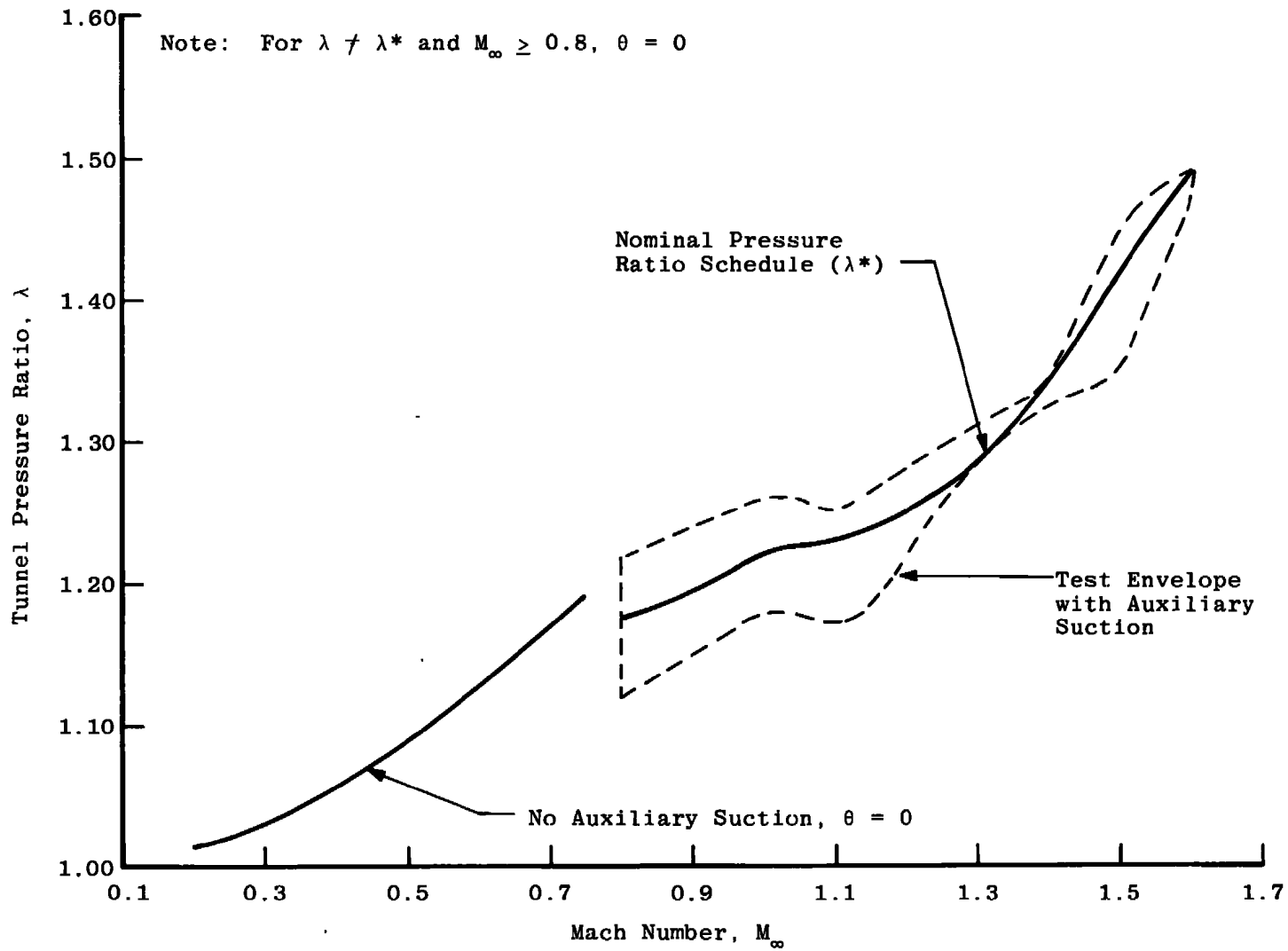


Figure 2. Variation of tunnel pressure ratio.

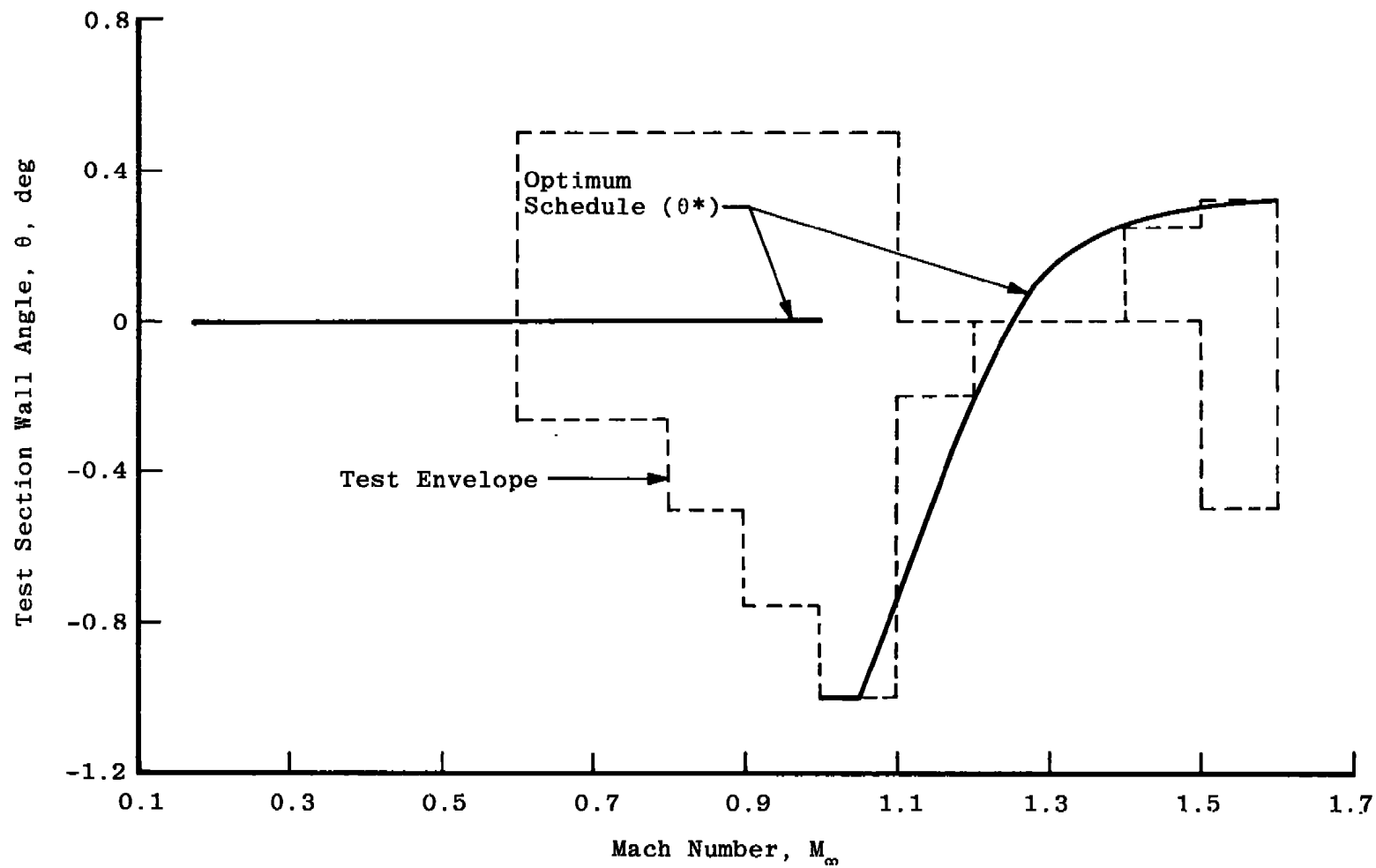


Figure 3. Variation of test section wall angle.

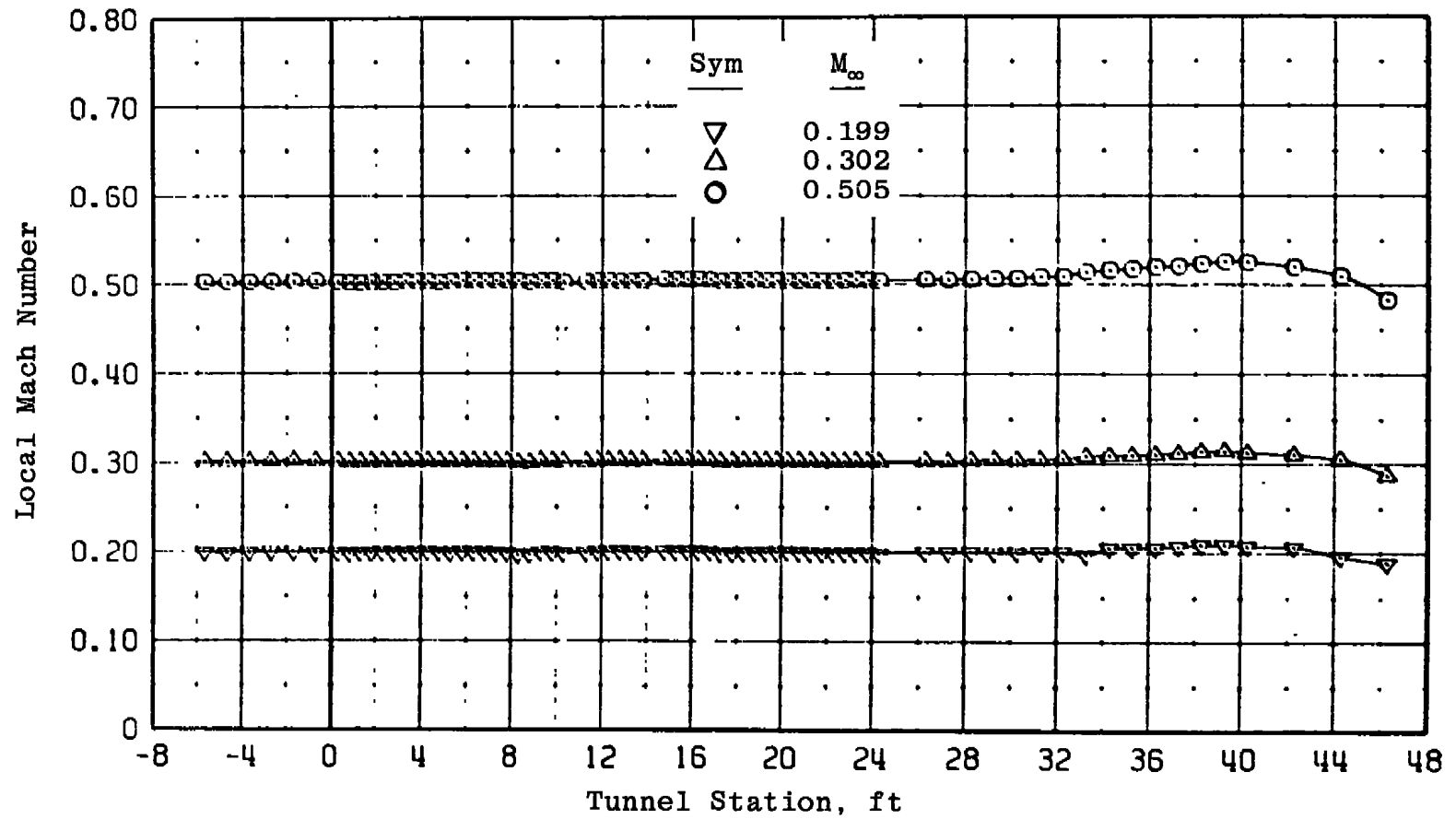
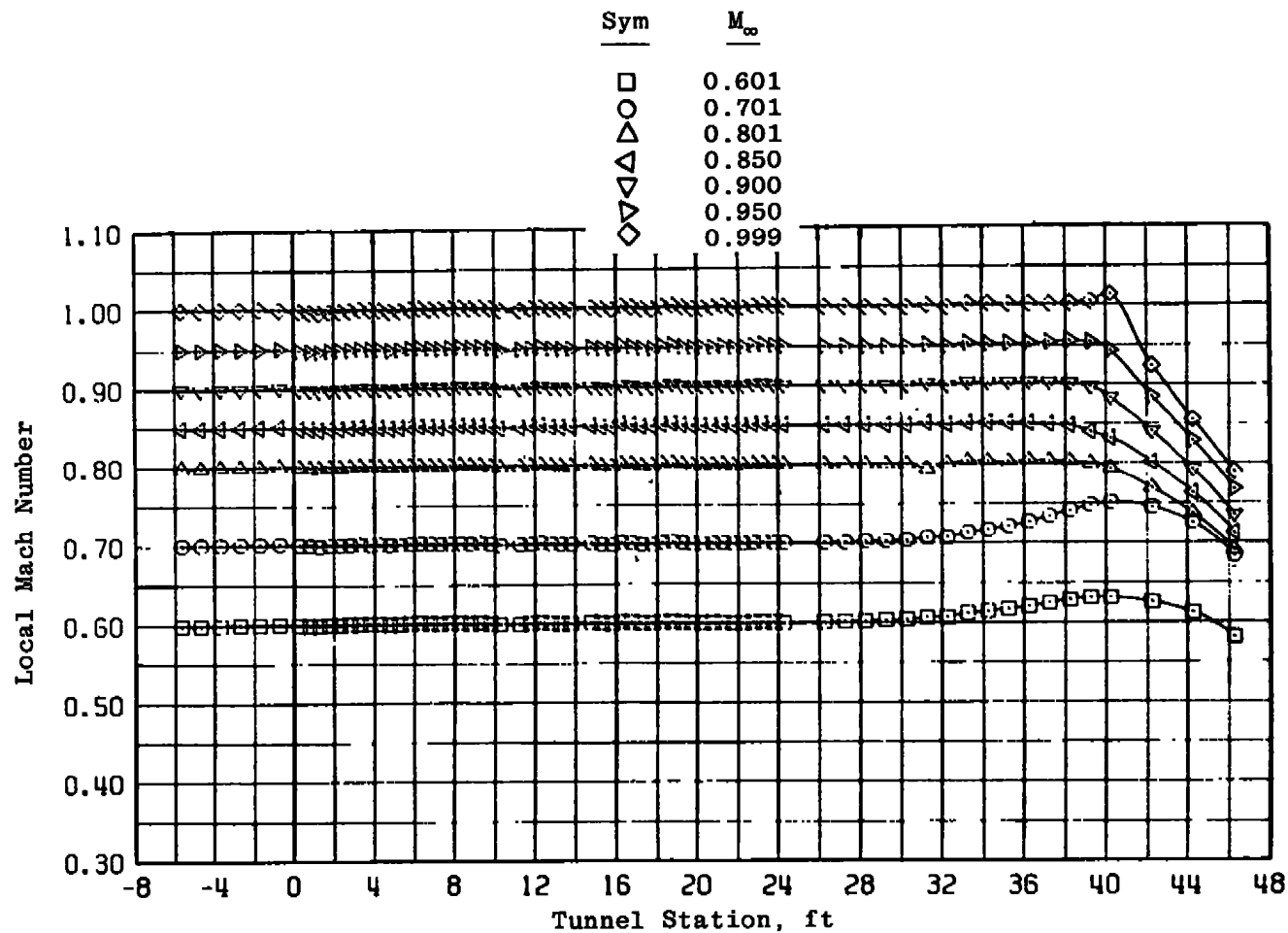
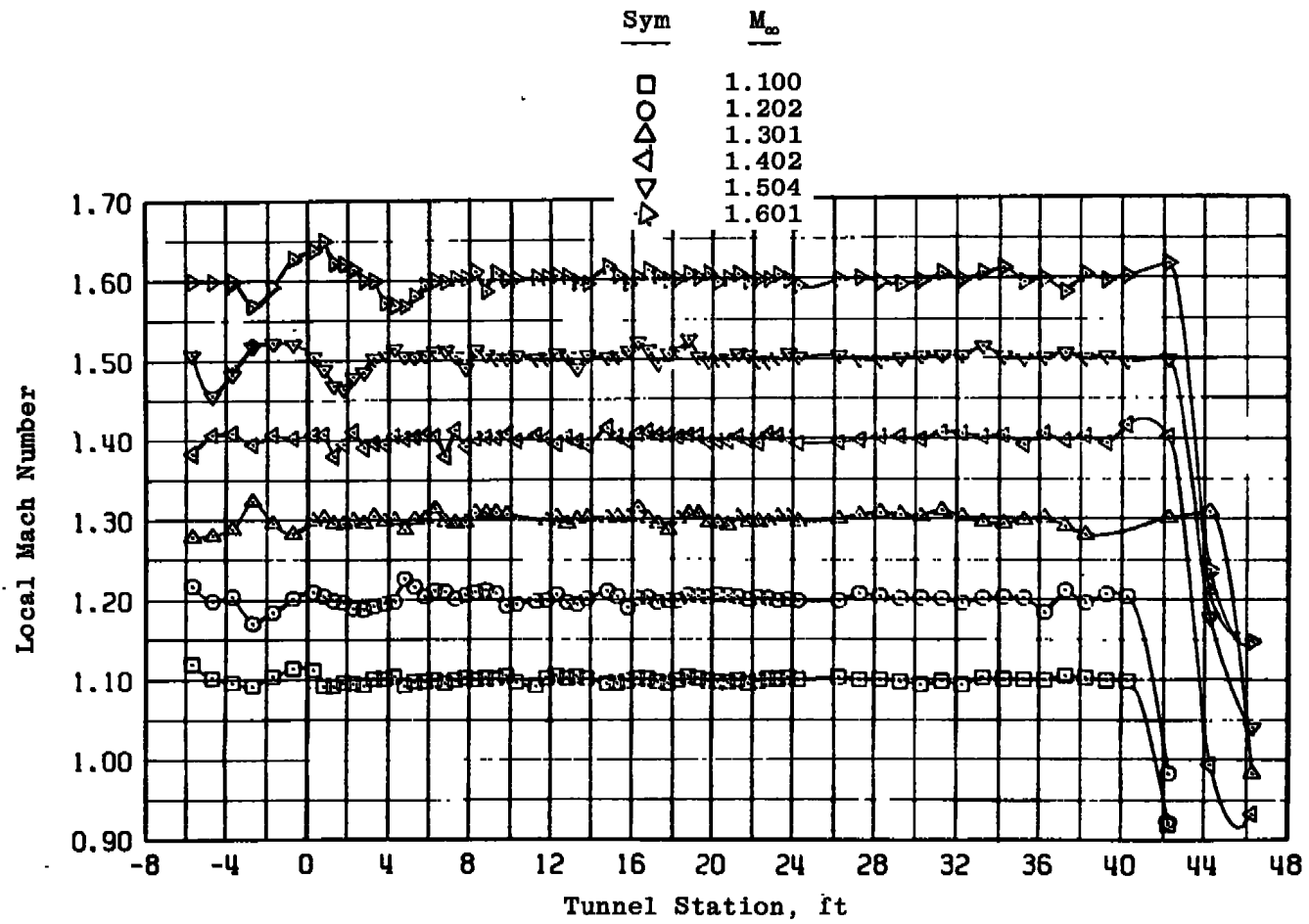


Figure 4. Tunnel 16T centerline Mach number distributions at $M_\infty = 0.2$ to 0.5 with $\lambda = \lambda^*$, $\theta = 0$, and $P_t \cong 1,200$ psfa.

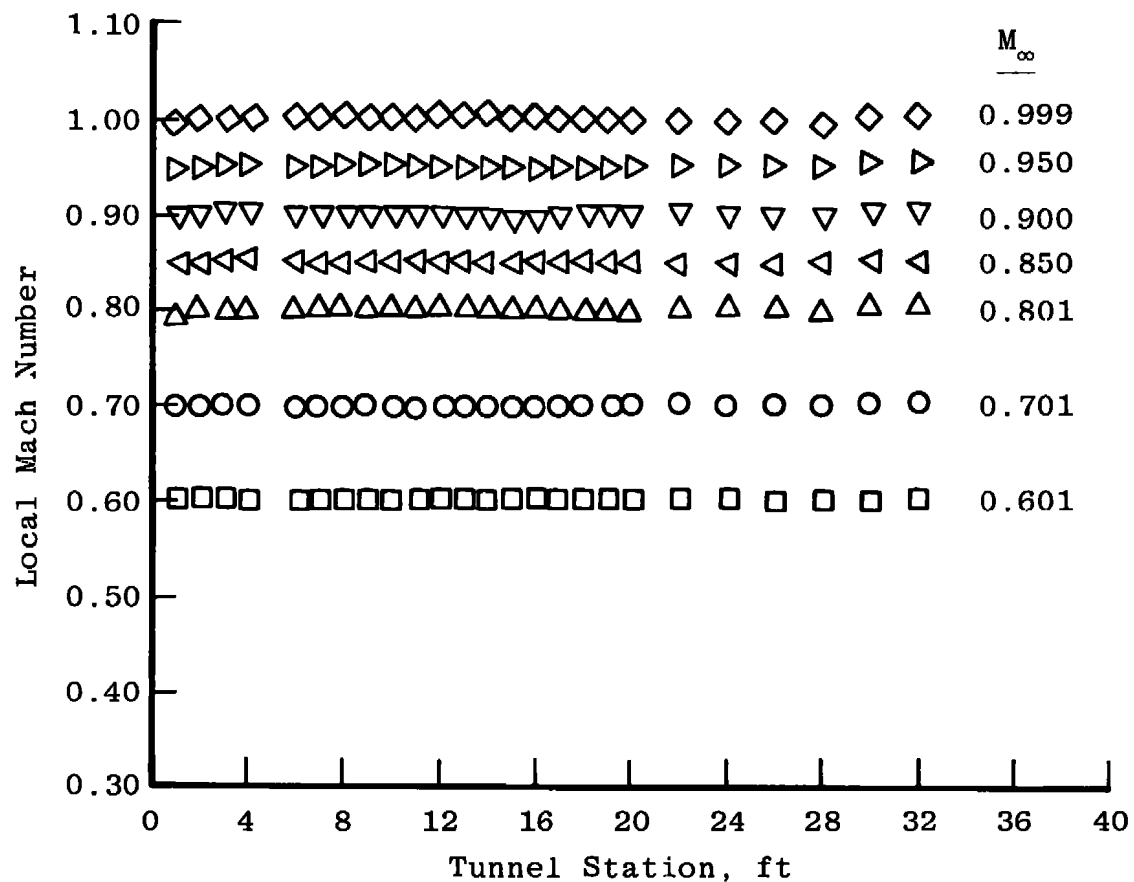


a. $M_\infty = 0.6$ to 1.0

Figure 5. Tunnel 16T centerline Mach number distributions with $\lambda = \lambda^*$, $\theta = 0$, and $P_t \approx 1,600$ psfa.

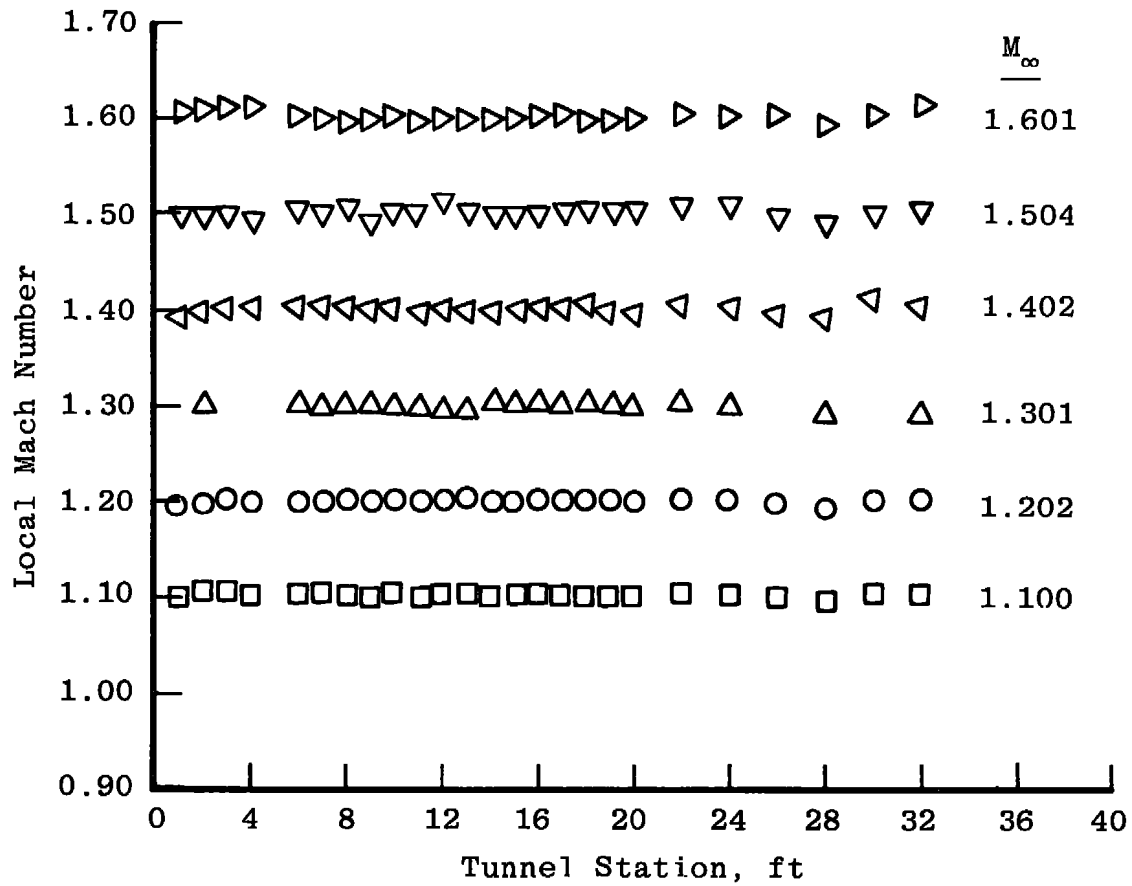


b. $M_\infty = 1.1$ to 1.6
Figure 5. Concluded.

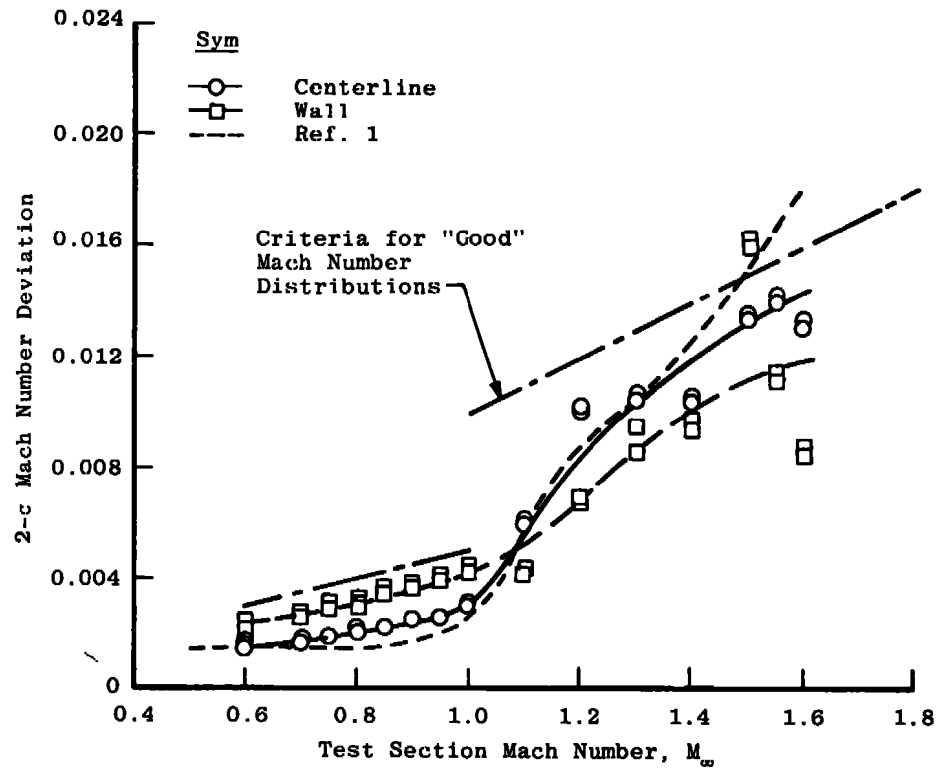


a. $M_\infty = 0.6$ to 1.0

Figure 6. Tunnel 16T wall Mach number distributions with $\lambda = \lambda^*$, $\theta = 0$, and $P_t \cong 1,600$ psfa.

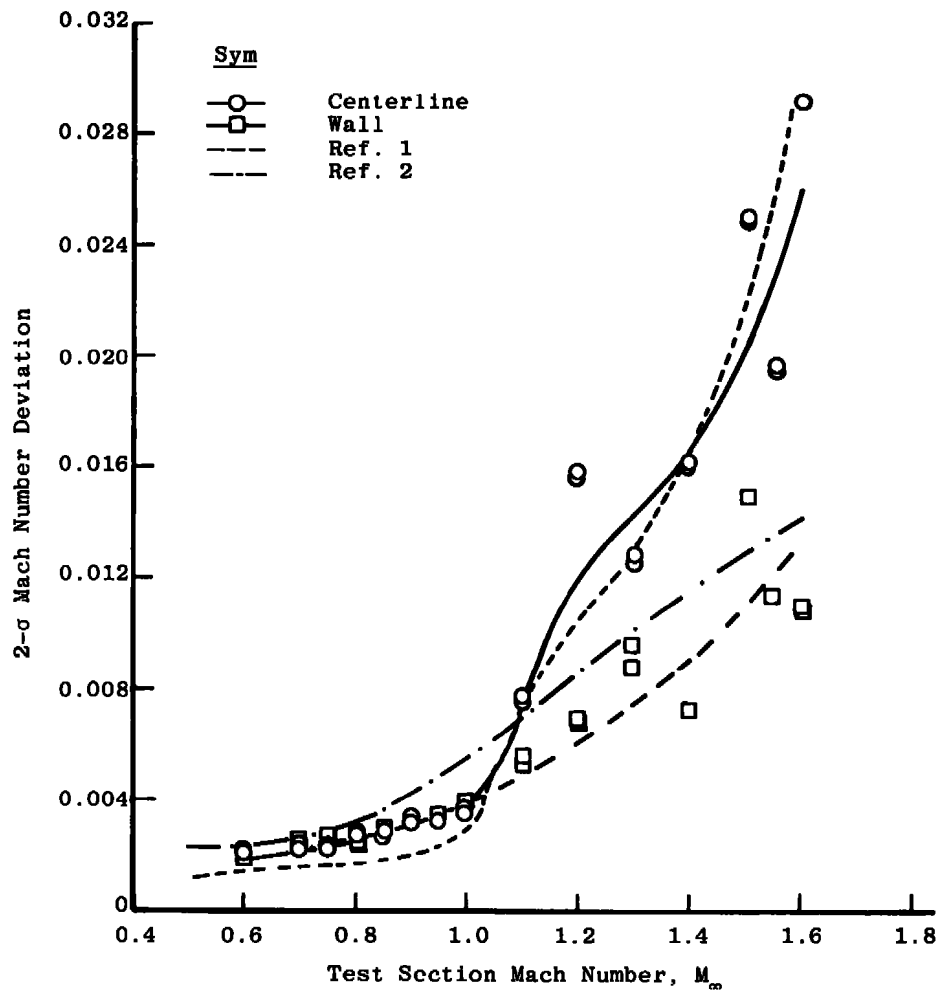


b. $M_\infty = 1.1$ to 1.6
Figure 6. Concluded.

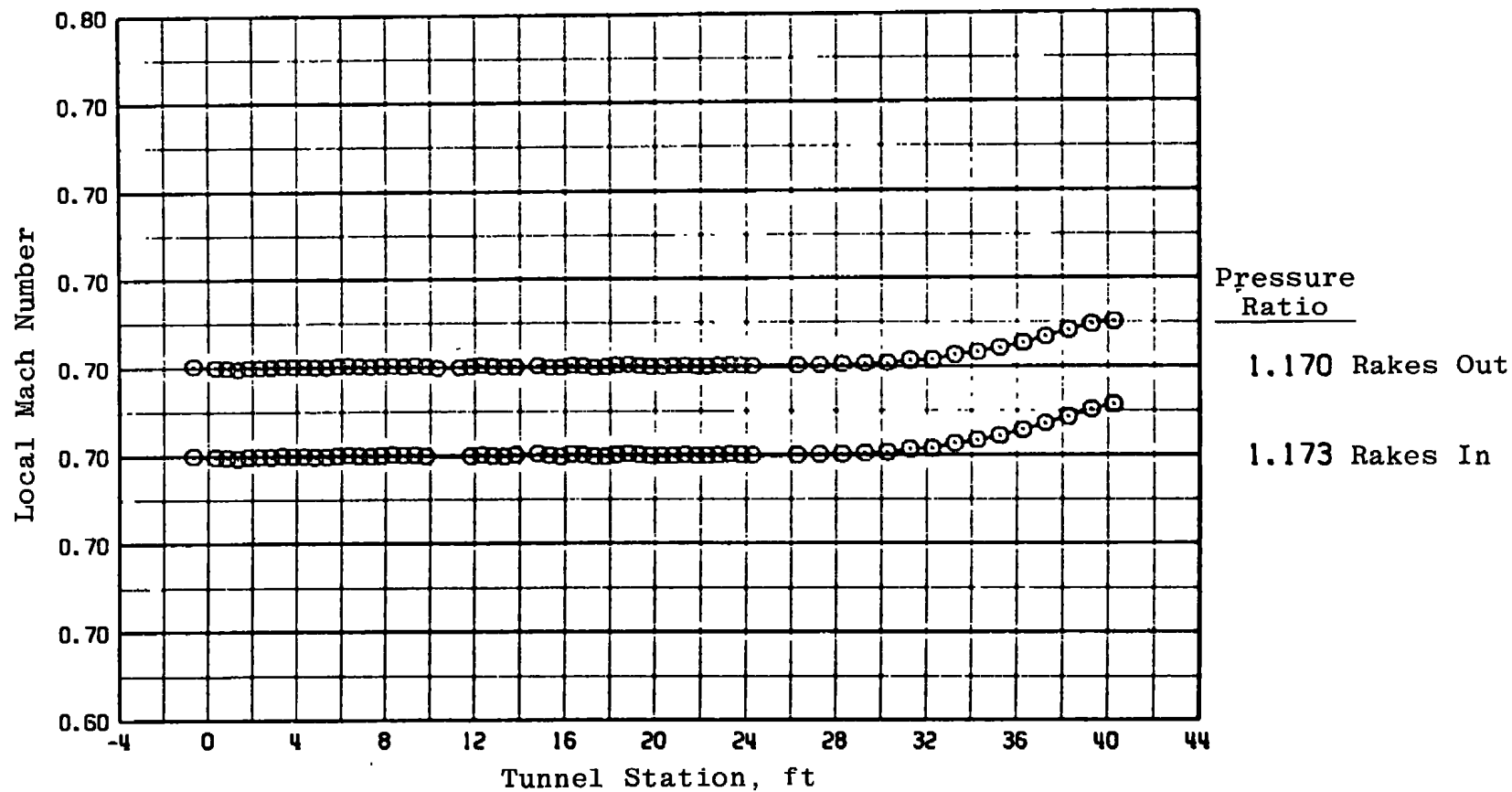


a. Tunnel Stations 8 to 28

Figure 7. Effect of Mach number on the Mach number deviations with $\lambda = \lambda^*$, $\theta = 0$, and $P_t \cong 1,600$ psfa.



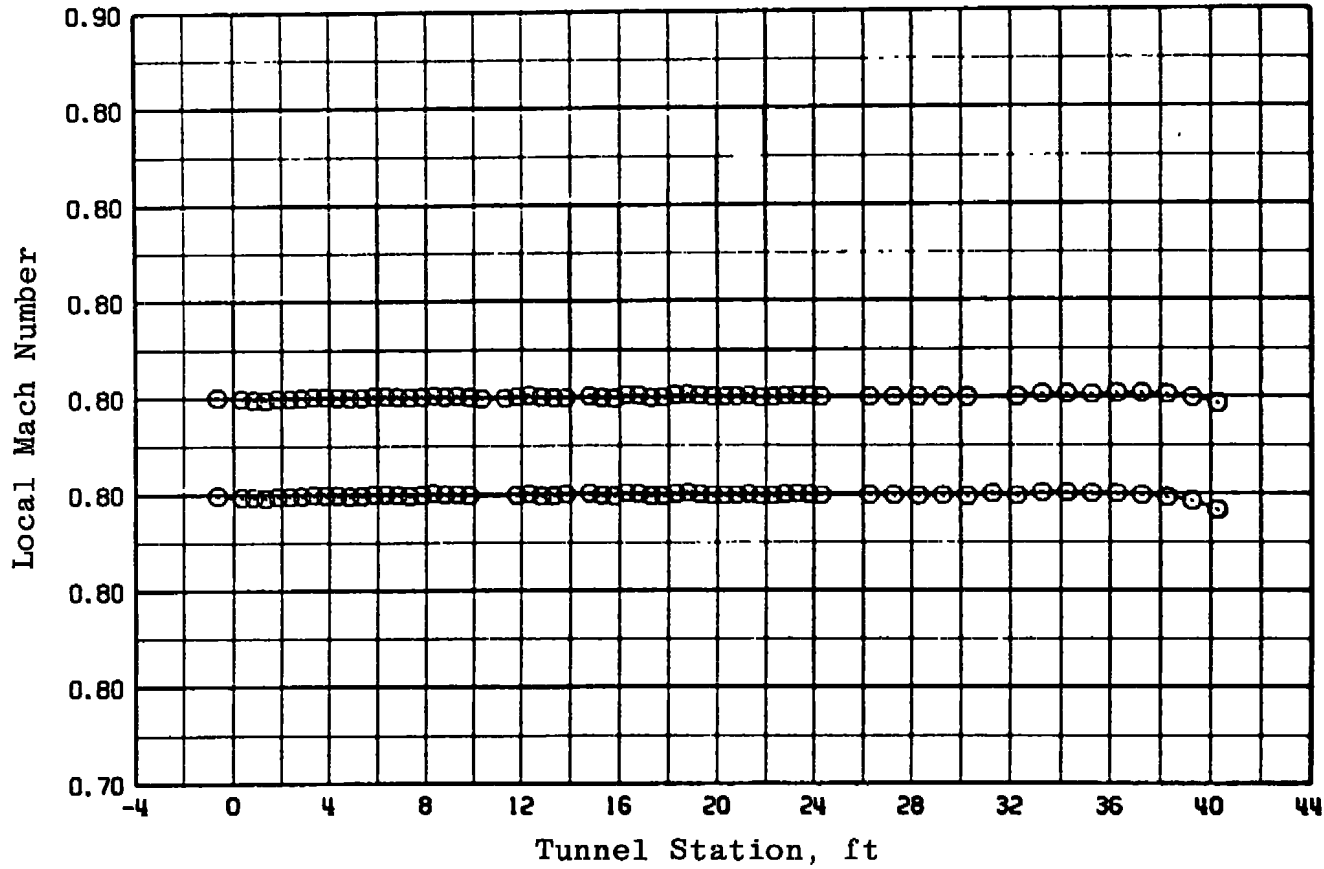
b. Tunnel Stations 1 to 20
Figure 7. Concluded.



a. $M_\infty = 0.70$

Figure 8. Effect of boundary-layer rakes on centerline Mach number distributions with $\theta = 0$, $\lambda = \lambda^*$, and $P_t = 1,600$ psfa.

38

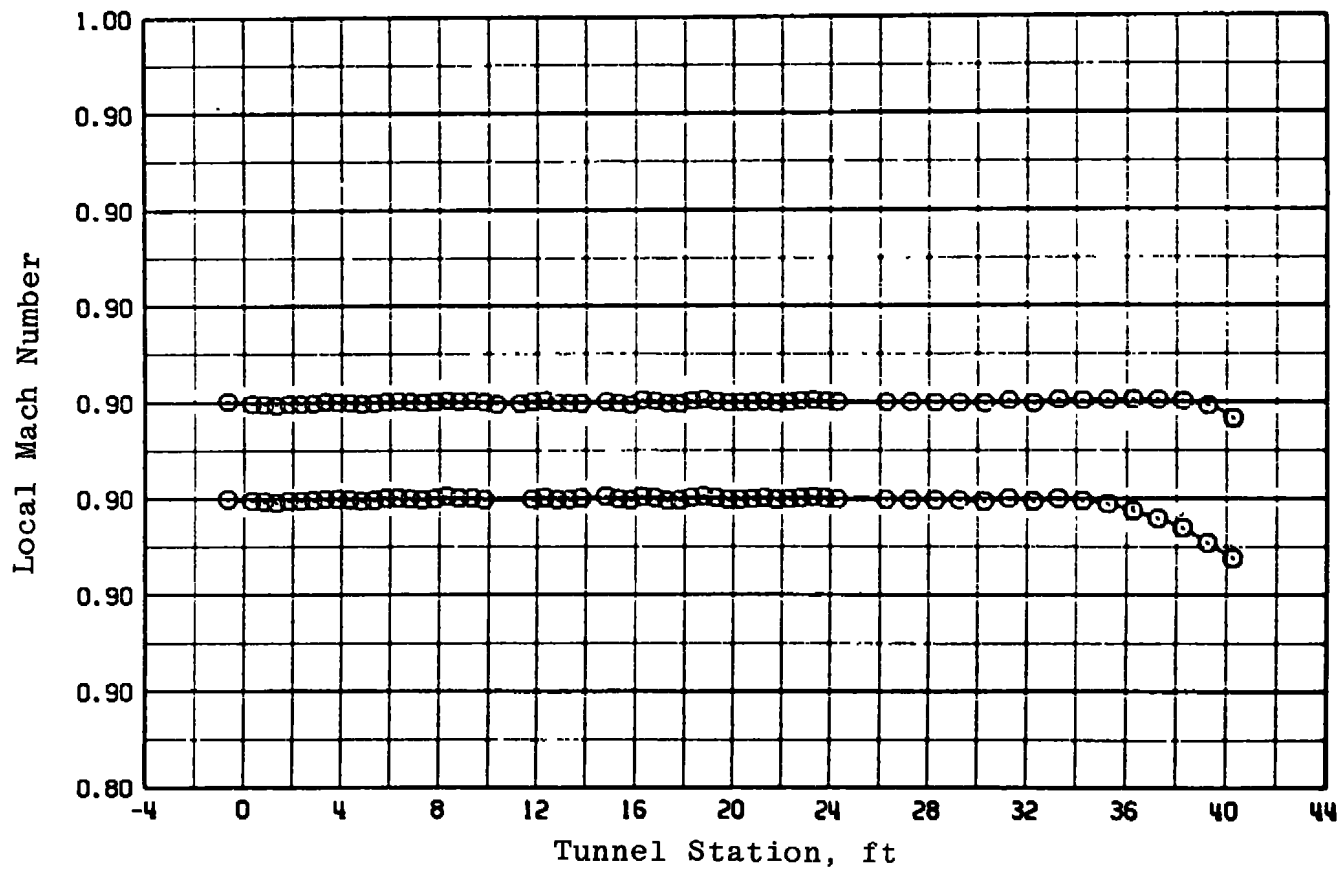


Pressure
Ratio

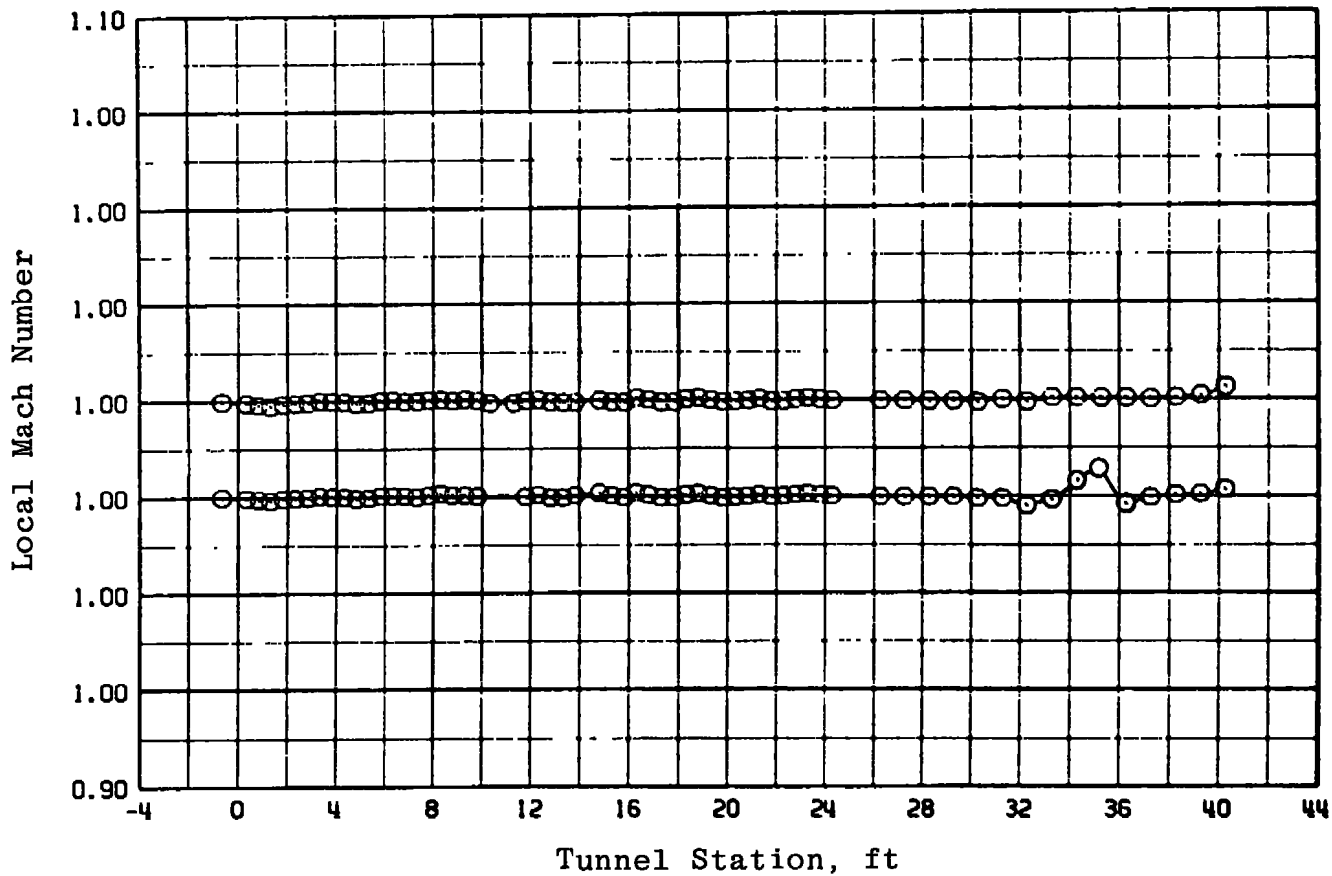
1.174 Rakes Out

1.176 Rakes In

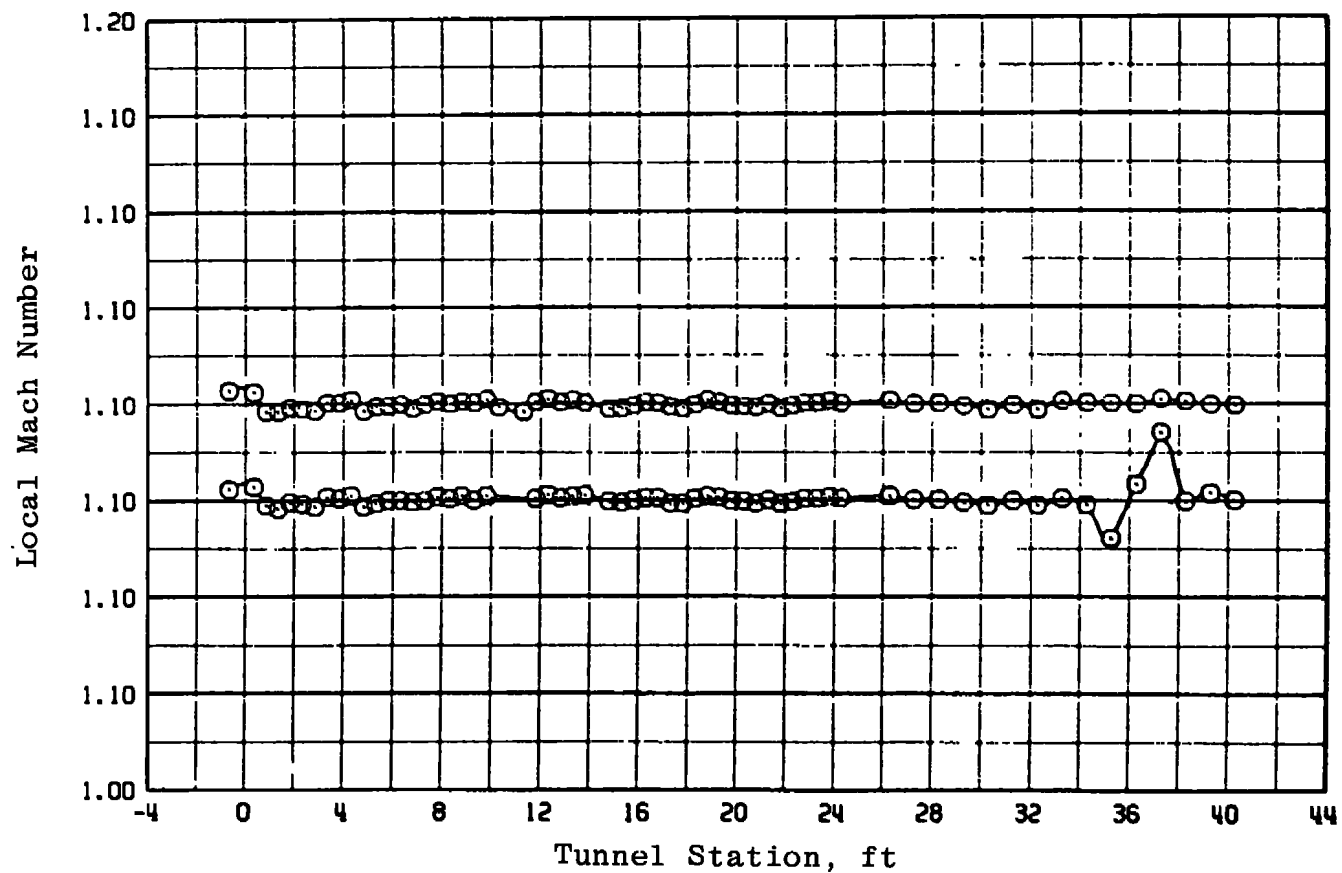
b. $M_{\infty} = 0.80$
Figure 8. Continued.



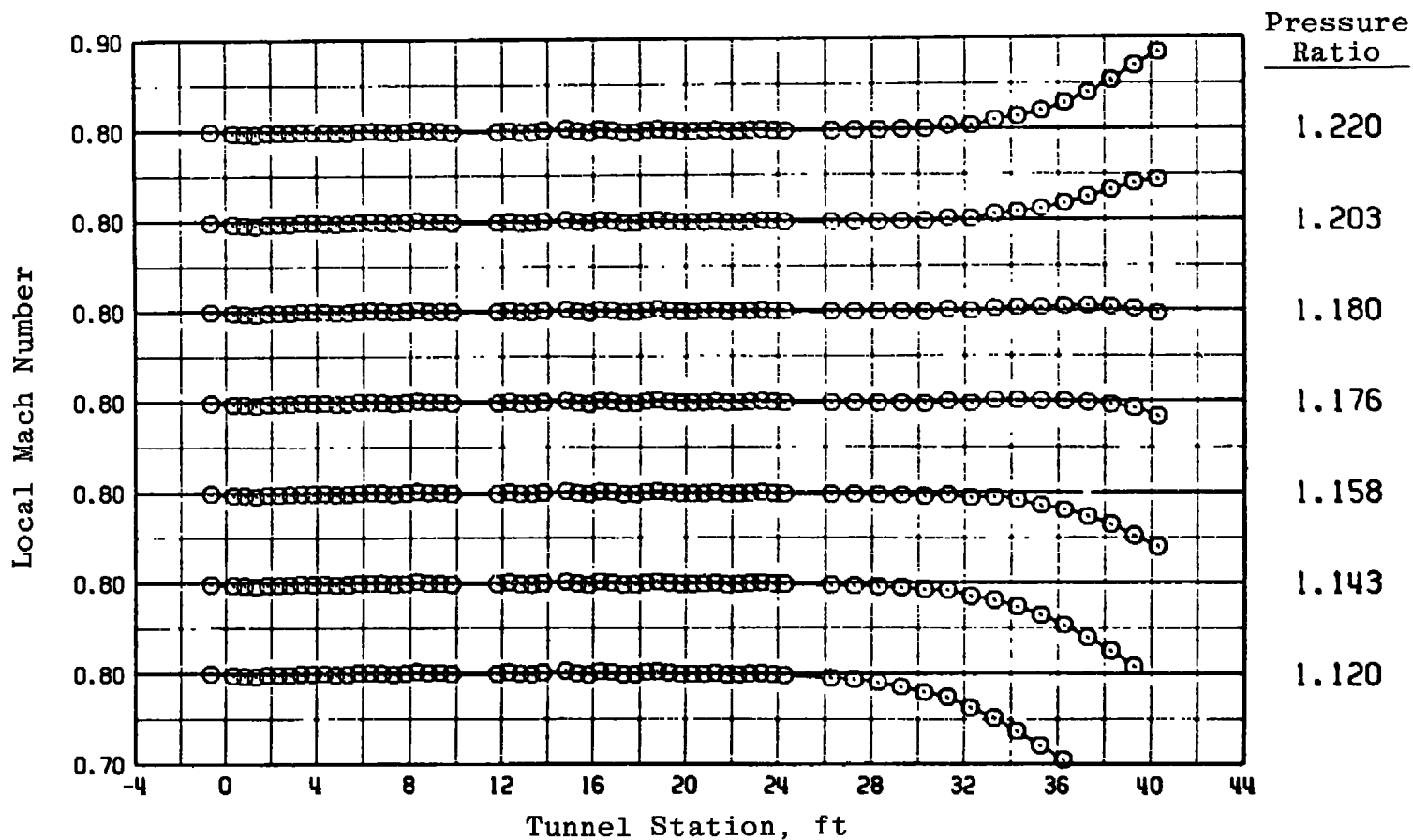
c. $M_{\infty} = 0.90$
Figure 8. Continued.



d. $M_\infty = 1.0$
Figure 8. Continued.

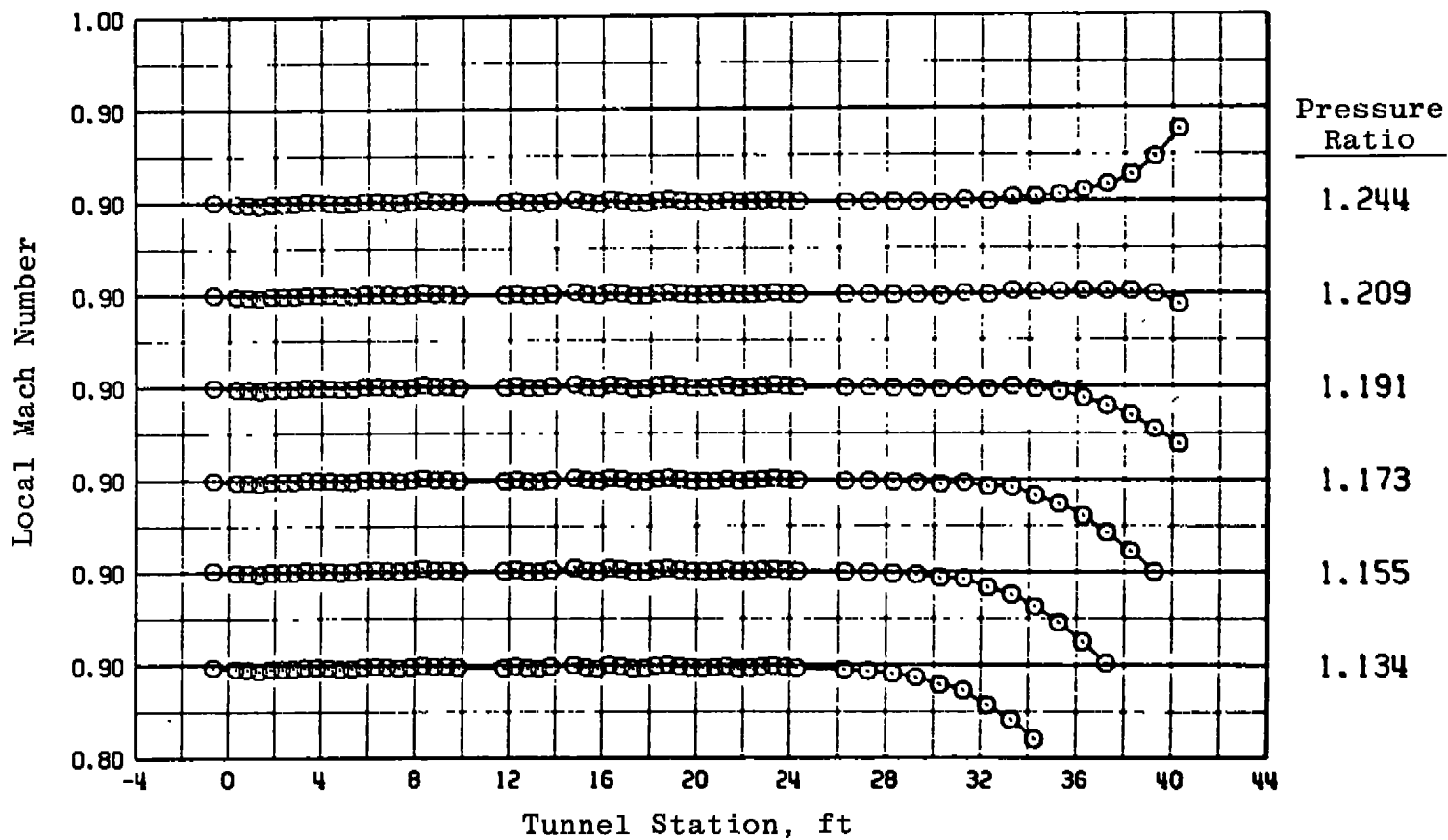


e. $M_\infty = 1.10$
Figure 8. Concluded.

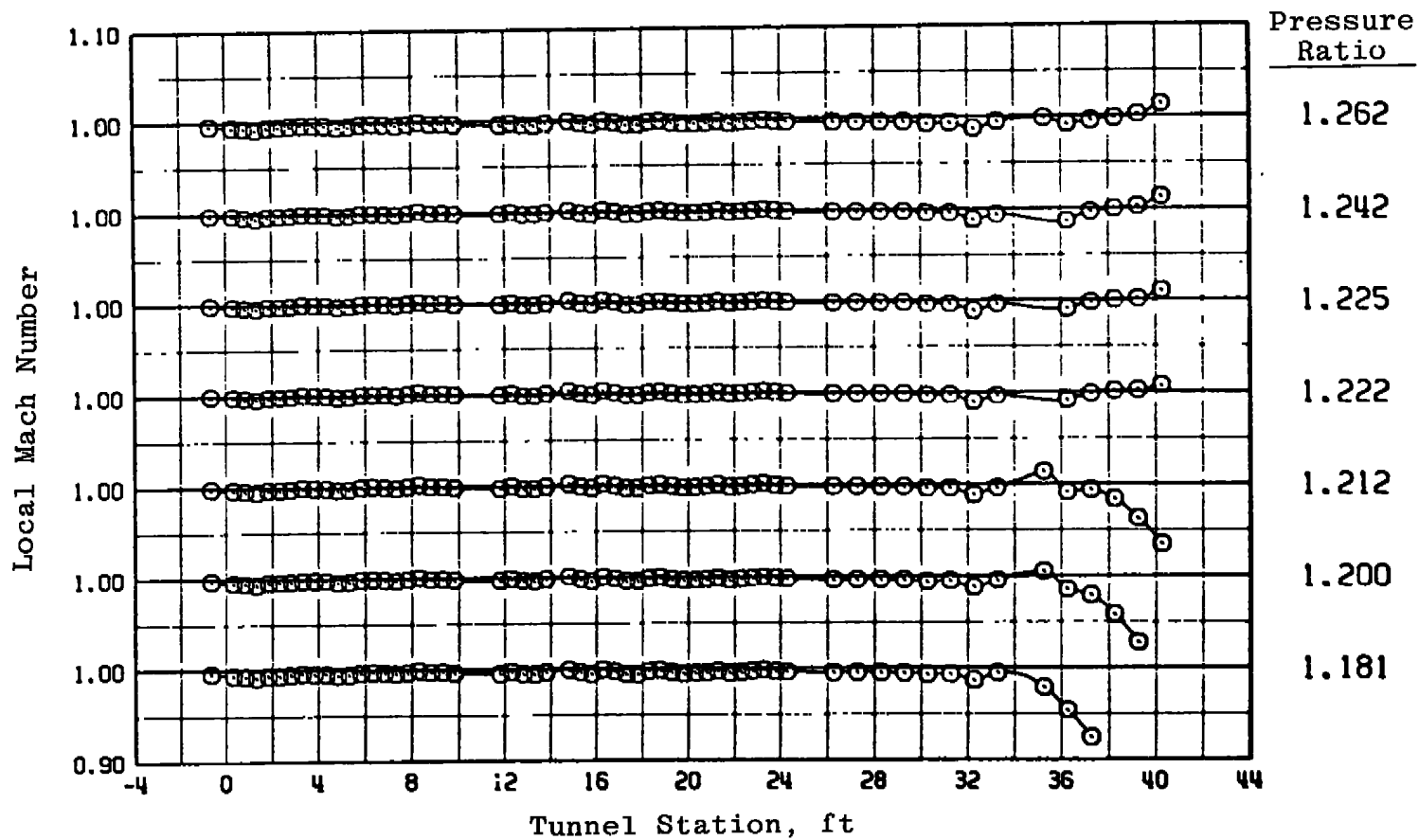


a. $M_{\infty} = 0.80$

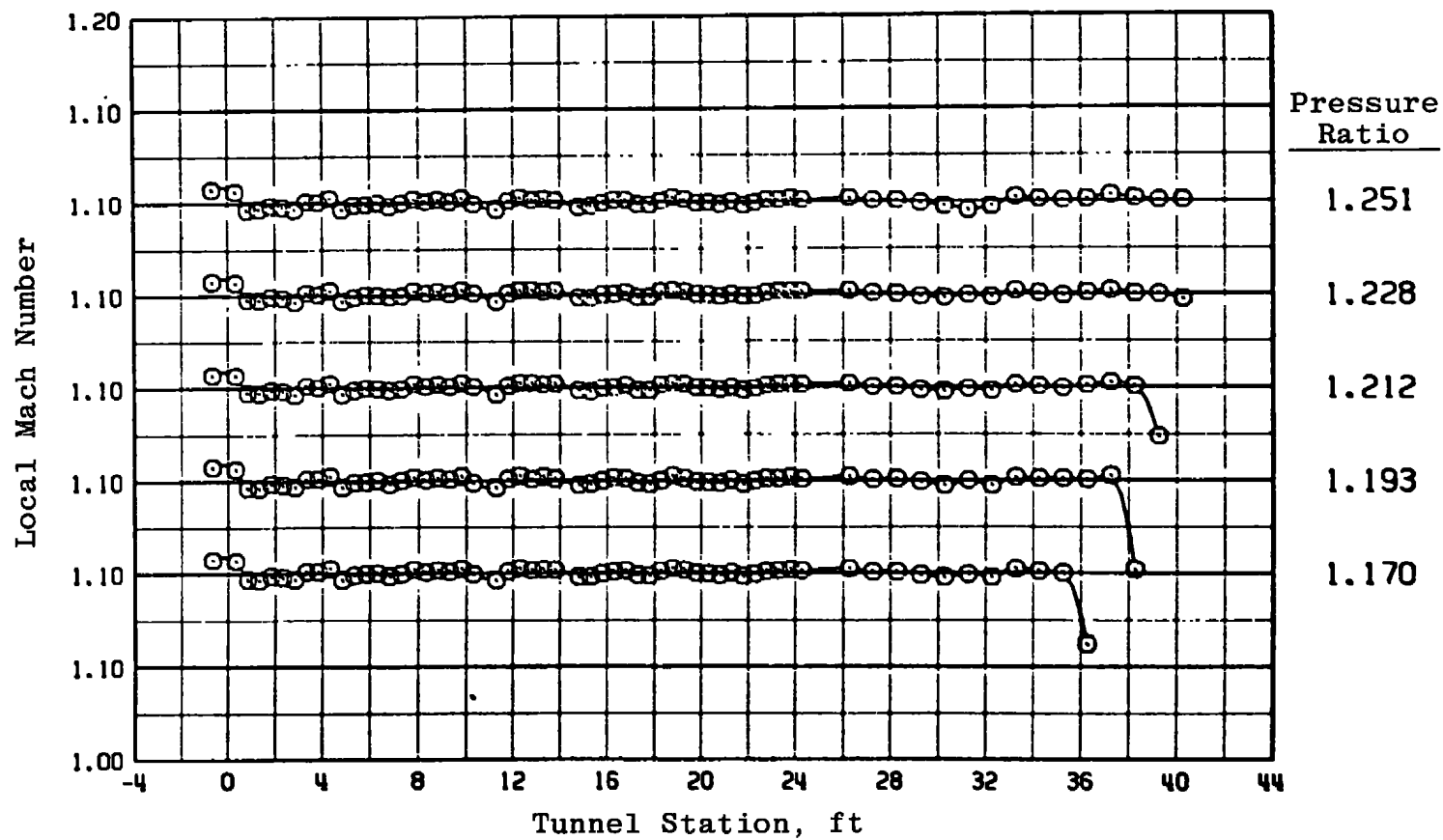
Figure 9. Tunnel 16T centerline Mach number distributions for various tunnel pressure ratios with $\theta = 0$ and $P_t = 1,600$ psfa.



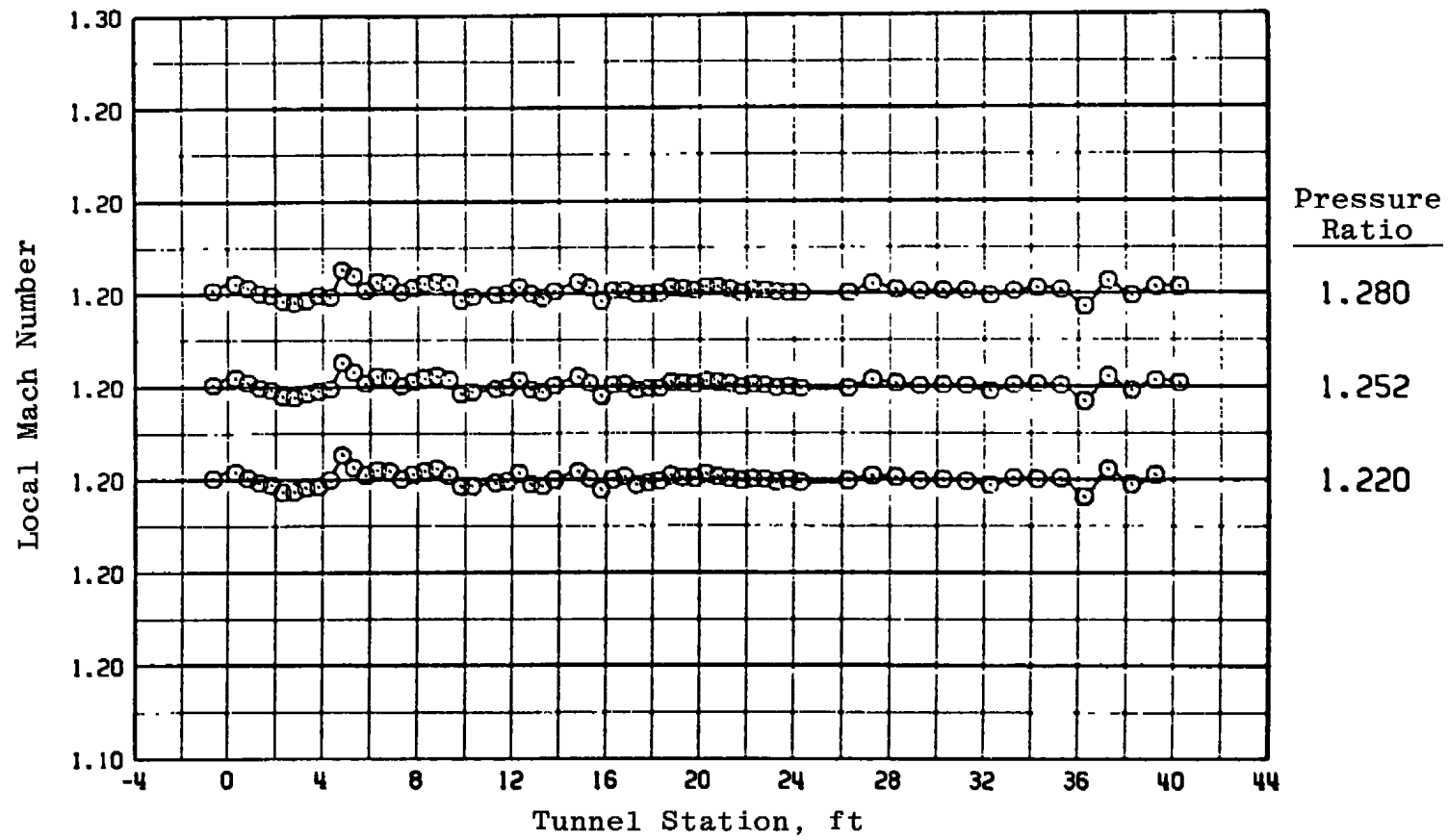
b. $M_\infty = 0.90$
Figure 9. Continued.



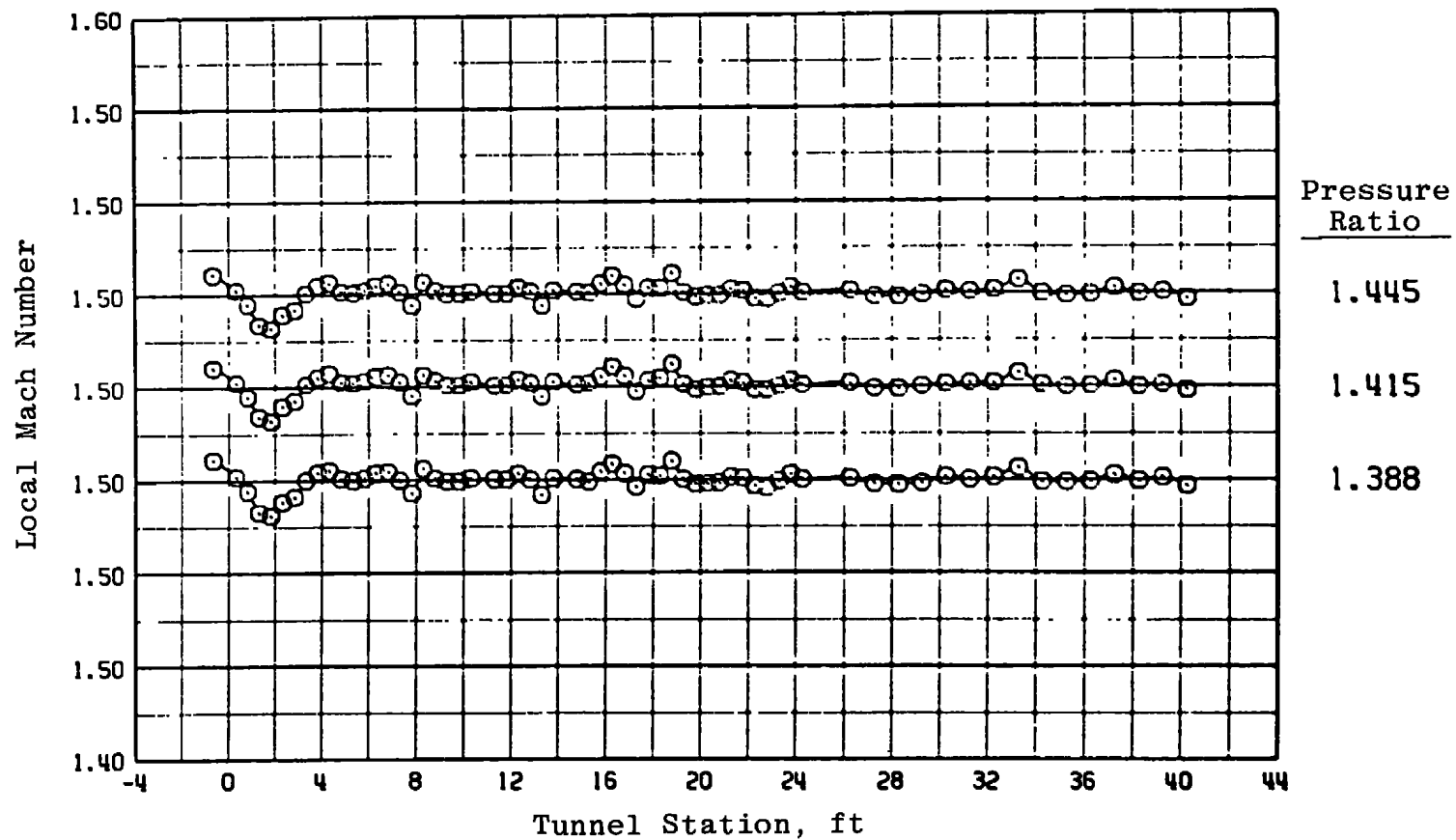
c. $M_{\infty} = 1.0$
Figure 9. Continued.



d. $M_{\infty} = 1.10$
Figure 9. Continued.



e. $M_\infty = 1.20$
Figure 9. Continued.



f. $M_{\infty} = 1.50$
Figure 9. Concluded.

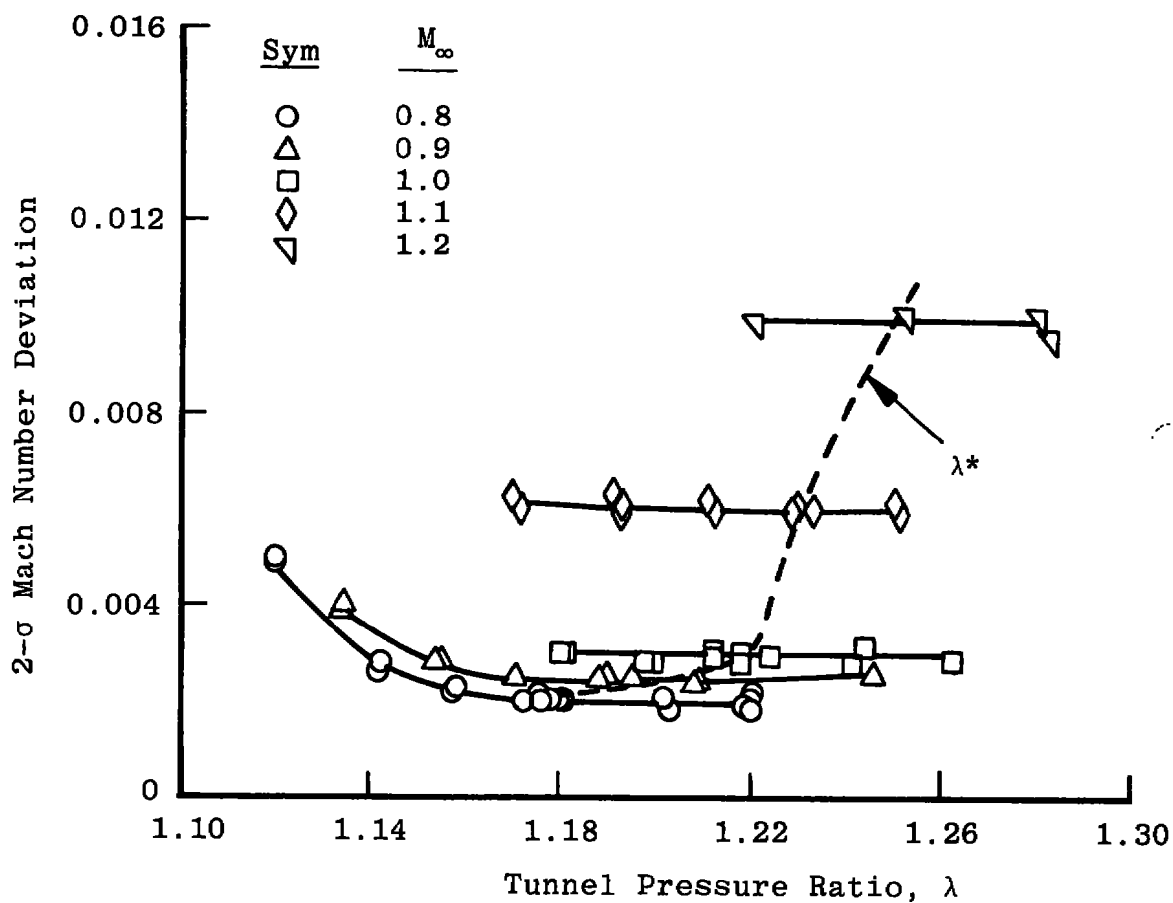


Figure 10. Effect of tunnel pressure ratio variation on the 2σ Mach number deviations for Tunnel Stations 8 to 28 with $\theta = 0$ and $P_t = 1,600$ psfa.

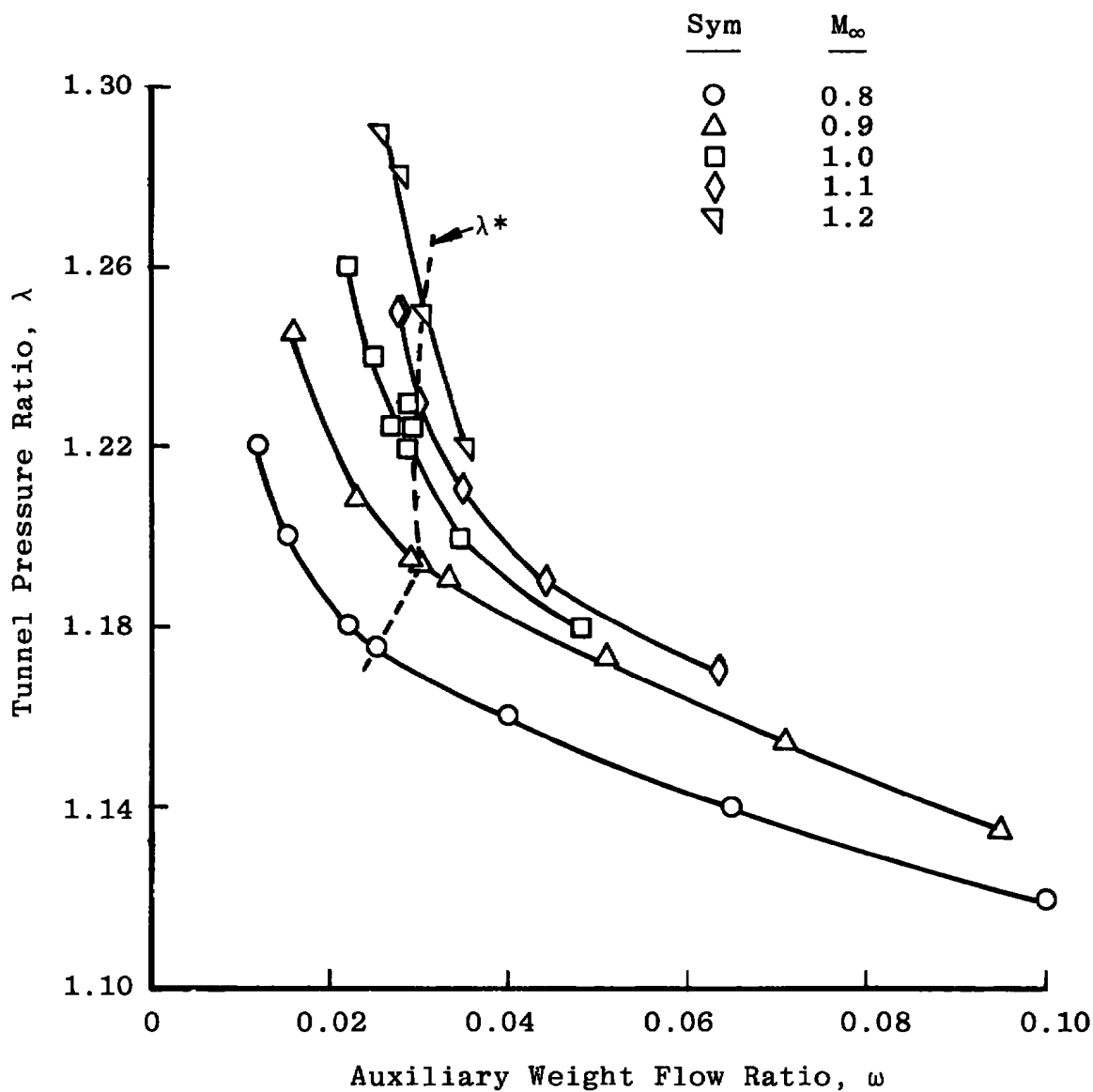


Figure 11. Effect of pressure ratio variation on auxiliary flow requirements with $\theta = 0$ and $P_t = 1,600$ psfa.

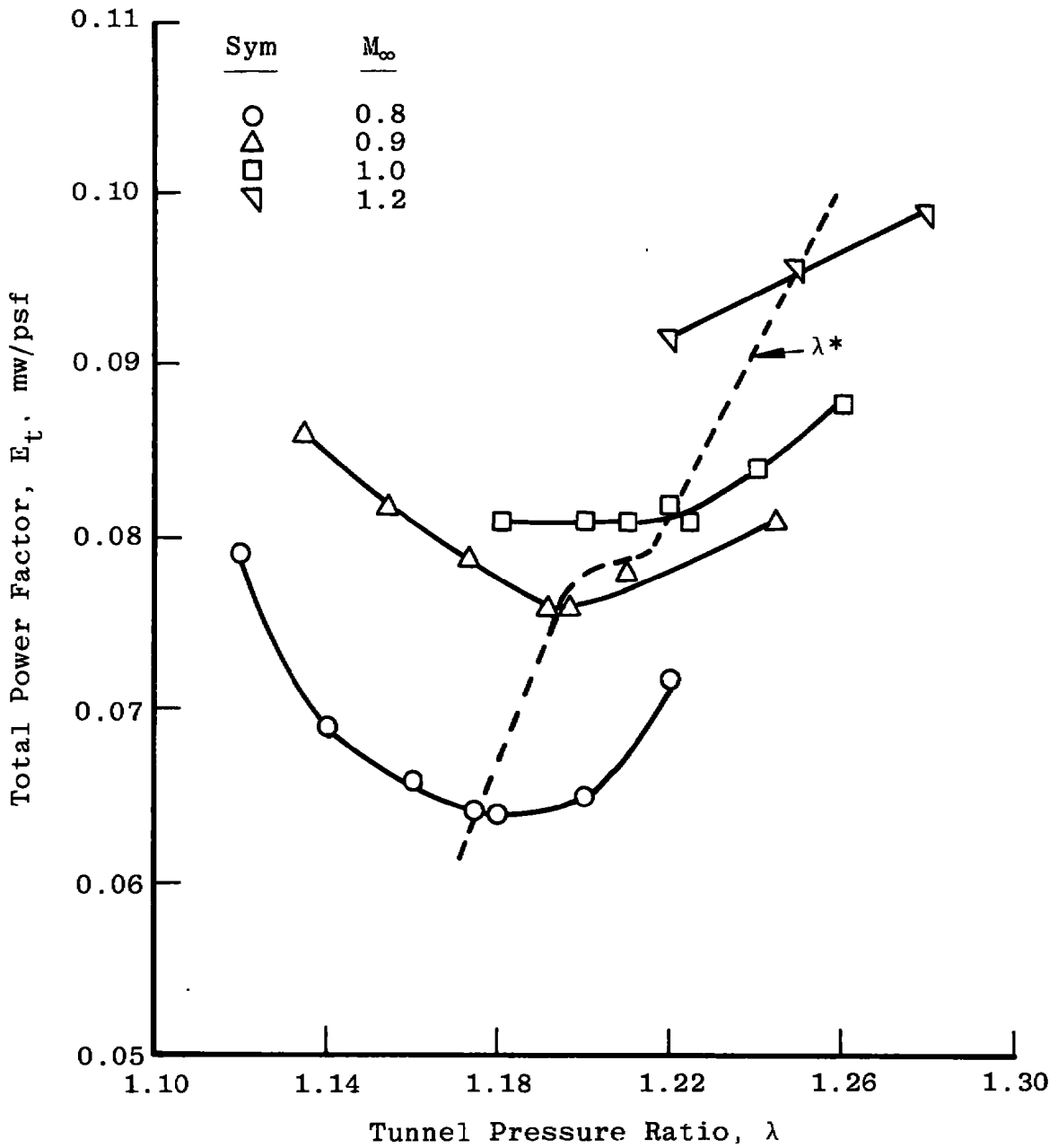


Figure 12. Effect of pressure ratio variation on tunnel total power requirements with $\theta = 0$ and $P_t = 1,600$ psfa.

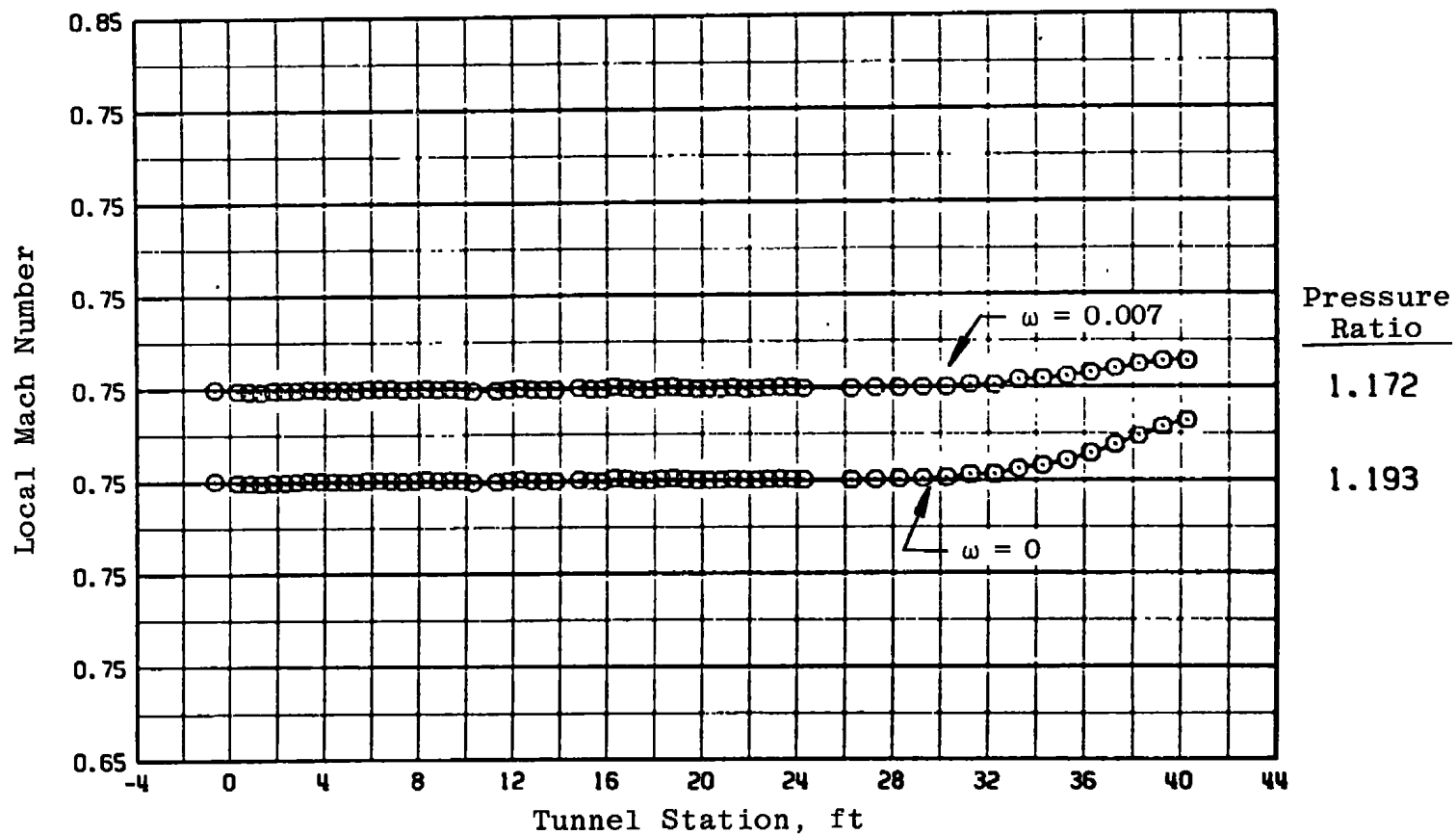
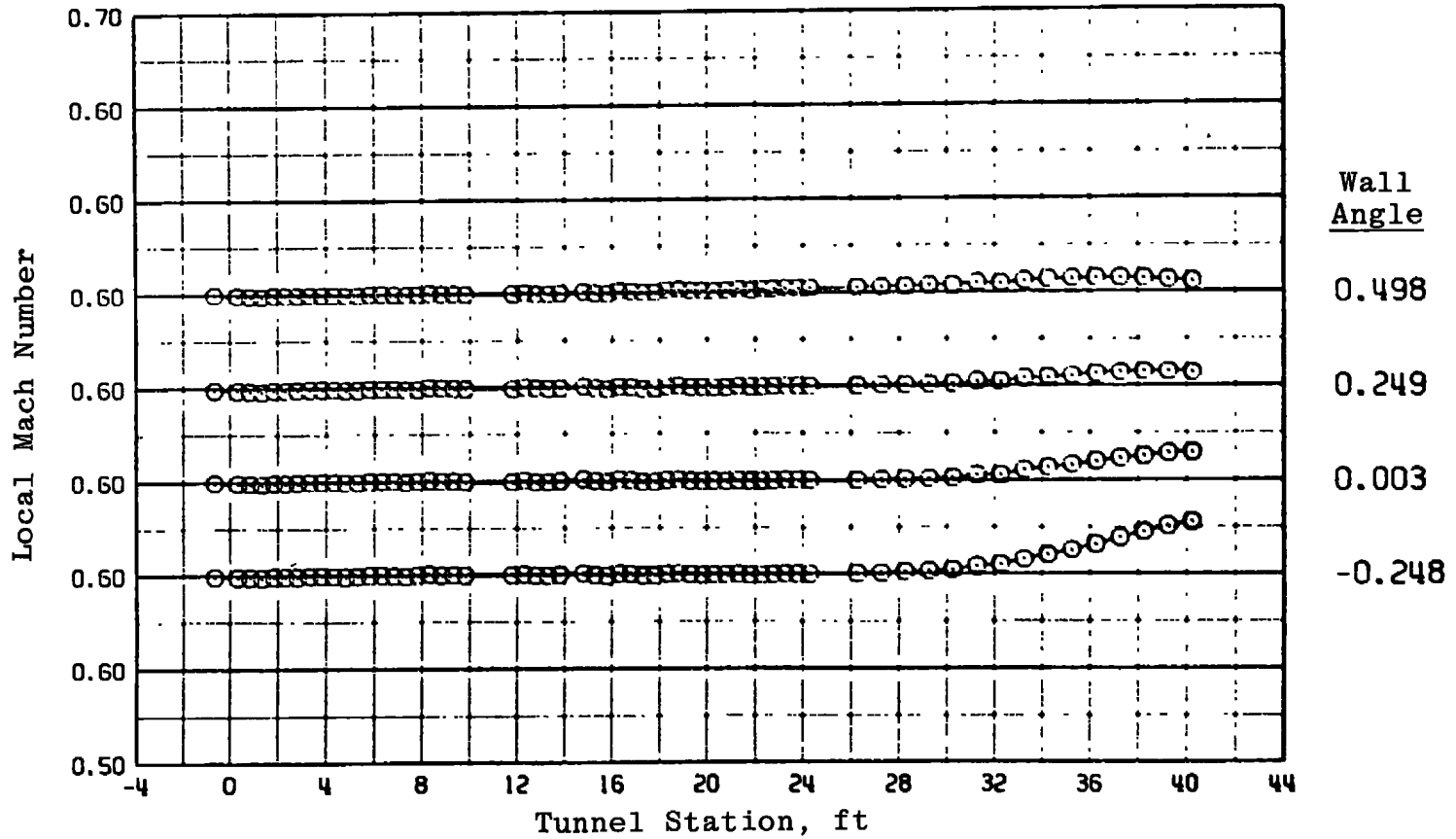
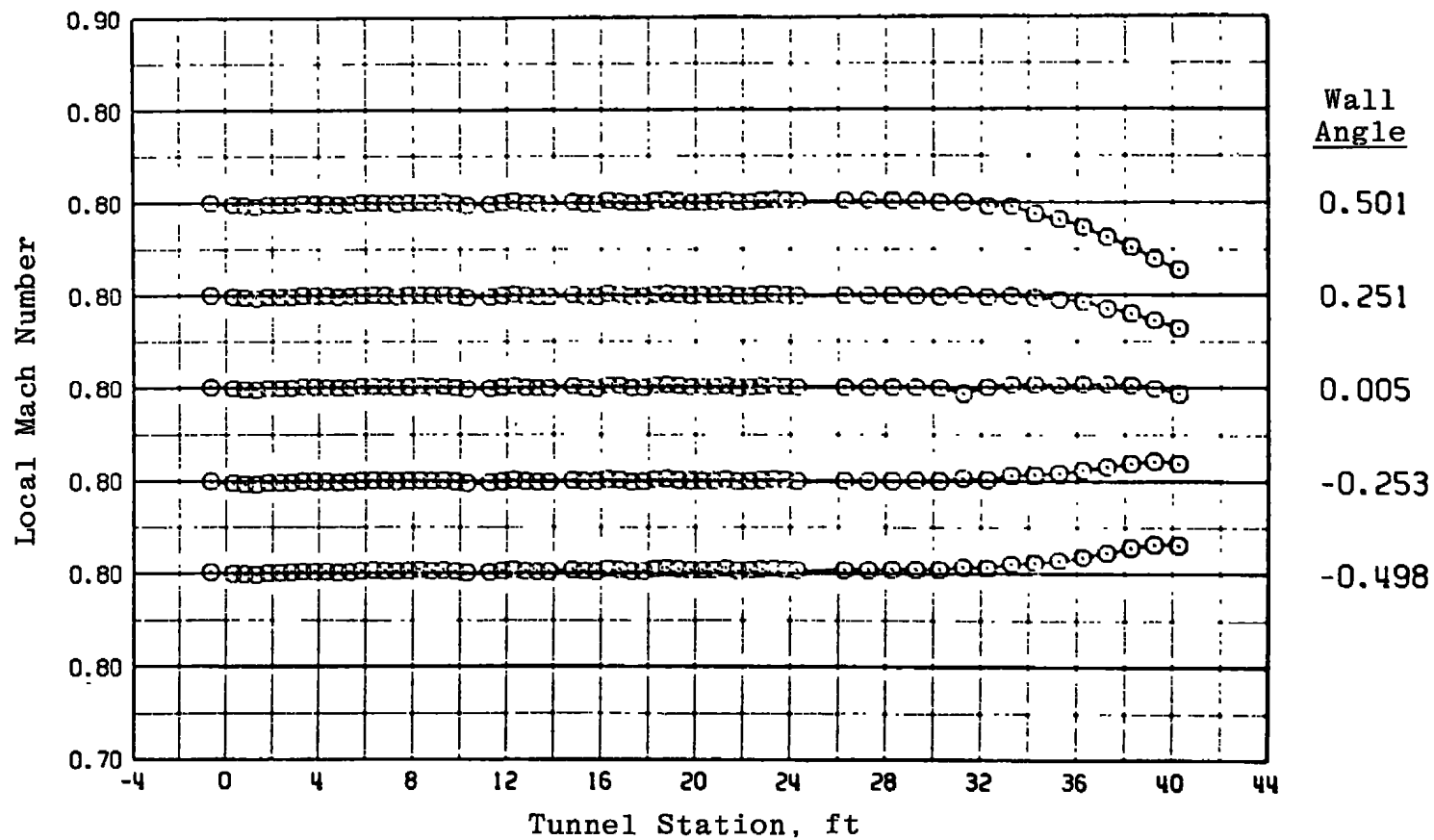


Figure 13. Effect of auxiliary flow utilization at $M_\infty = 0.75$, $\theta = 0$ and $P_t = 1,600$ psfa.

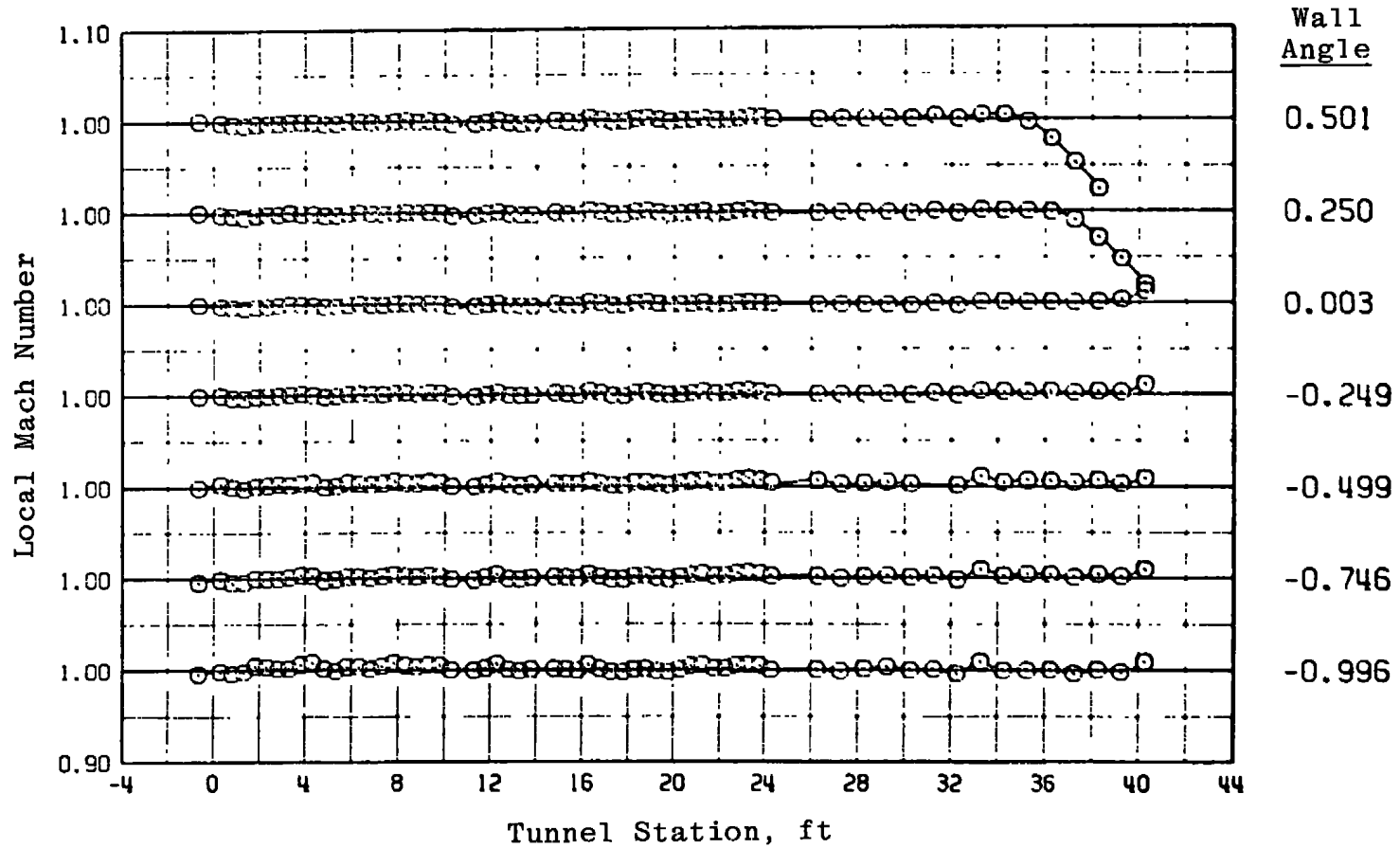


a. $M_{\infty} = 0.6$

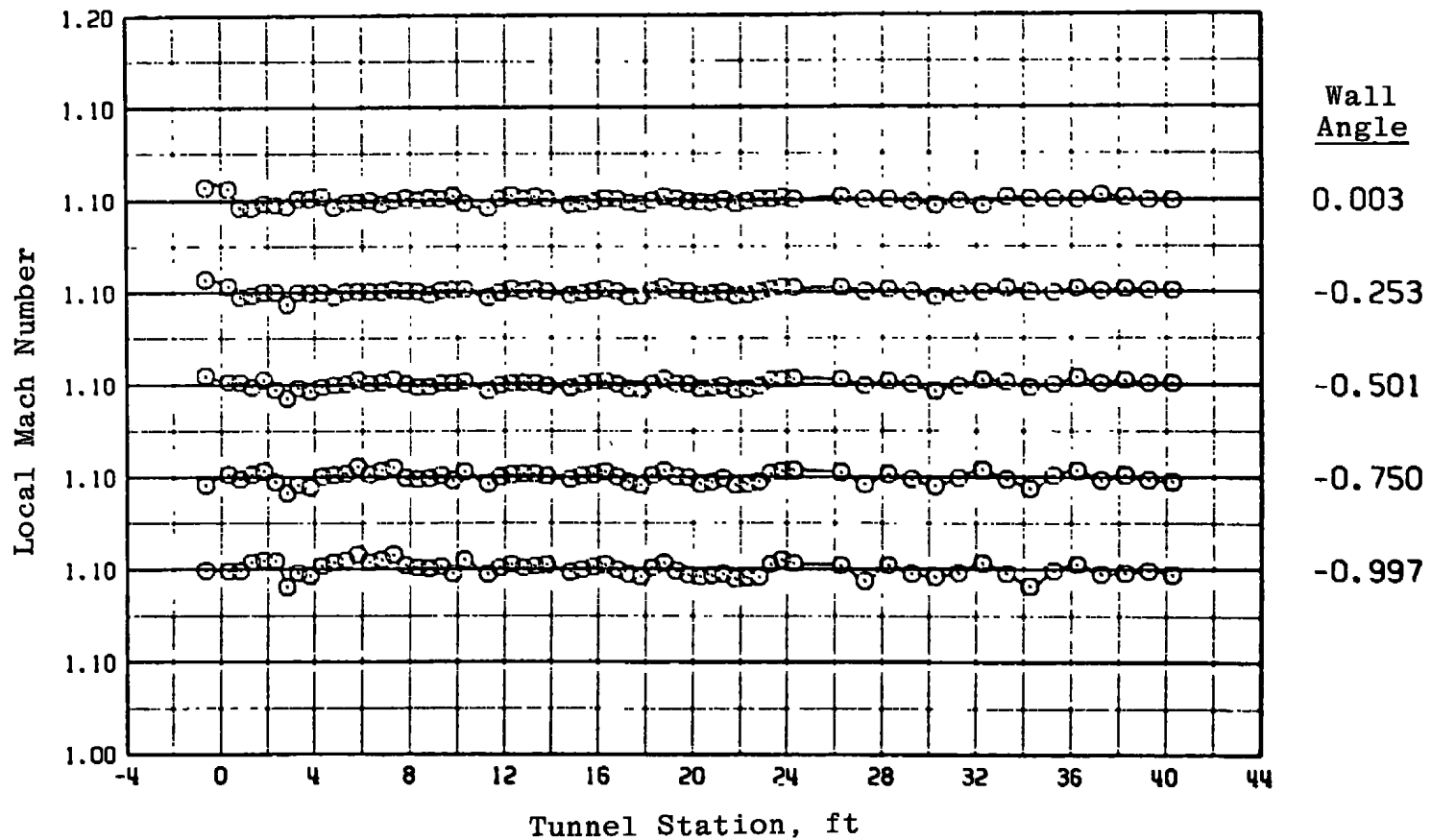
Figure 14. Tunnel 16T centerline Mach number distributions for various test section wall angles with $\lambda = \lambda^*$ and $P_t = 1,600$ psfa.



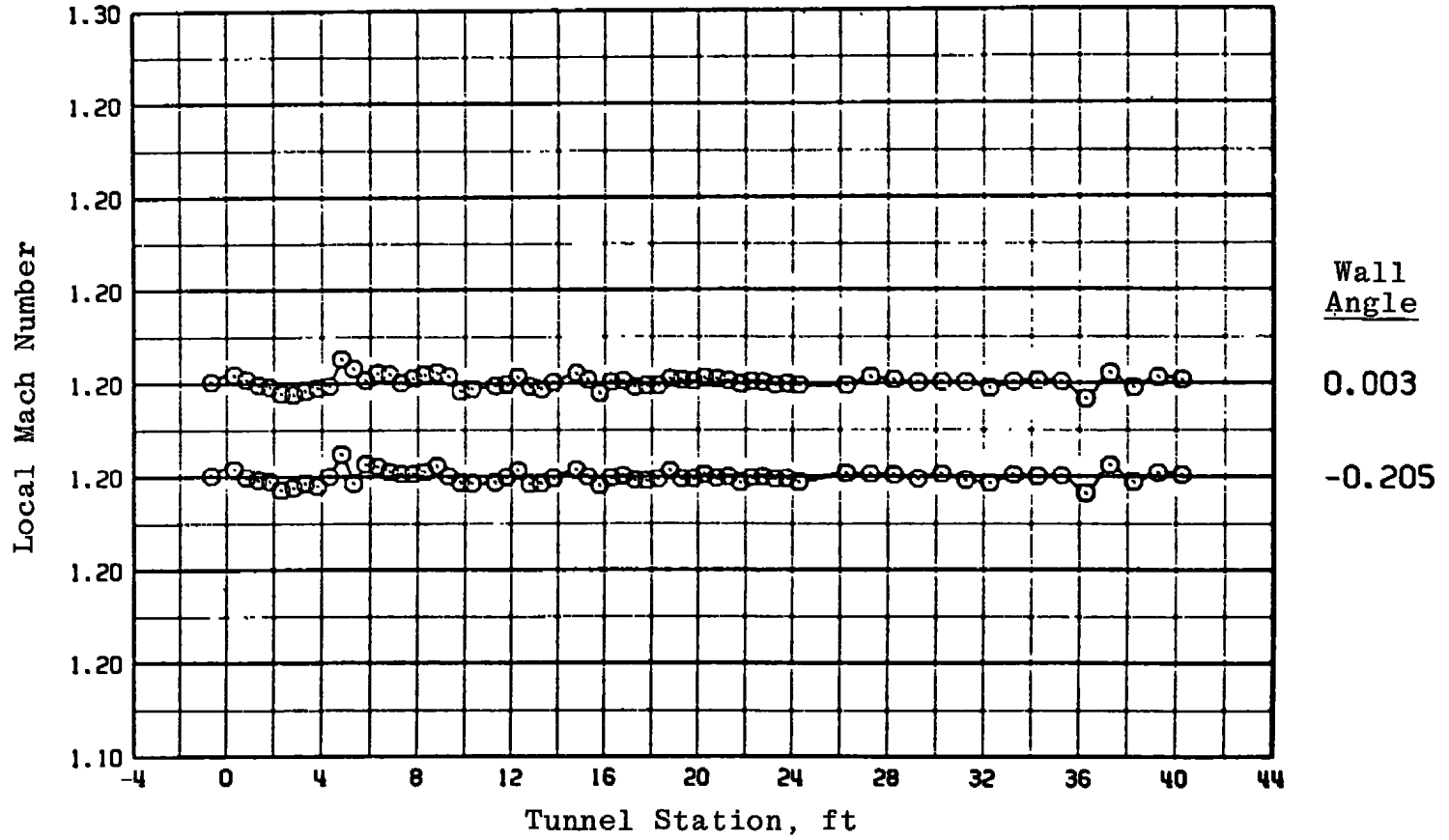
b. $M_\infty = 0.80$
Figure 14. Continued.



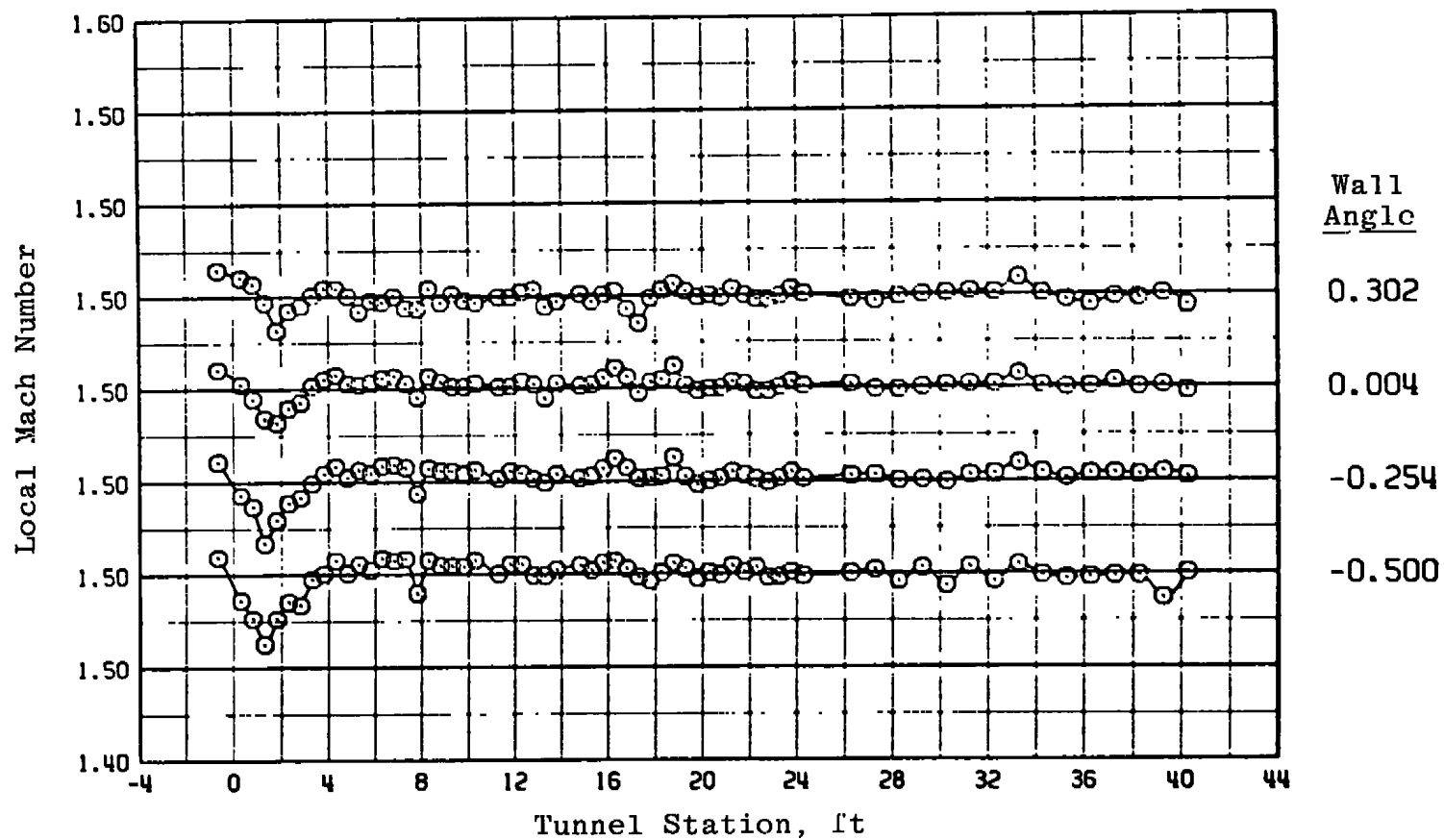
c. $M_{on} = 1.0$
Figure 14. Continued.



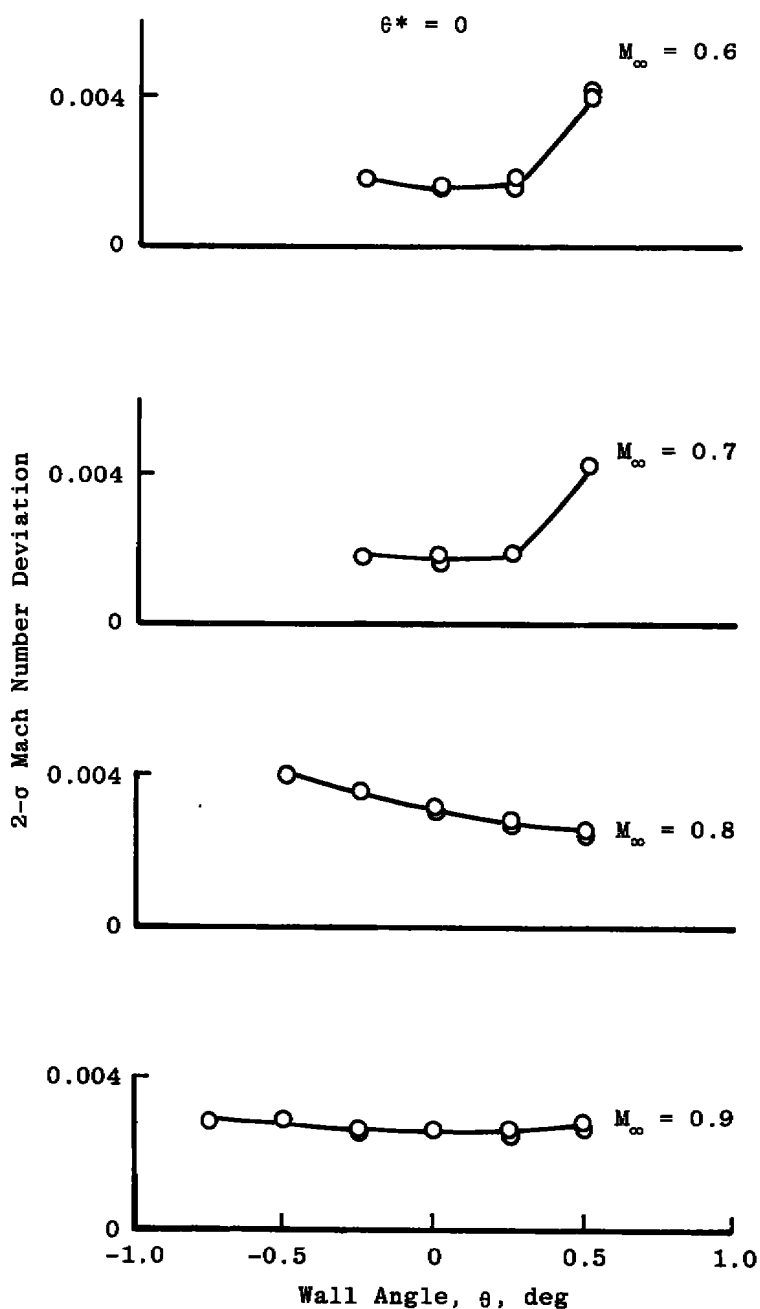
d. $M_\infty = 1.10$
Figure 14. Continued.



e. $M_{\infty} = 1.20$
Figure 14. Continued.

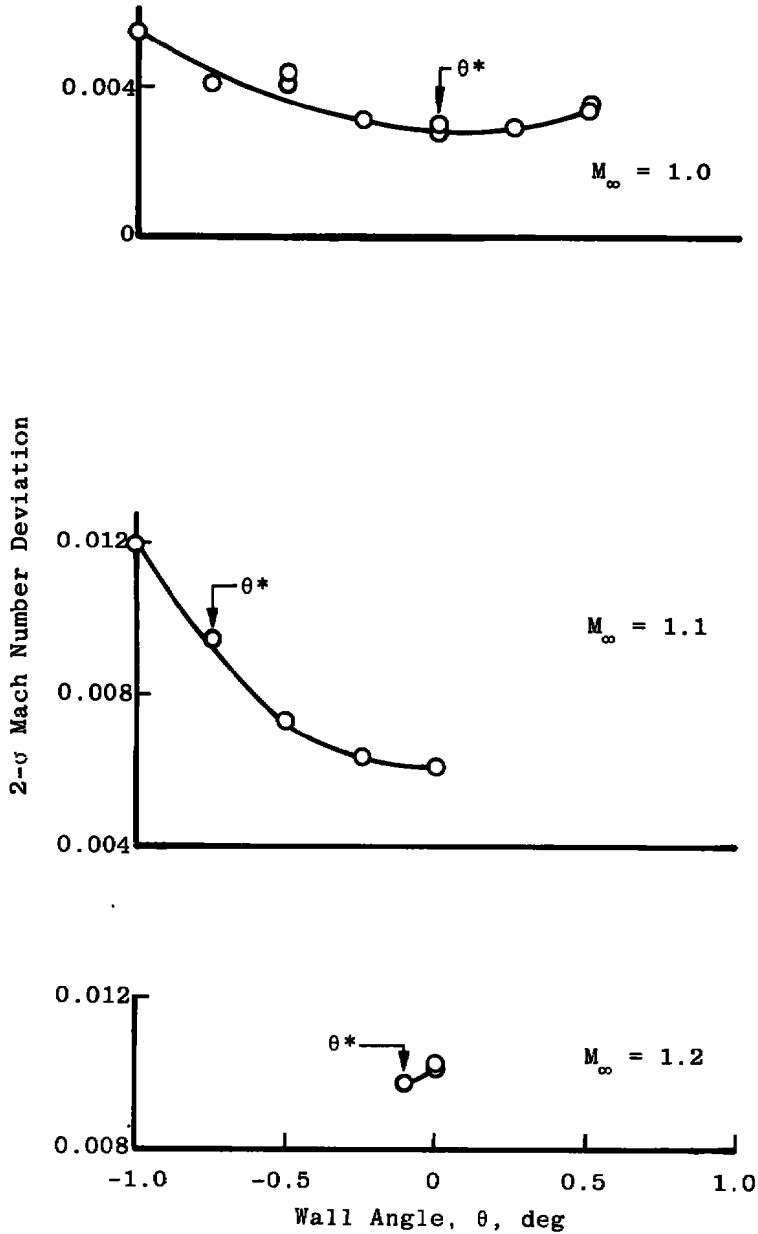


f. $M_{\infty} = 1.50$
Figure 14. Concluded.

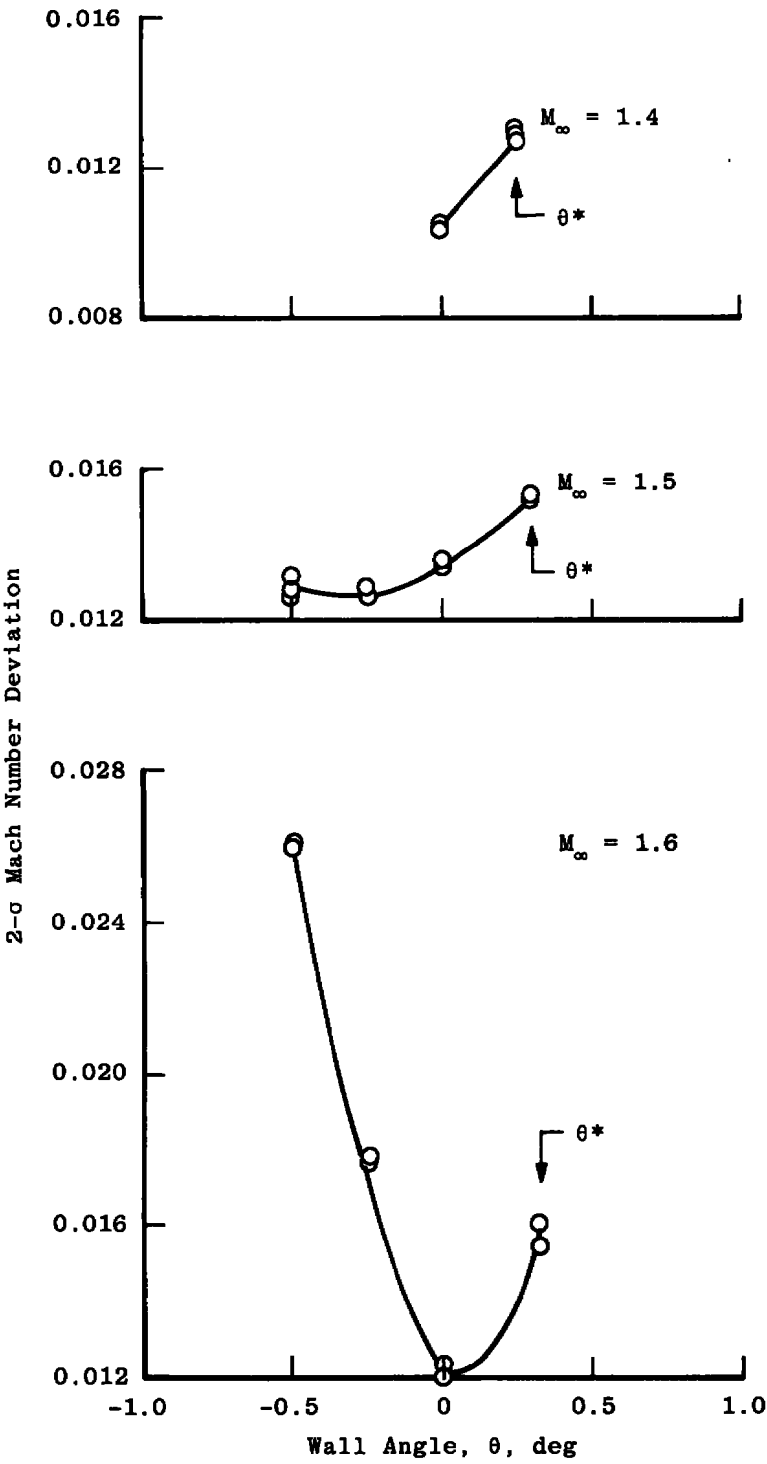


a. $M_\infty = 0.6$ to 0.9

Figure 15. Effect of wall angle variations on the 2- σ Mach number deviations for Tunnel Stations 8 to 28 with $\lambda = \lambda^*$ and $P_t = 1,600$ psfa.



b. $M_\infty = 1.0$ to 1.2
Figure 15. Continued.



c. $M_\infty = 1.4$ to 1.6
Figure 15. Concluded.

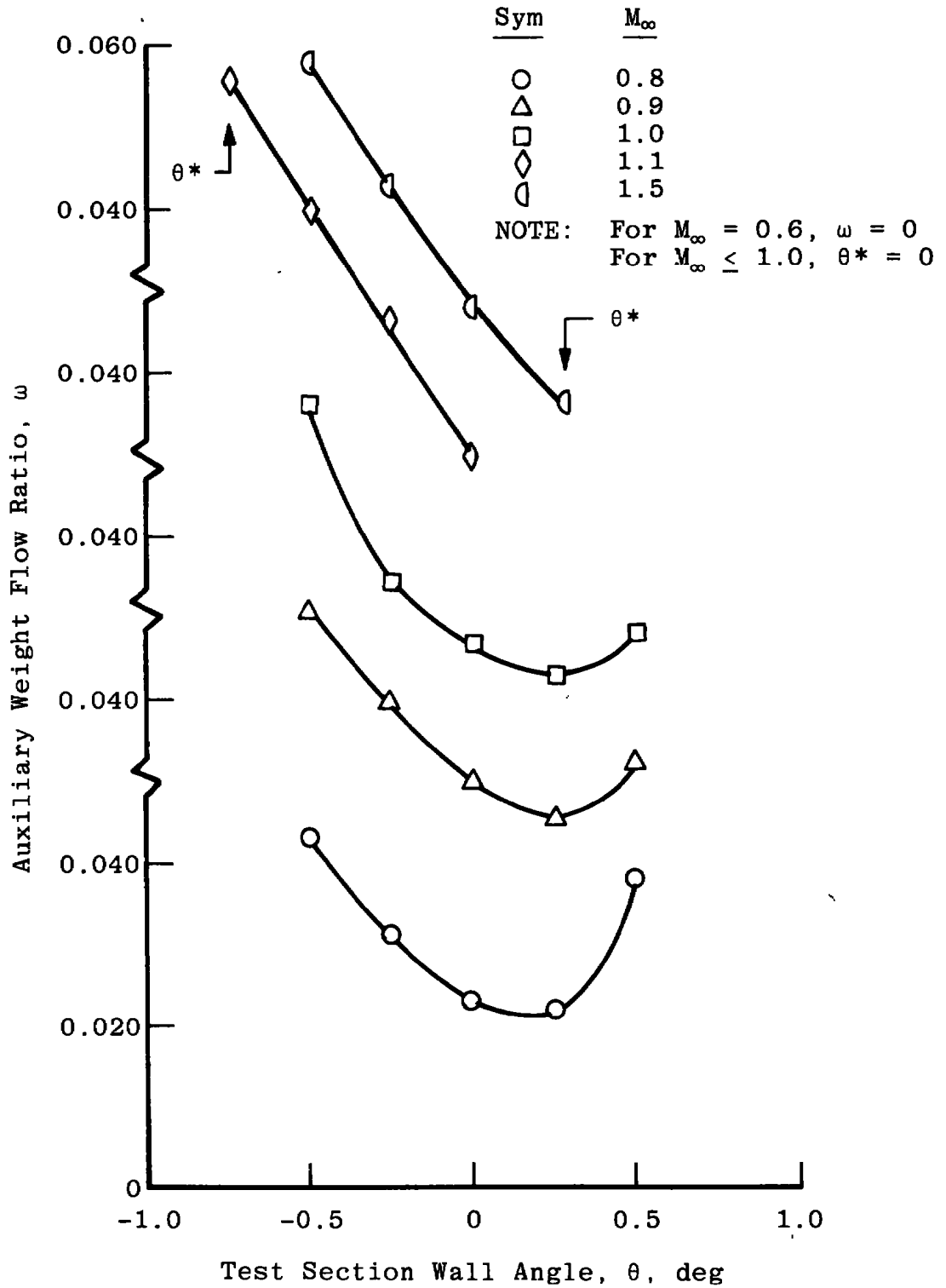


Figure 16. Effect of wall angle variation on auxiliary flow requirements with $\lambda = \lambda^*$ and $P_t = 1,600$ psfa.

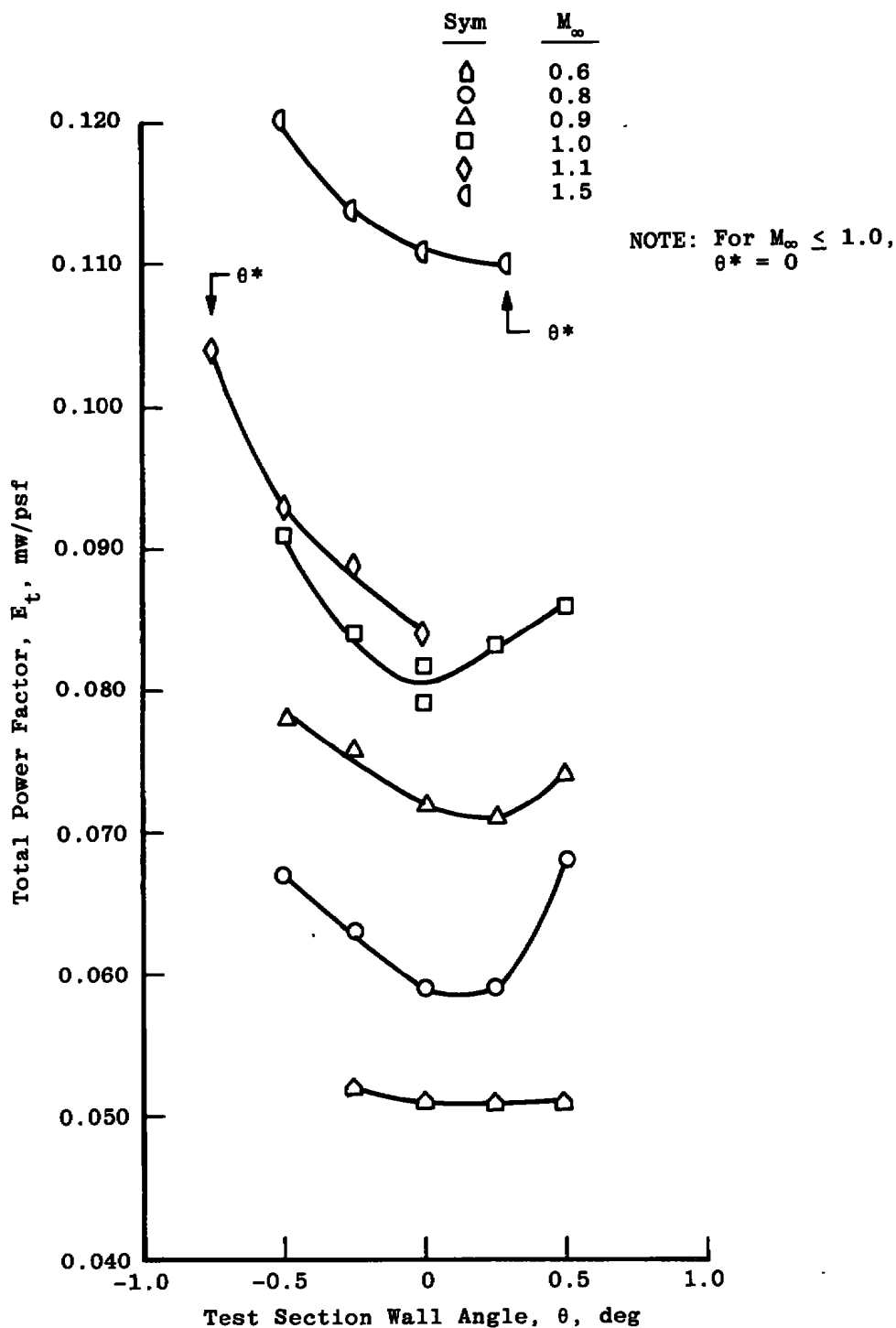
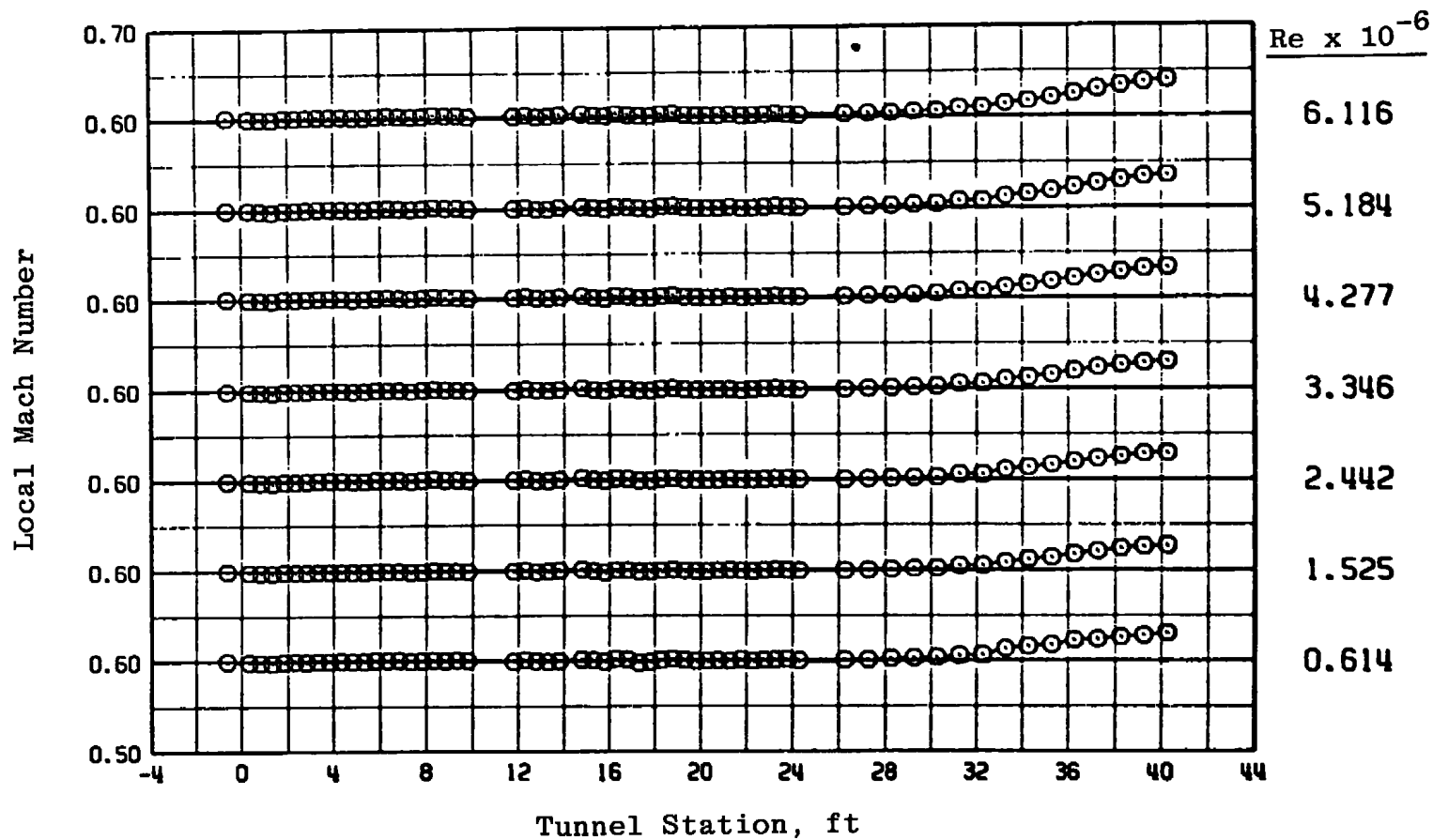
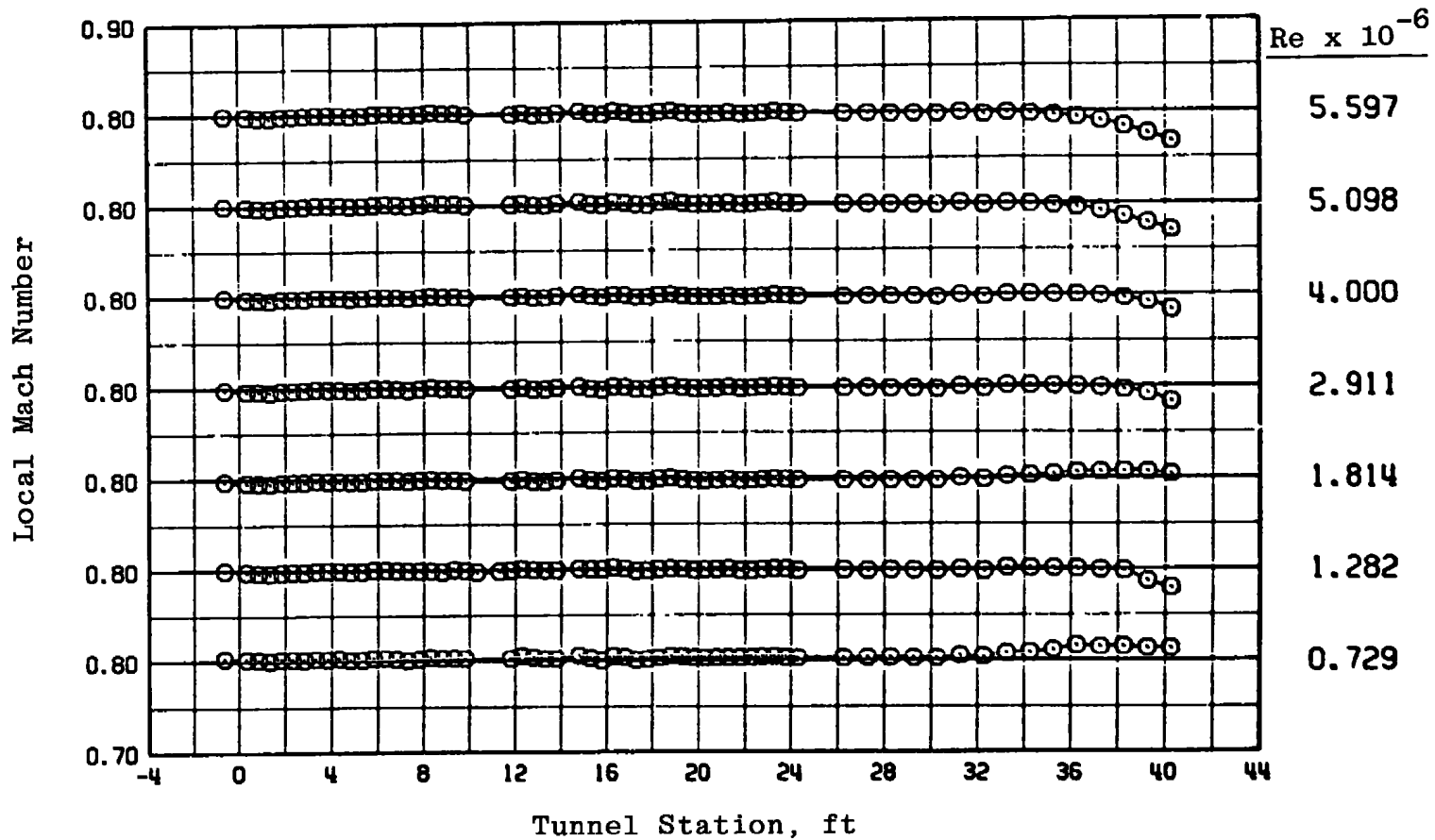


Figure 17. Effect of wall angle variation on tunnel total power requirements with $\lambda = \lambda^*$ and $P_t = 1,600$ psfa.

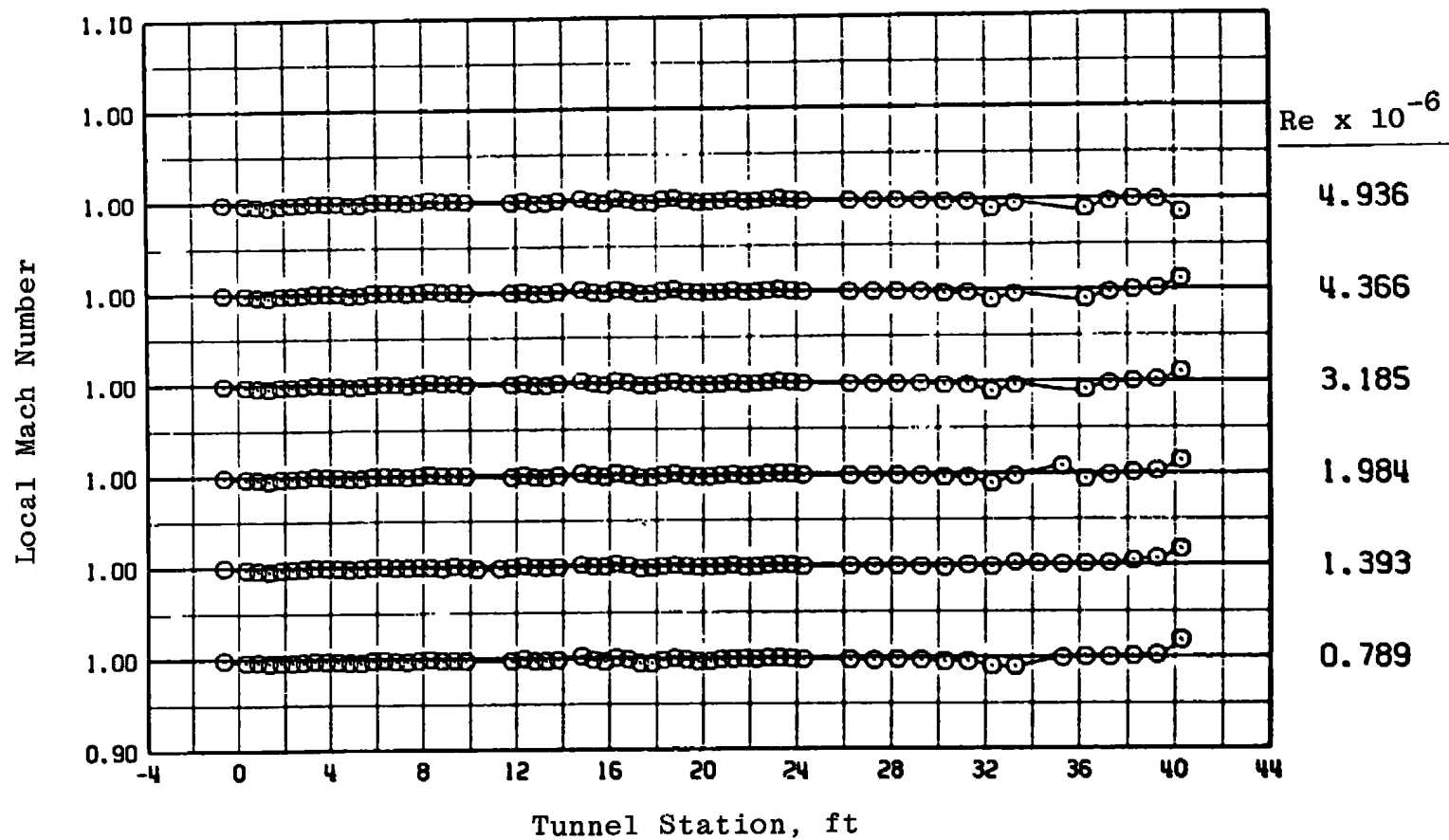


a. $M_{\infty} = 0.6$

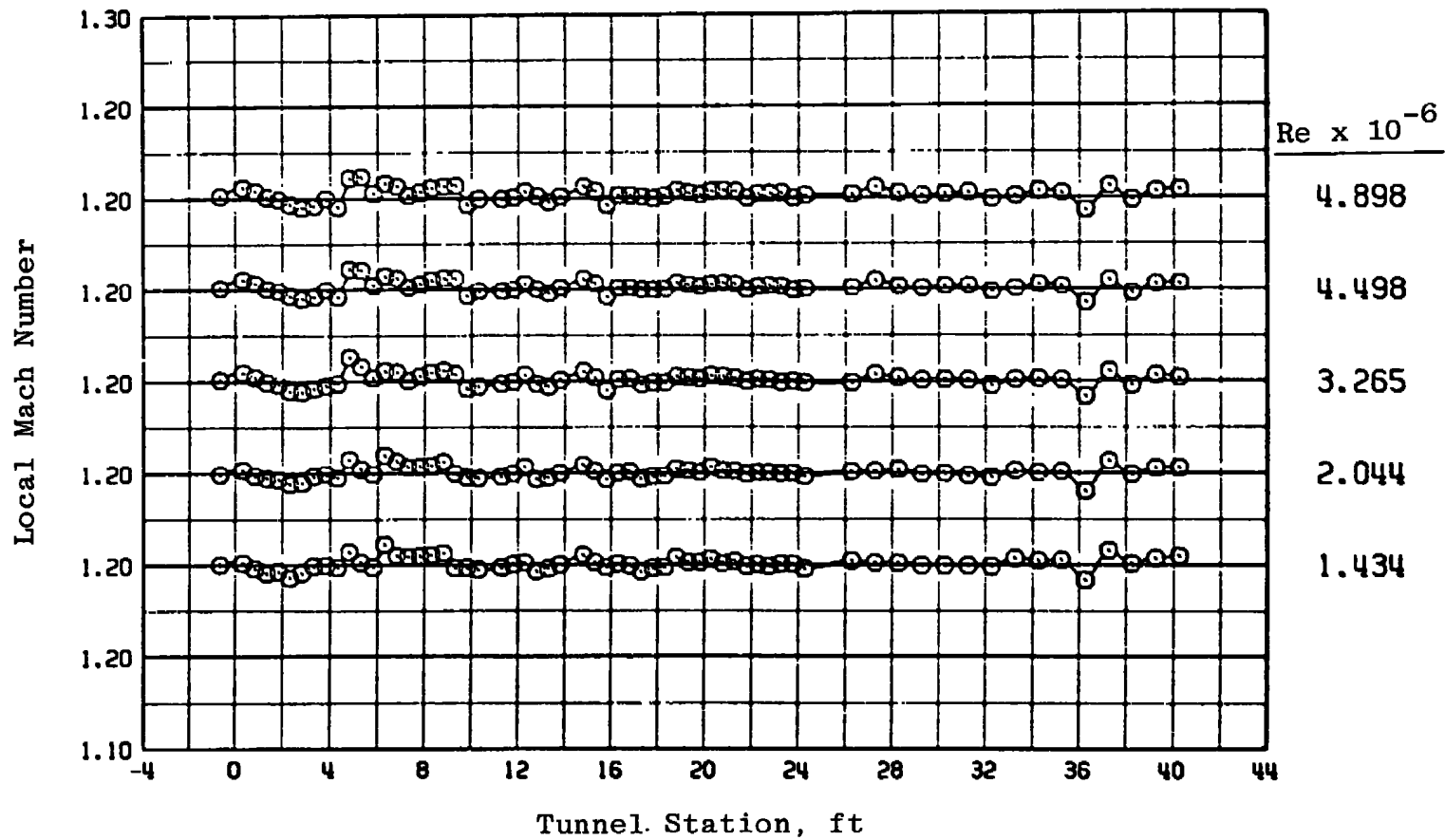
Figure 18. Tunnel 16T centerline Mach number distributions for various Reynolds numbers with $\theta = 0$ and $\lambda = \lambda^*$.



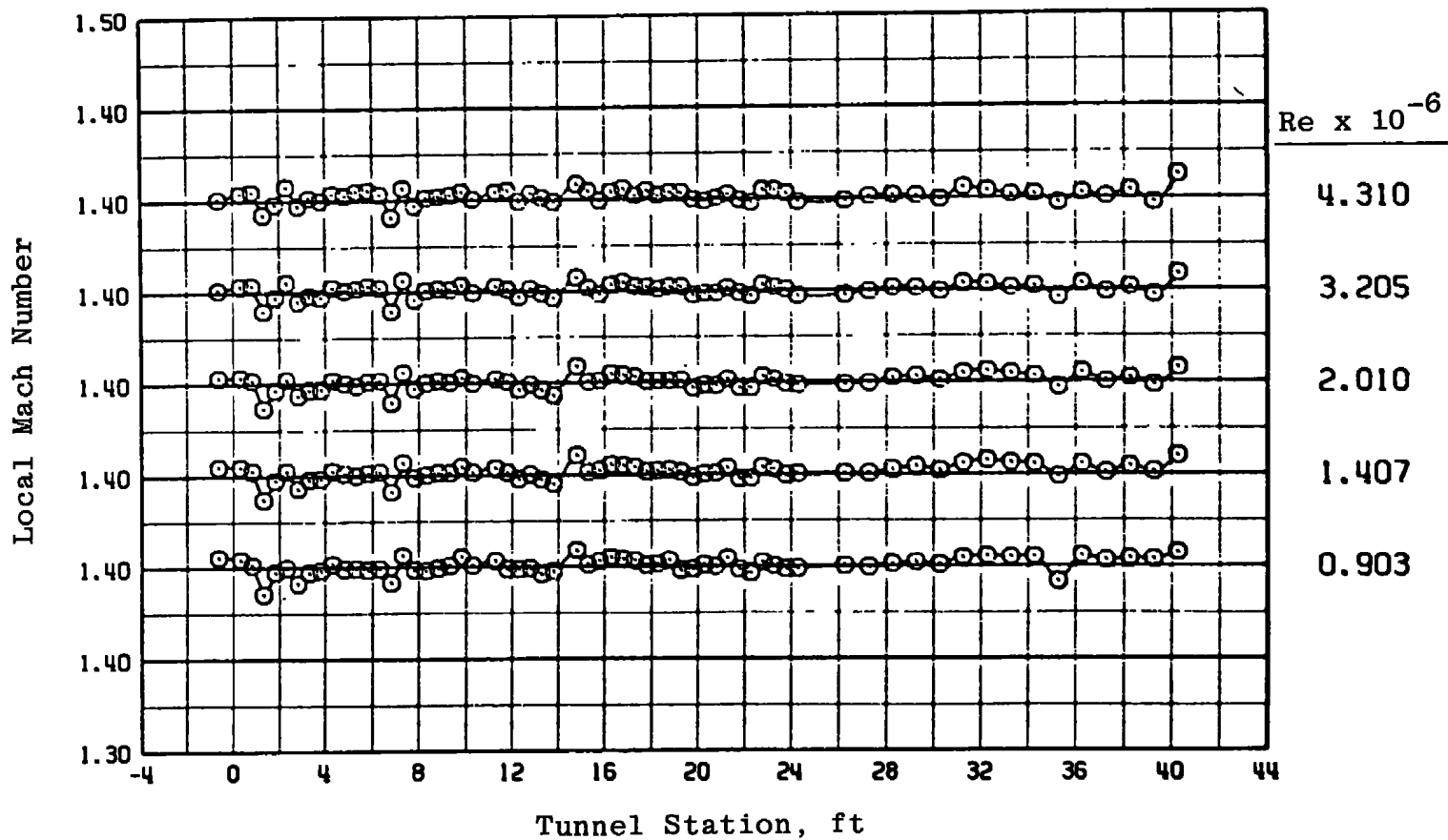
b. $M_{\infty} = 0.8$
Figure 18. Continued.



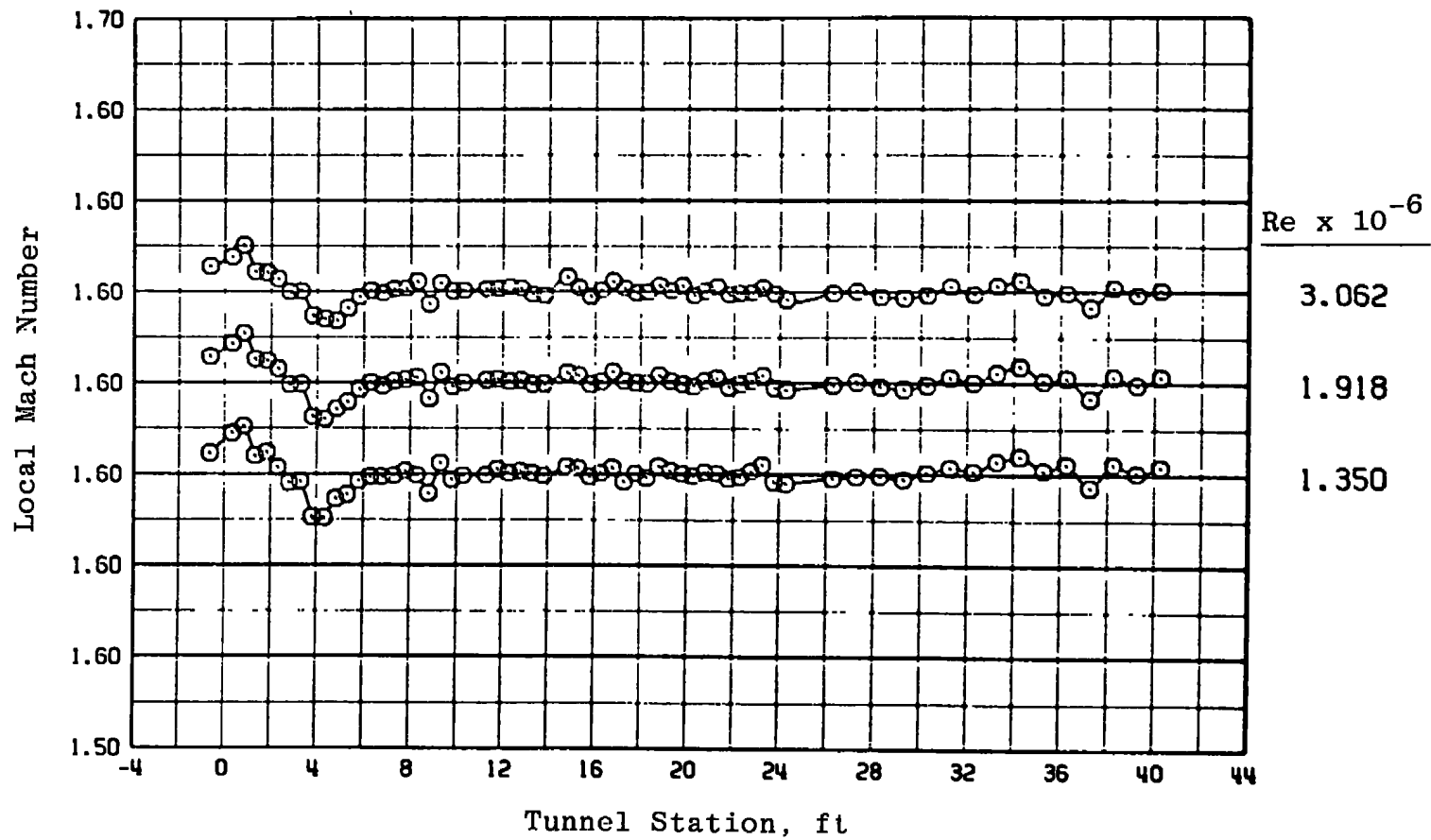
c. $M_{\infty} = 1.0$
Figure 18. Continued.



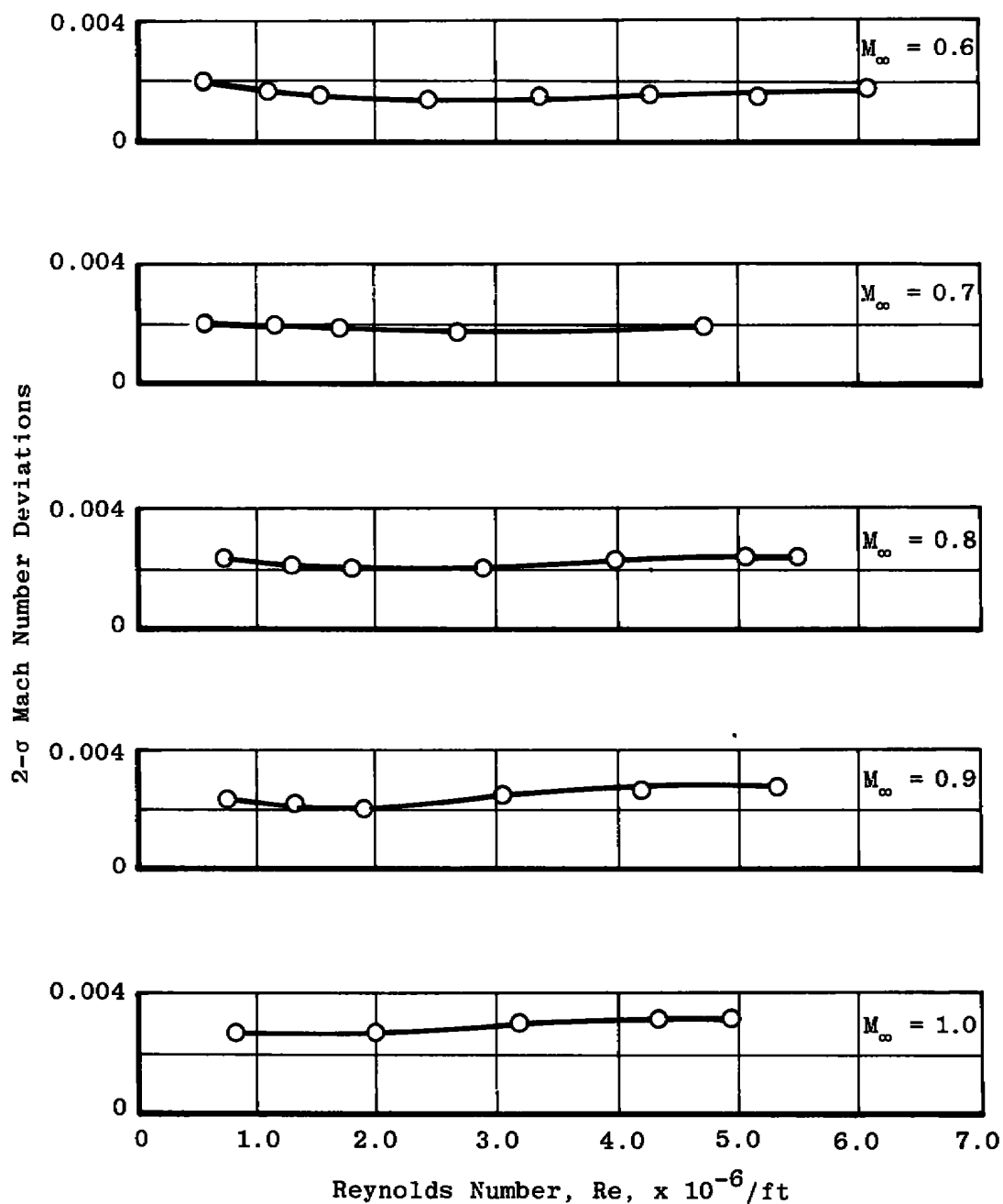
d. $M_{\infty} = 1.2$
Figure 18. Continued.



e. $M_{\infty} = 1.40$
Figure 18. Continued.

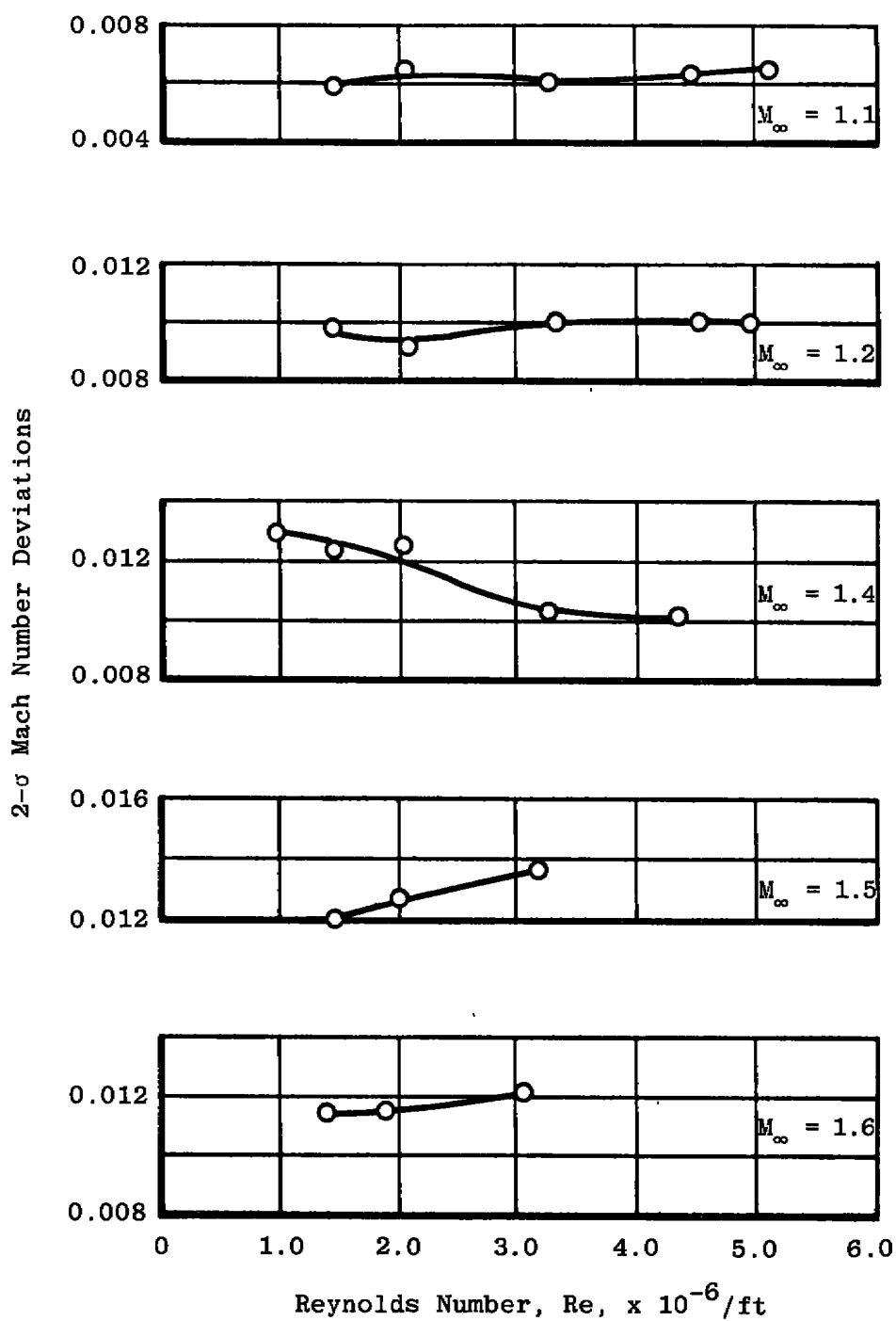


$f. M_\infty = 1.6$
Figure 18. Concluded.



a. $M_\infty = 0.6$ to 1.0

Figure 19. Effect of Reynolds number variation on the 2- σ Mach number deviations for Tunnel Stations 8 to 28 at $\lambda = \lambda^*$ and $\theta = 0$.



b. $M_\infty = 1.1$ to 1.6
Figure 19. Concluded.

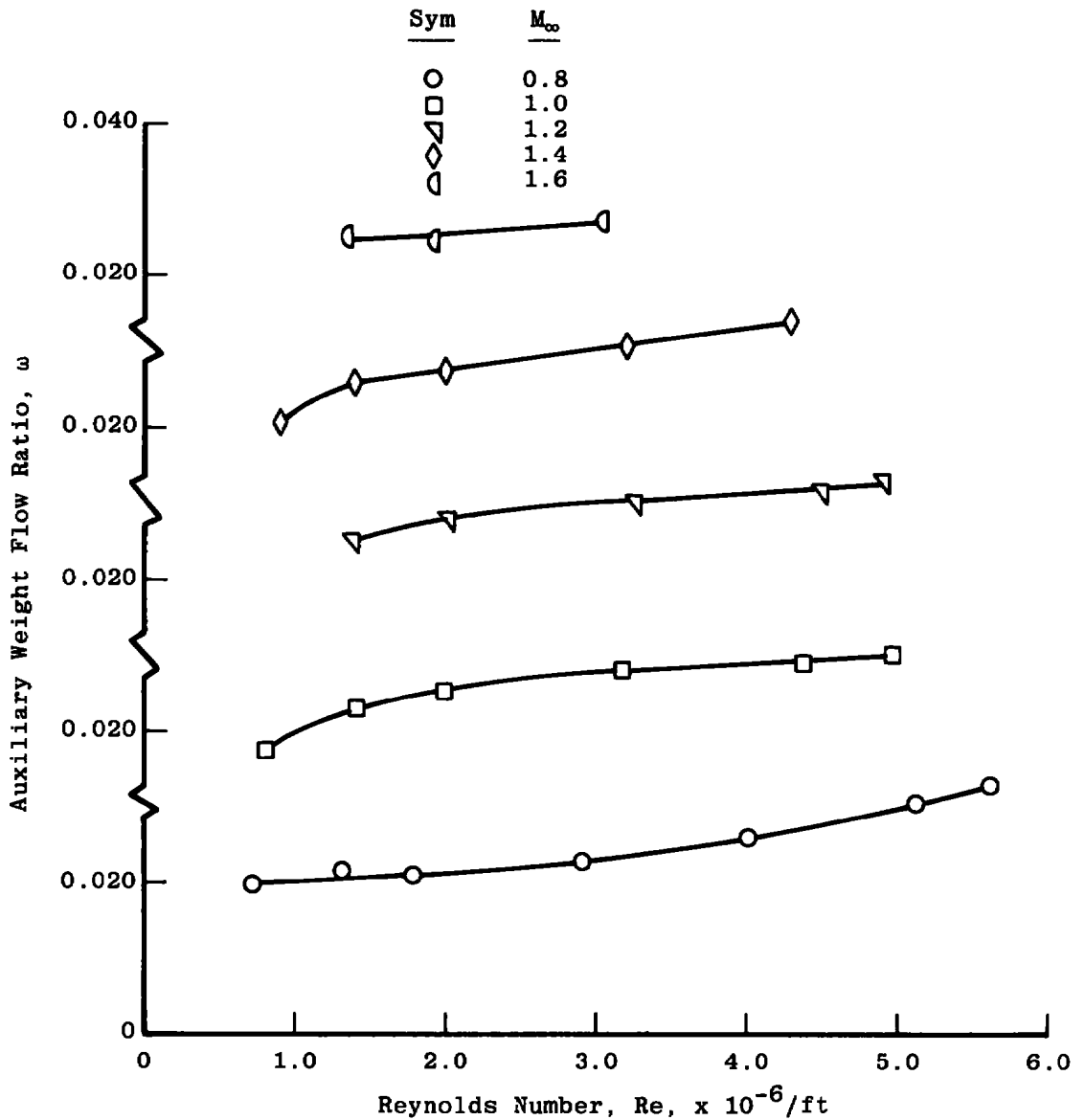


Figure 20. Effect of Reynolds number variations on the auxiliary flow requirements with $\theta = 0$ and $\lambda = \lambda^*$.

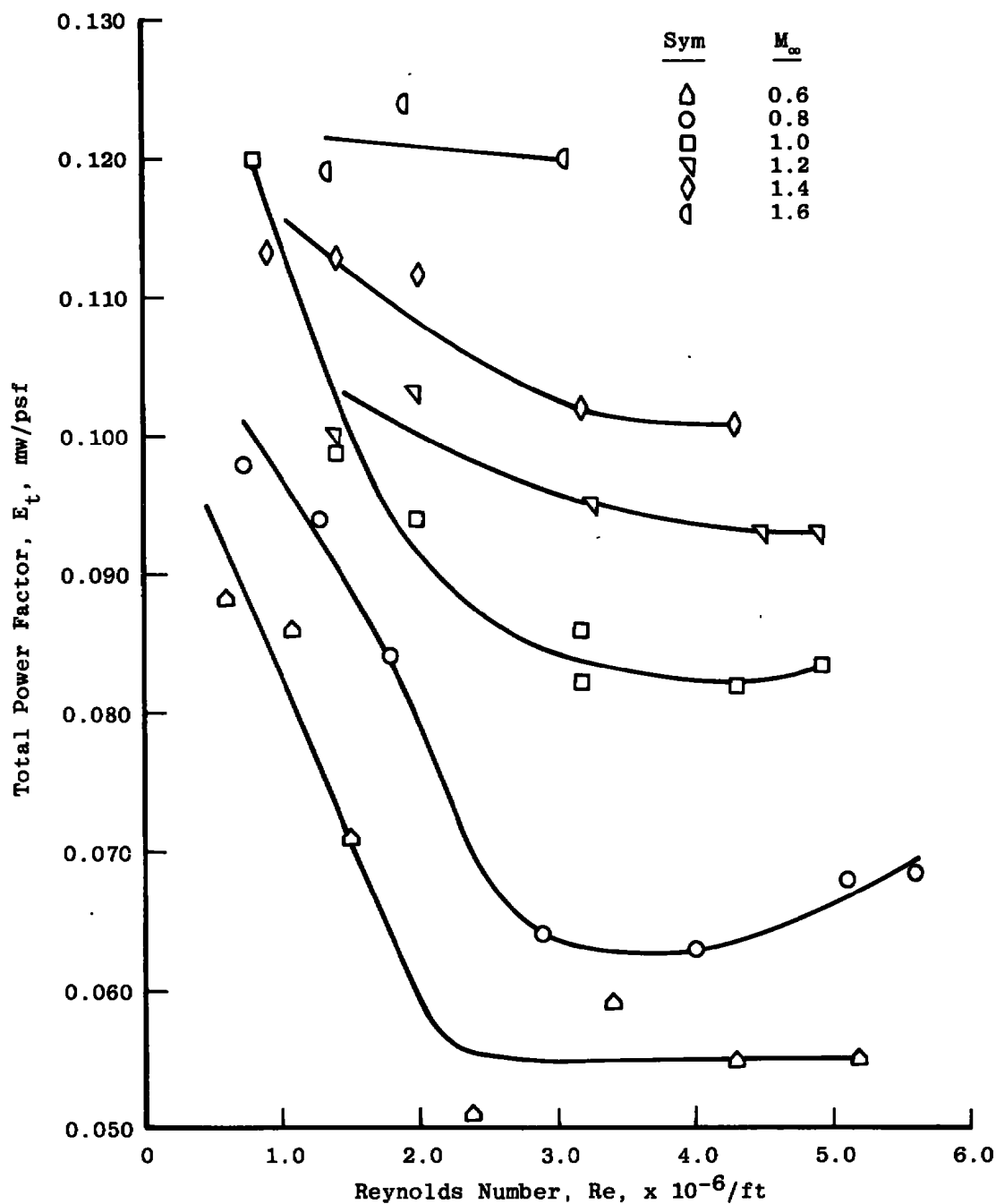
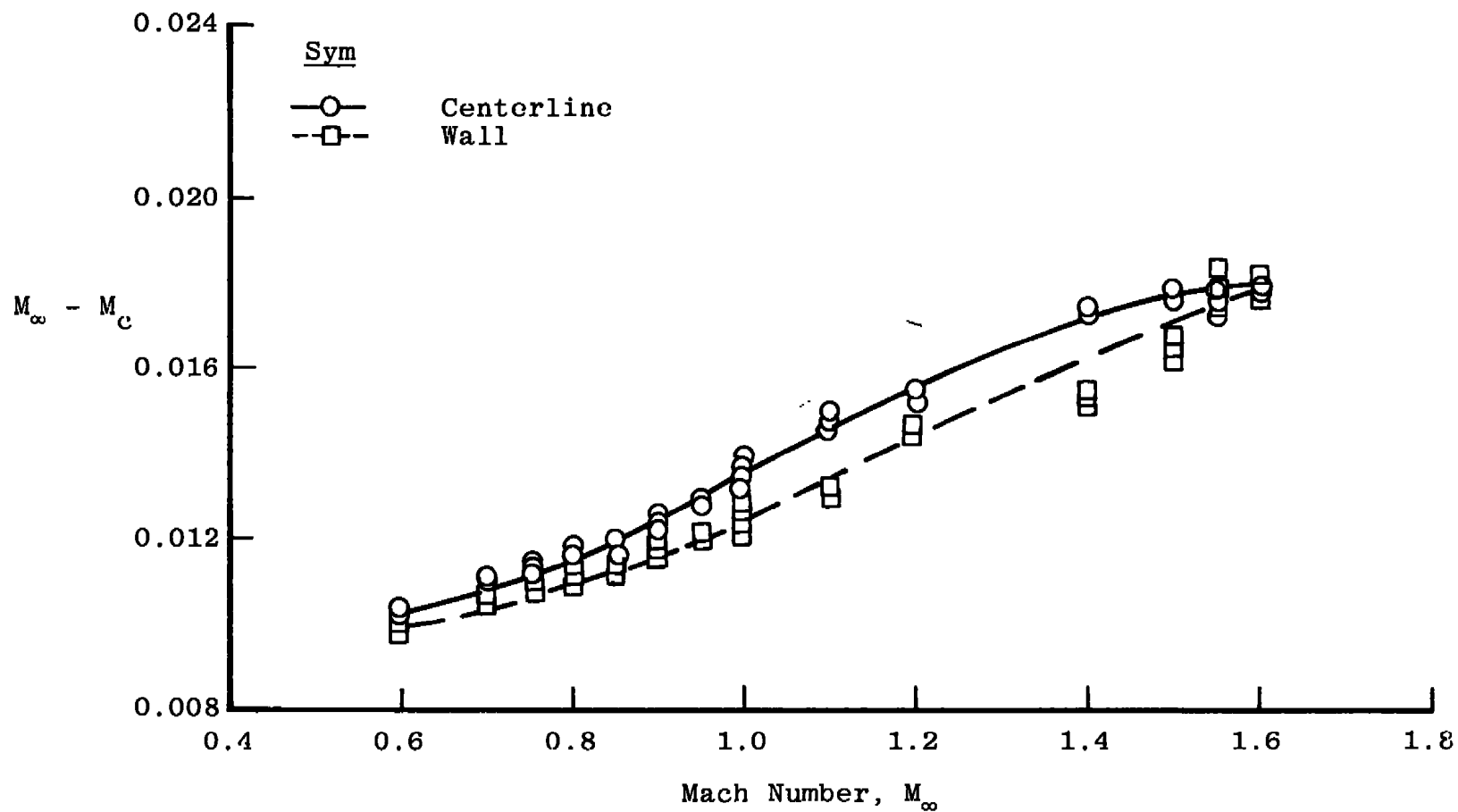
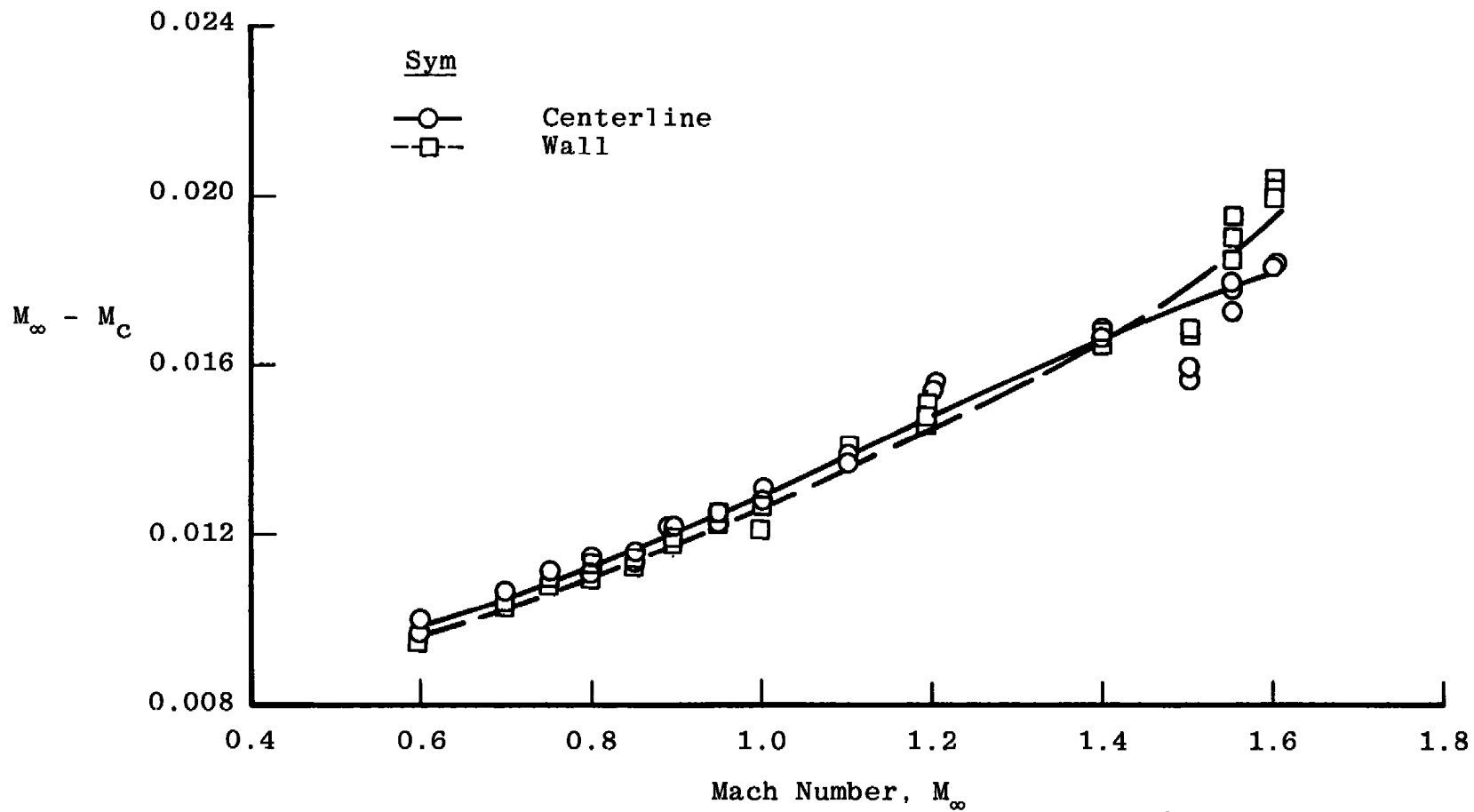


Figure 21. Effect of Reynolds number variation on tunnel total power requirements with $\theta = 0$ and $\lambda = \lambda^*$.



a. Stations 8 to 28

Figure 22. Effect of orifice selection on the Tunnel 16T Mach number calibration with $\lambda = \lambda^*$, $\theta = 0$, and $P_t = 1,600$ psfa.



b. Station 1 to 20
Figure 22. Concluded.

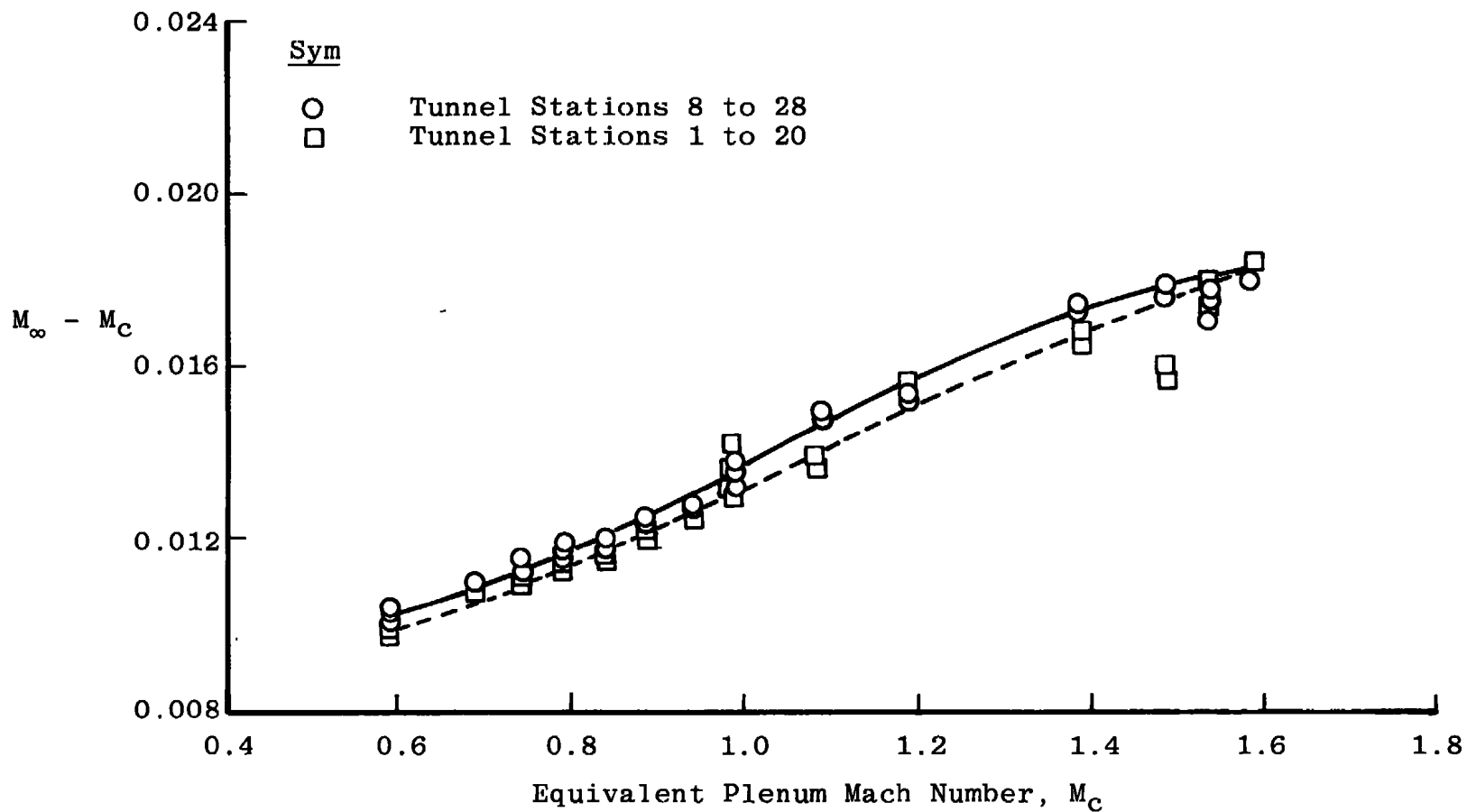
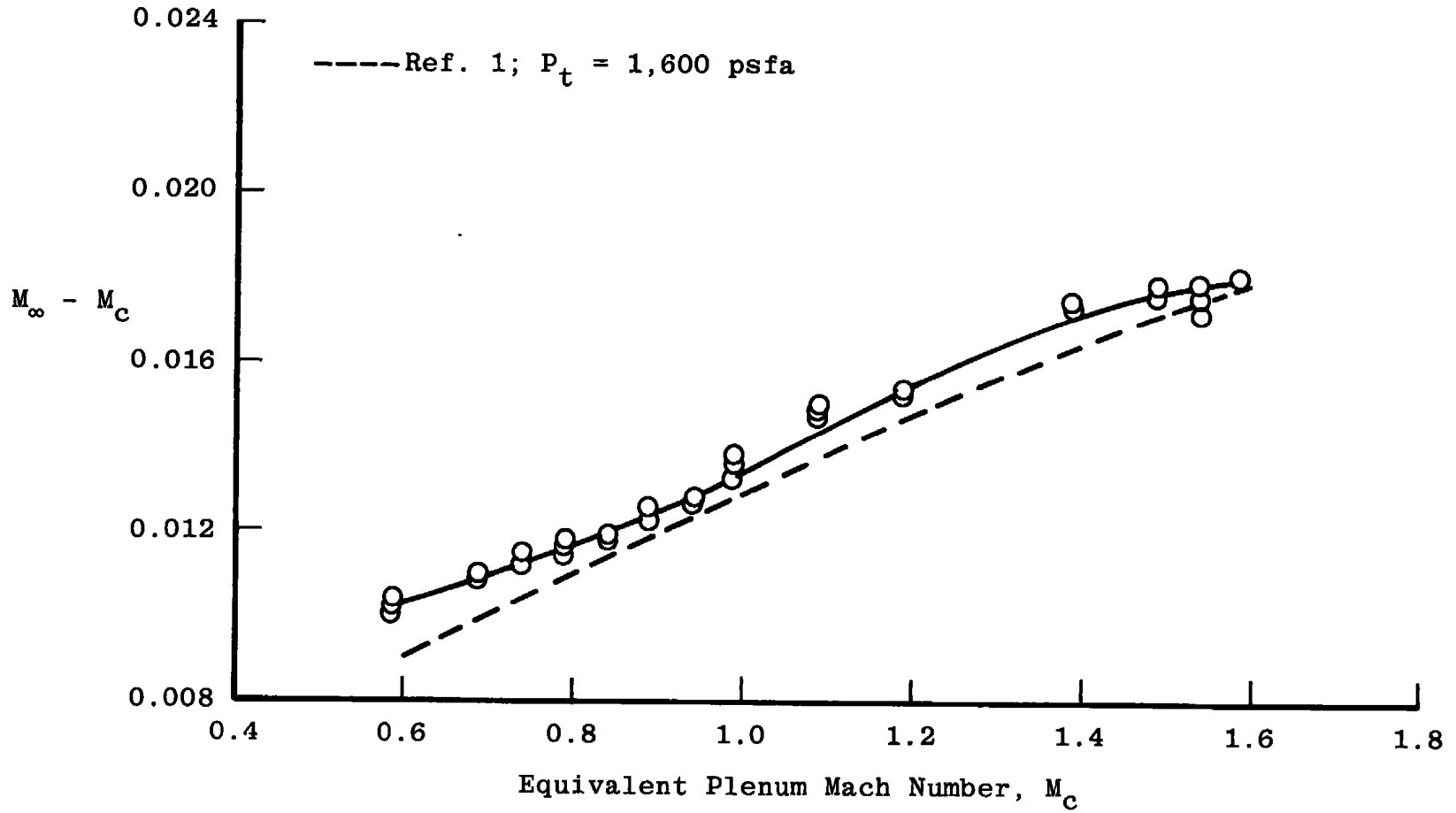
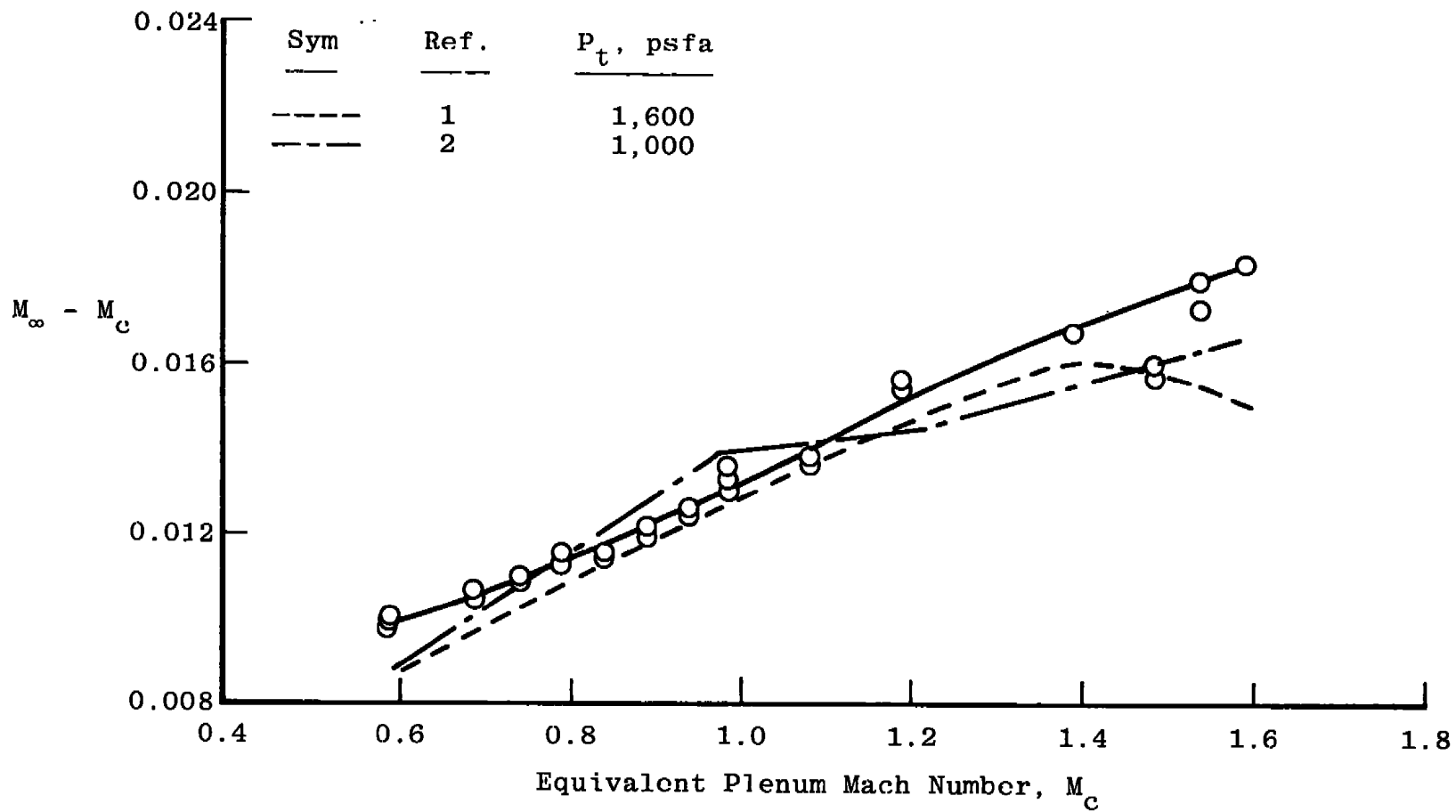


Figure 23. Effect of test section region on the Tunnel 16T Mach number calibration at $\theta = 0$, $\lambda = \lambda^*$, and $P_t = 1,600$ psfa.



a. Tunnel Stations 8 to 28

Figure 24. Comparison of Tunnel 16T calibration with $\lambda = \lambda^*$
 $\theta = 0$, and $P_t = 1,600$ psfa to previous results.



b. Tunnel Stations 1 to 20
Figure 24. Concluded.

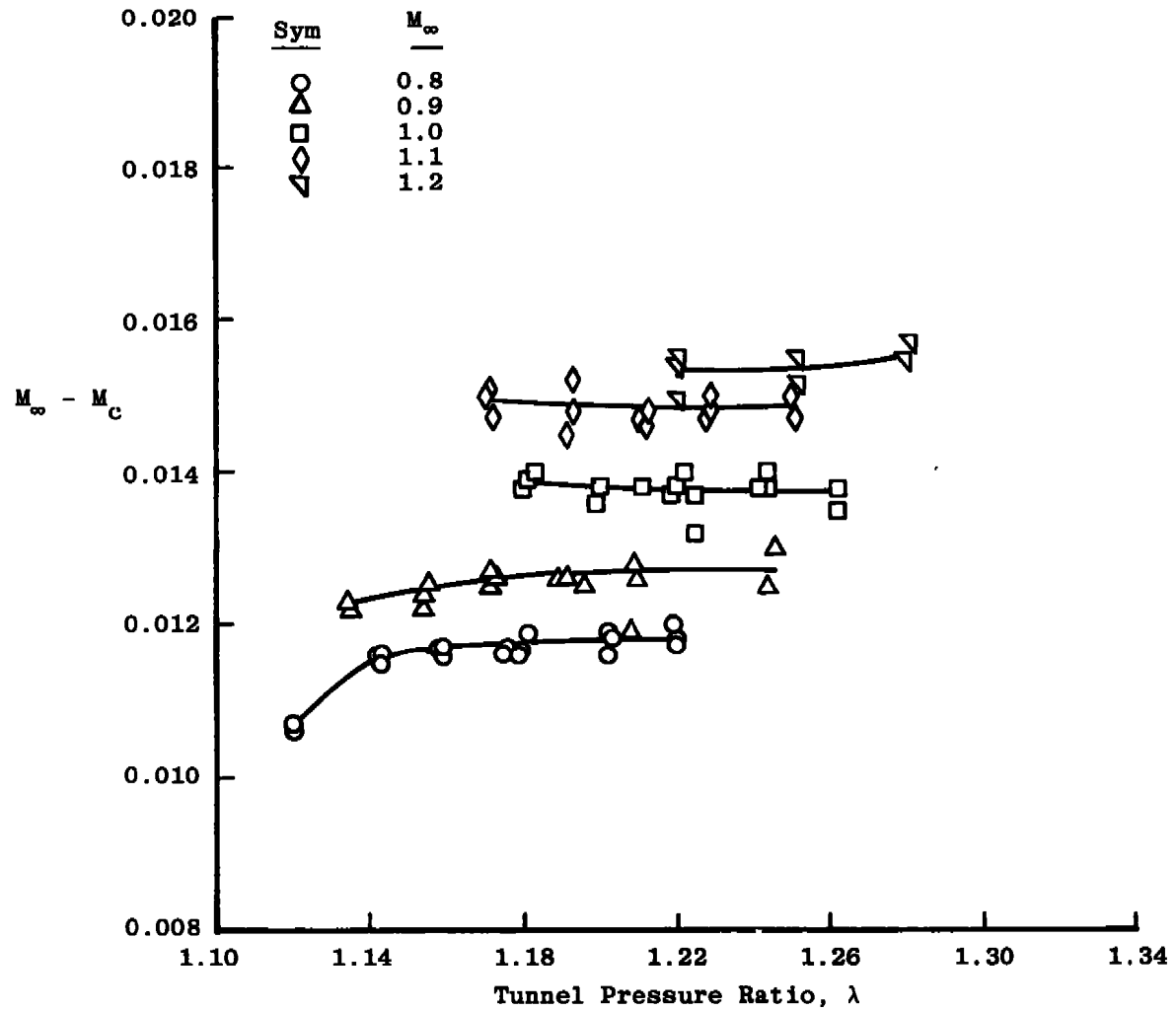


Figure 25. Effect of pressure ratio variation on the Tunnel 16T calibration with $\theta = 0$ and $P_t = 1,600$ psfa.

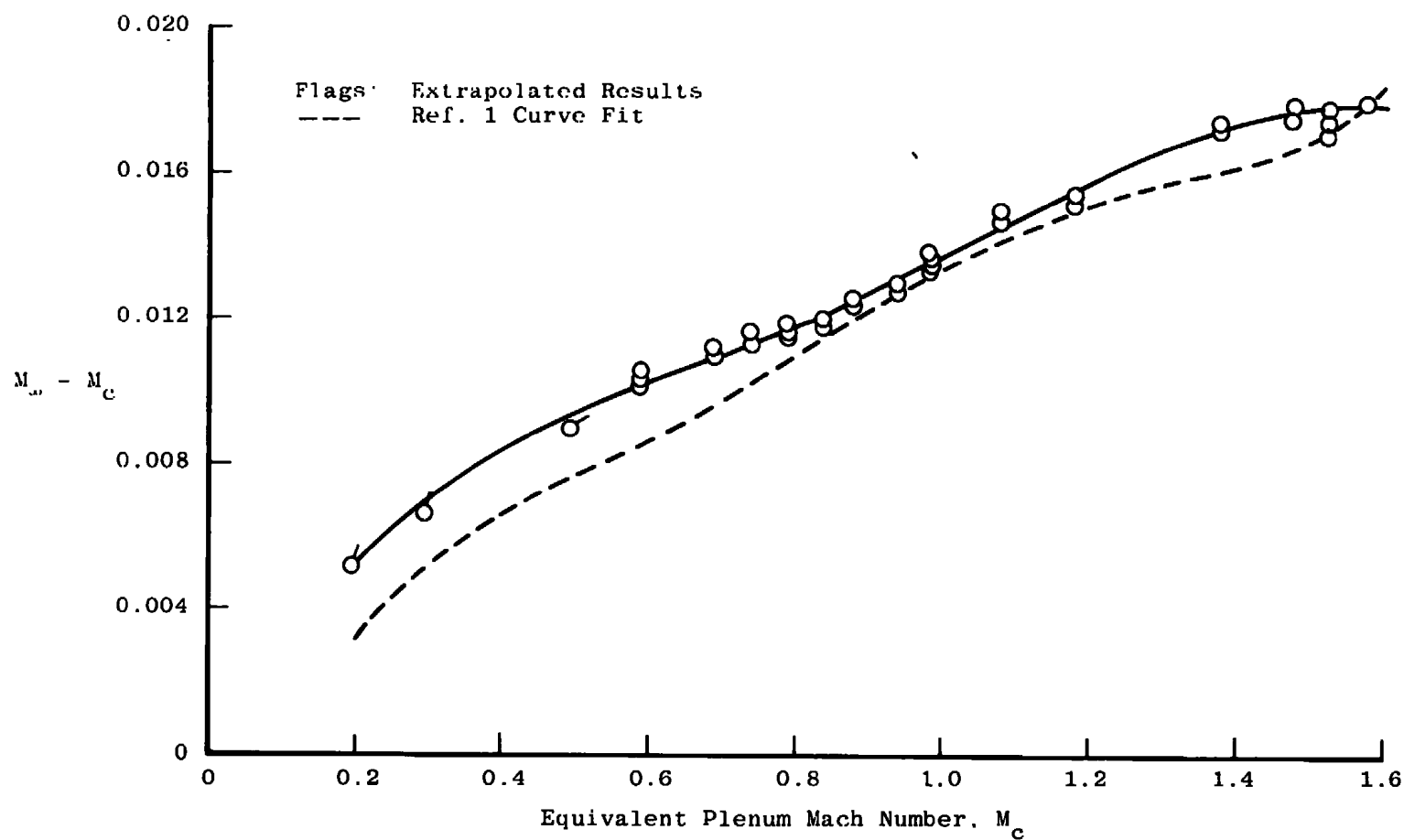


Figure 26. Tunnel 16T calibration with $\lambda = \lambda^*$, $\theta = 0$, and $P_t = 1,600$ psfa.

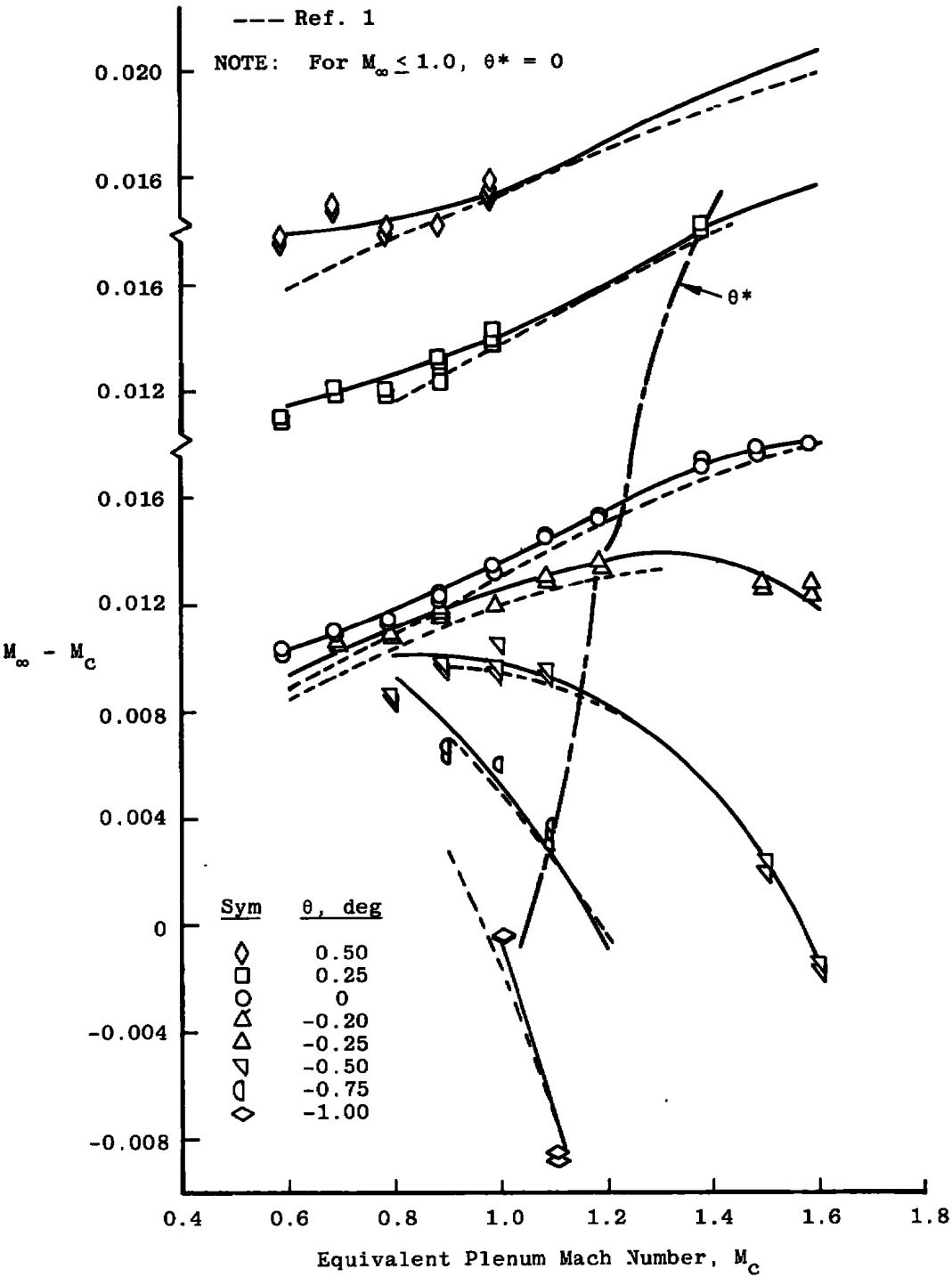


Figure 27. Tunnel 16T Mach number calibration for various test section wall angles at $\lambda = \lambda^*$ and $P_t = 1,600$ psfa.

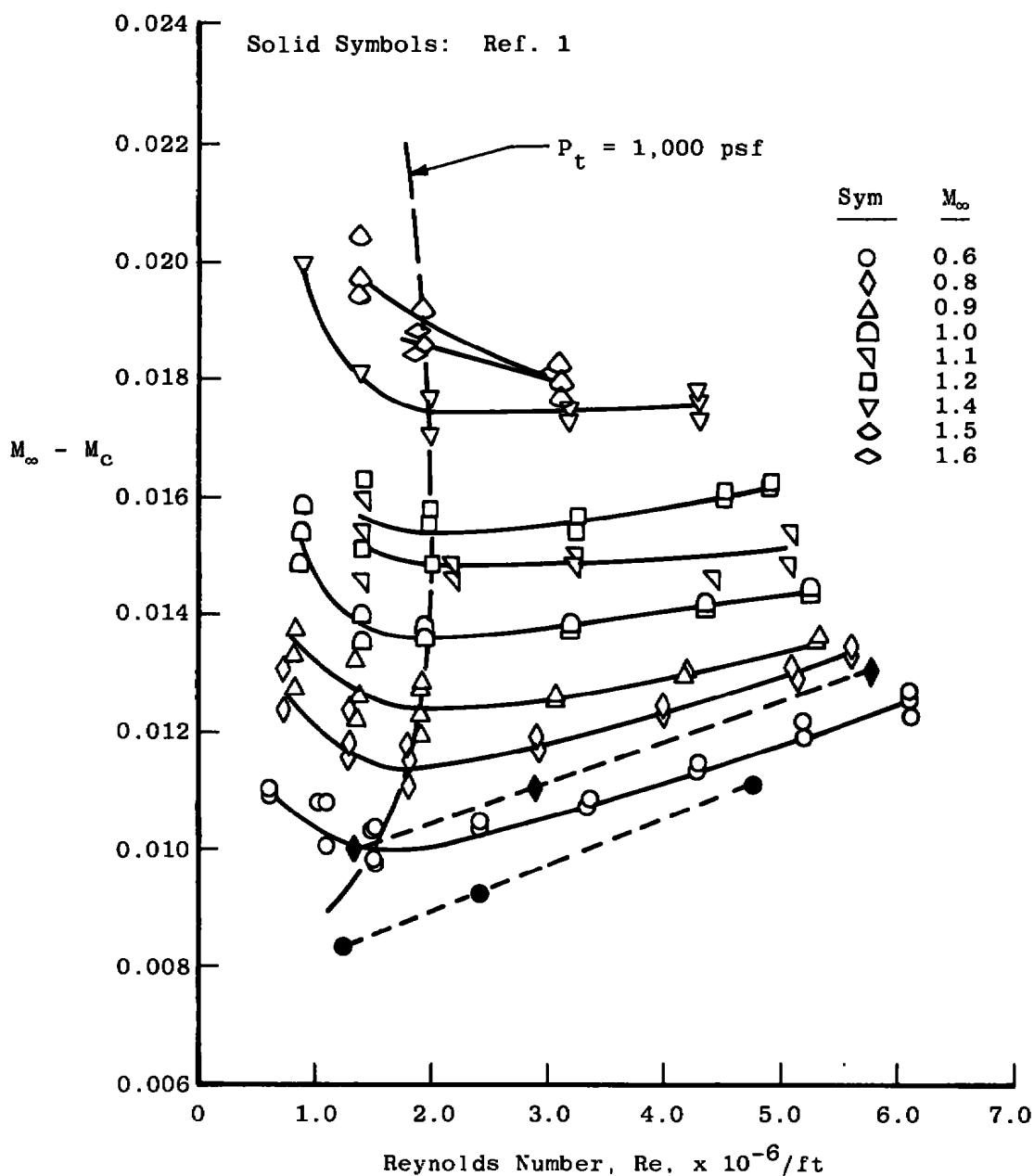


Figure 28. Tunnel 16T Mach number calibration for various Reynolds numbers with $\lambda = \lambda^*$ and $\theta = 0$.

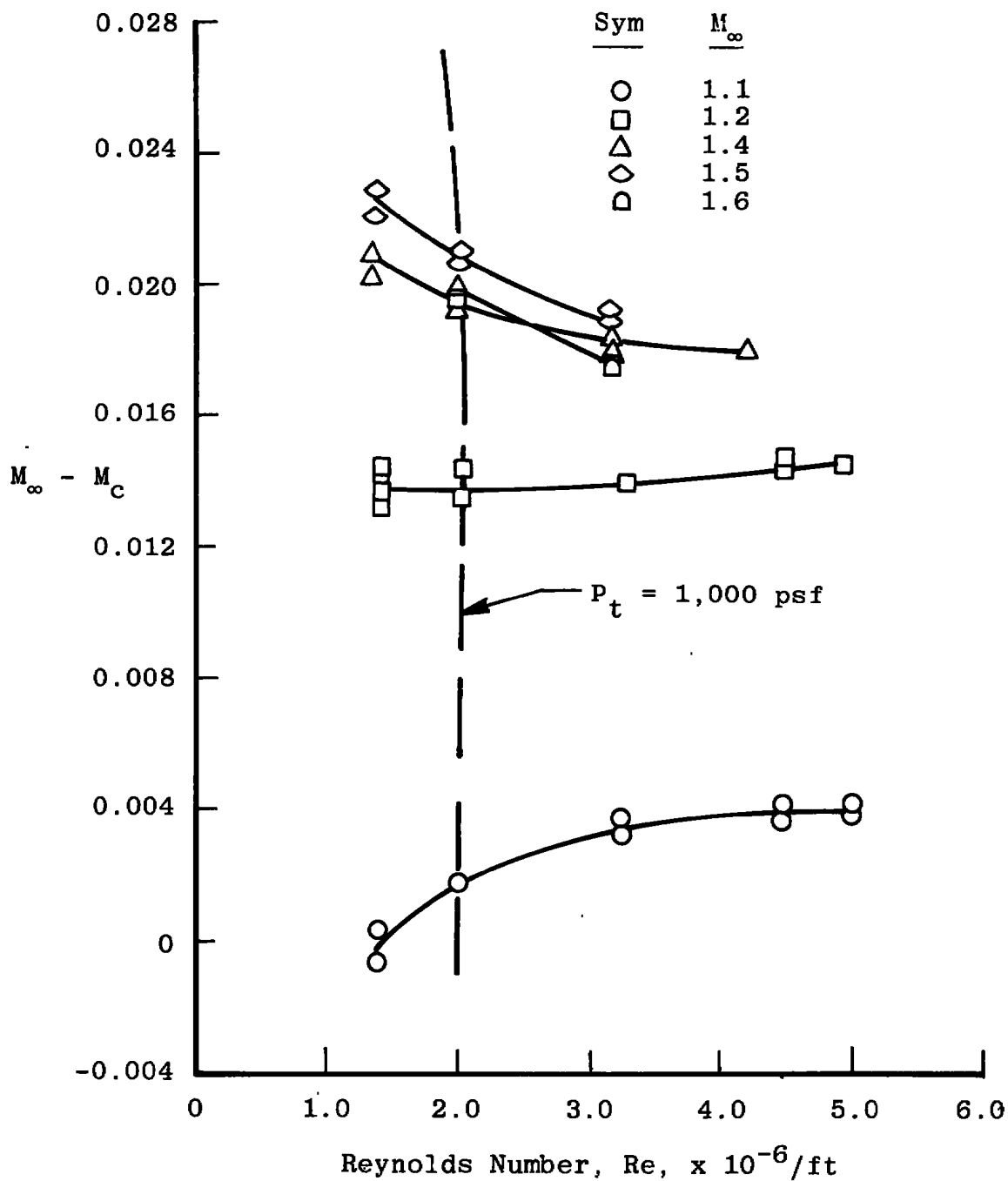
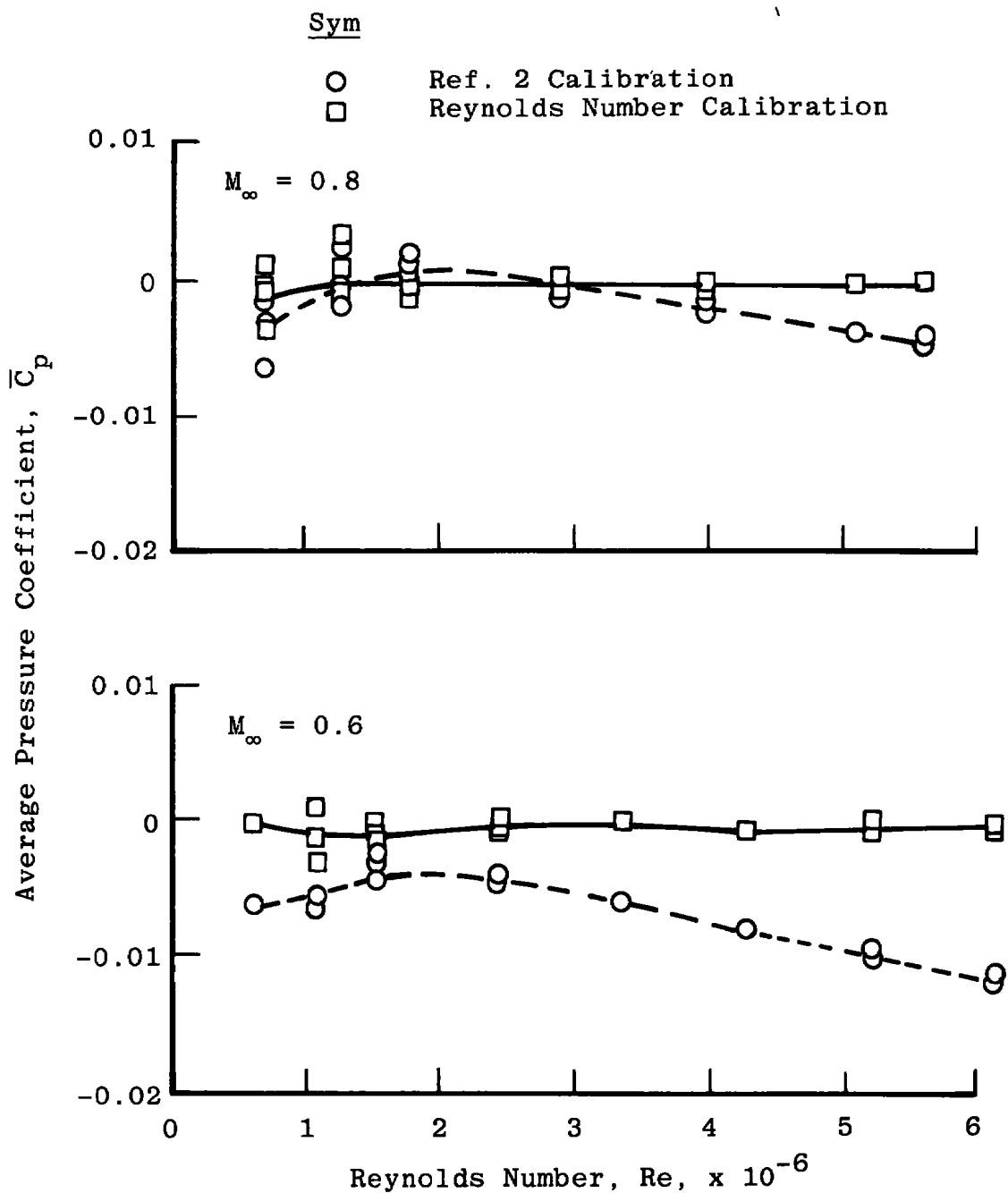
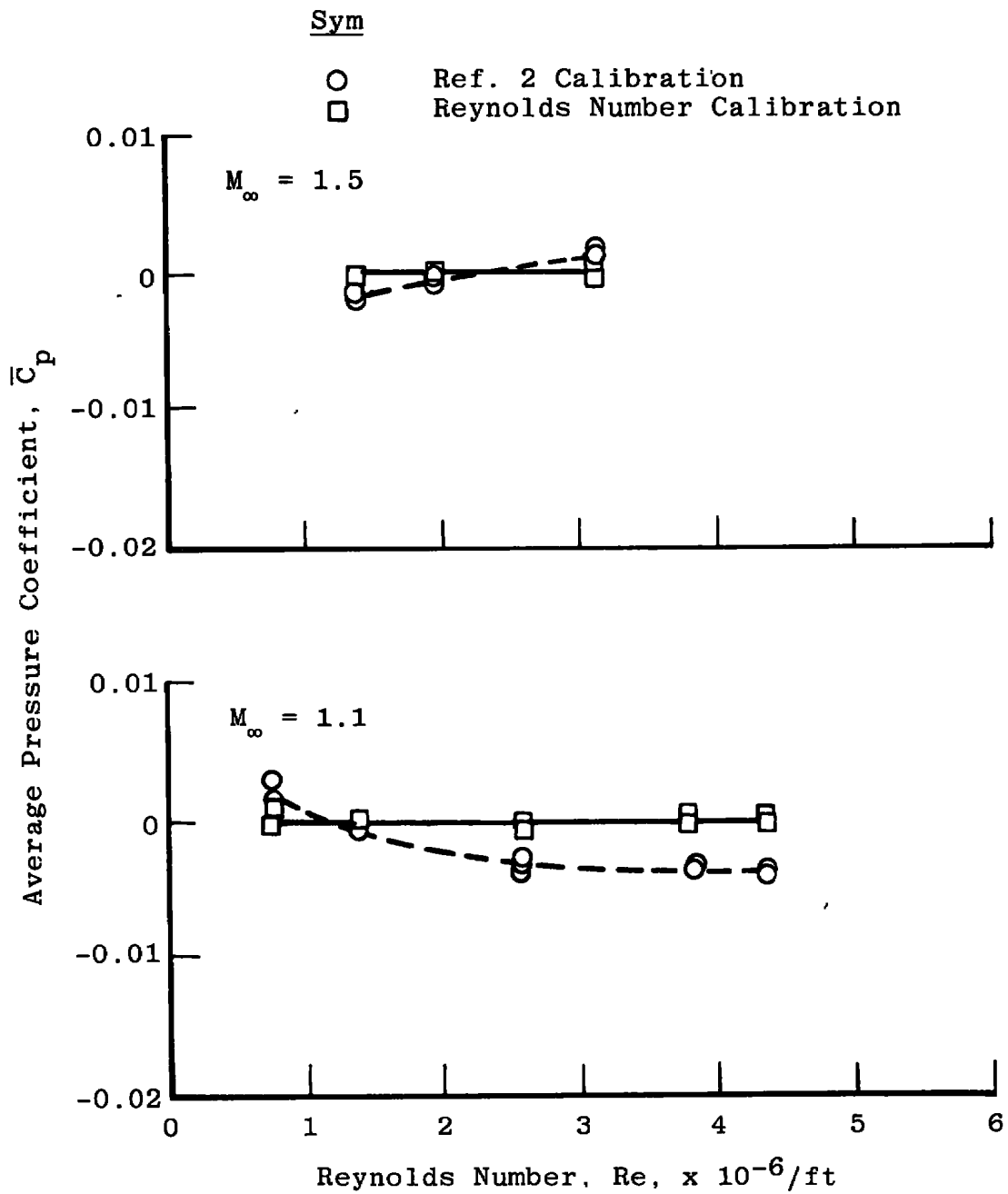


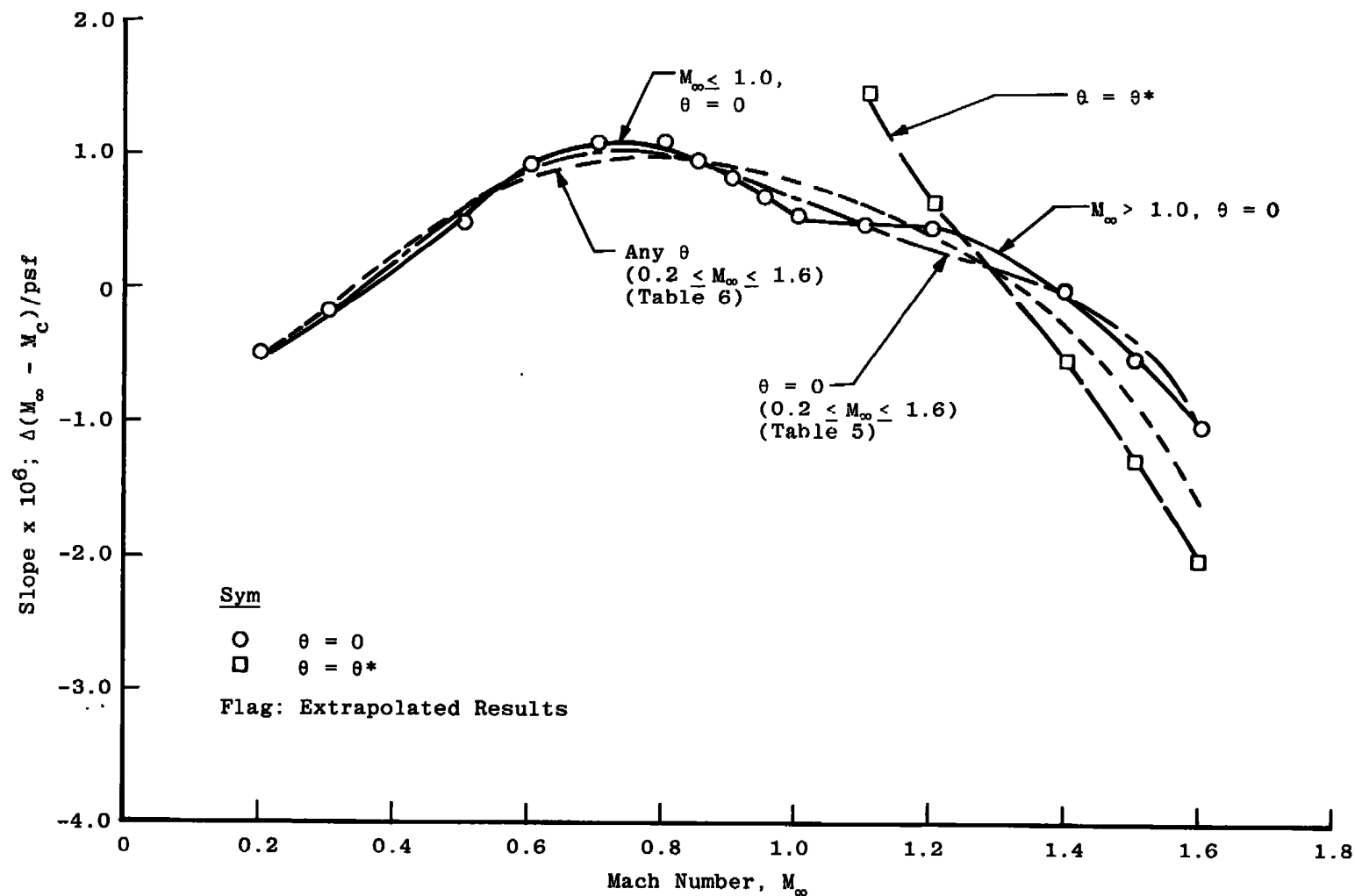
Figure 29. Tunnel 16T Mach number calibration for various Reynolds numbers with $\lambda = \lambda^*$ and $\theta = \theta^*$.



a. $M_\infty = 0.6$ and $0.8, \theta = 0$
Figure 30. Effect of Reynolds number corrections on the centerline pipe average pressure coefficient for Tunnel Stations 8 to 28 with $\theta = 0$ and $\lambda = \lambda^*$.

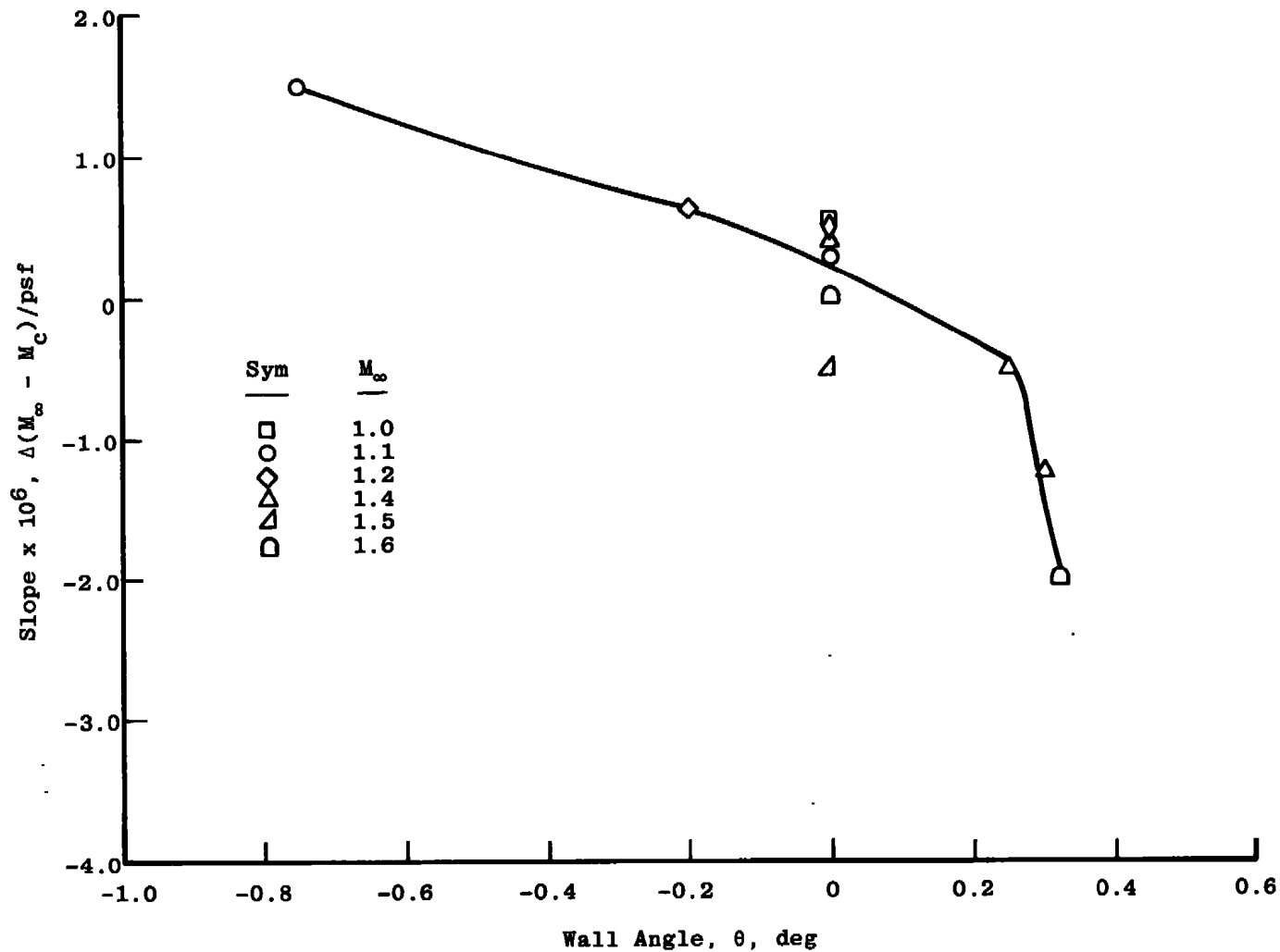


b. $M_\infty = 1.1$ and $1.5, \theta = \theta^*$
Figure 30. Concluded.

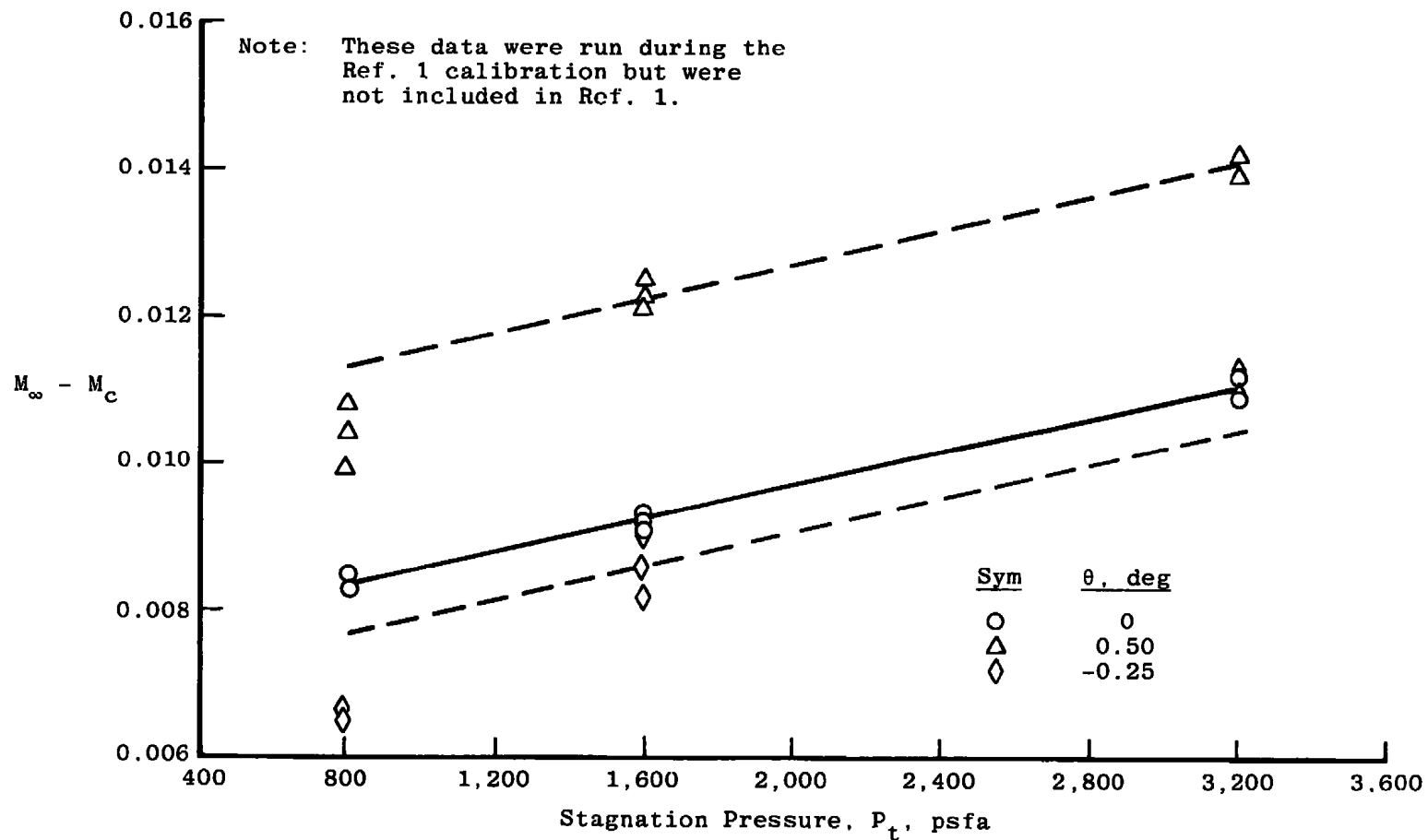


a. Slope = $f(M_\infty)$

Figure 31. Slopes of Reynolds number correction curves.

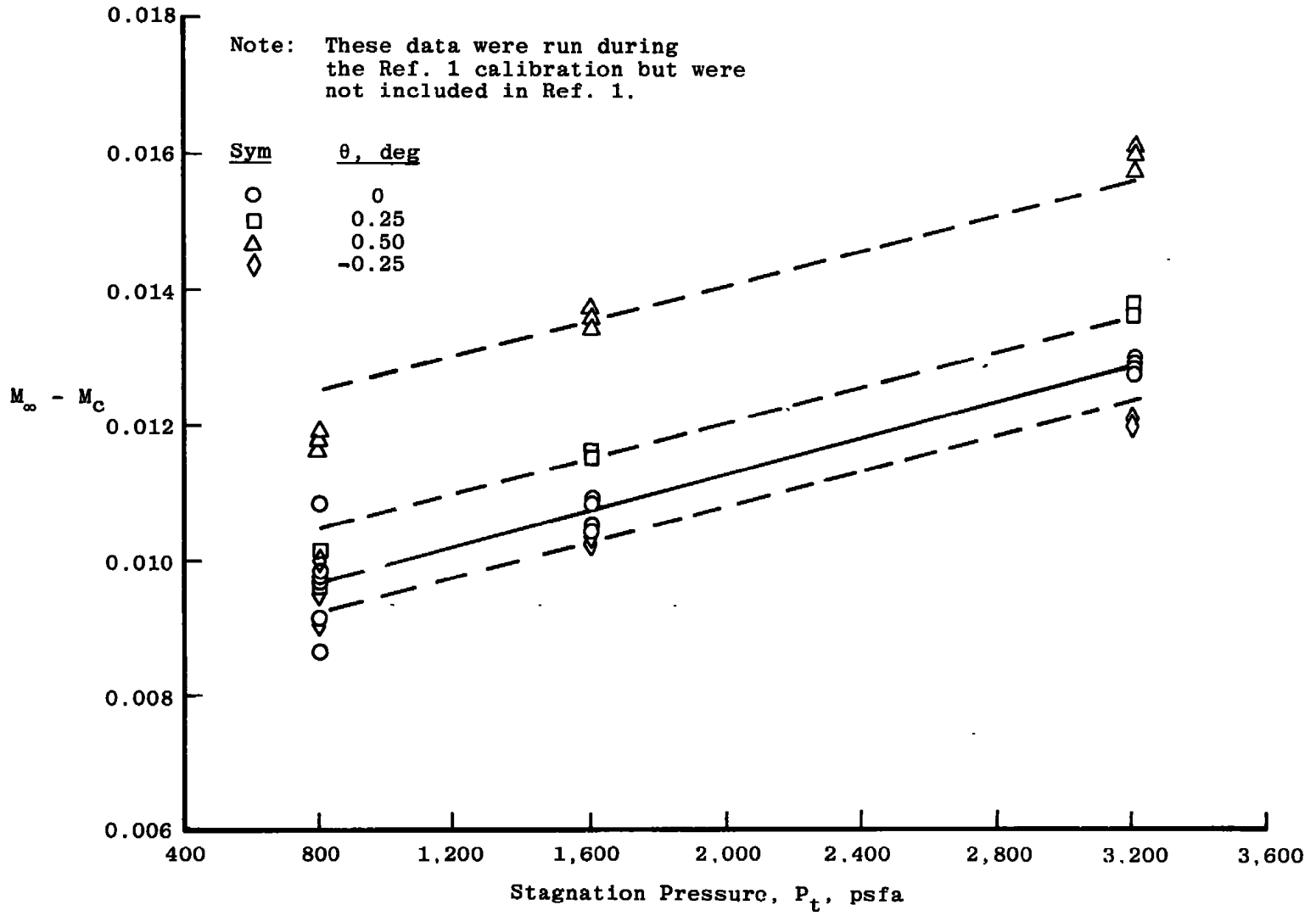


b. Slope = $f(\theta)$; $M_\infty > 1.0$
Figure 31. Concluded.



a. $M_\infty = 0.60$

Figure 32. Effect of wall angle on the Tunnel 16T Reynolds number calibration at subsonic Mach numbers.



b. $M_\infty = 0.80$
Figure 32. Concluded.

**Table 1. Coefficients of the Tunnel 16T Calibration Curve Fit
for $\theta = 0$ and $P_t = 1,600$ psfa**

$$0.2 \leq M_\infty \leq 1.6$$

<u>i</u>	<u>A_i</u>
0	-2.0805-03
1	5.1296-02
2	-9.3145-02
3	9.0721-02
4	-3.8655-02
5	5.5289-03
Maximum Residual	0.0007
Maximum Residual for 95% Data	0.0004

Where the curve is of the form

$$M_\infty - M_c = \sum_{i=0}^{i=\max} A_i M_c^i$$

**Table 2. Coefficients of the Tunnel 16T Calibration Surface Fit
for Variable Test Section Wall Angle**

$$0.2 \leq M_{\infty} \leq 1.6$$

<u>i</u>	<u>j</u>	<u>A_{ij}</u>
0	0	-8.1598-04
1	0	4.0772-02
0	1	9.8913-03
2	0	-6.1531-02
1	1	-5.9310-03
0	2	9.4553-04
3	0	4.8397-02
2	1	-1.3261-02
1	2	2.0631-02
0	3	-1.9259-02
4	0	-1.3308-02
3	1	1.1500-02
2	2	-2.6858-02
1	3	3.3528-02
0	4	7.3451-03

Maximum
Residual 0.0011

Maximum Residual
for 95% Data 0.0008

Where the surface is of the form

$$M_{\infty} - M_c = \sum_{i,j=0}^{i,j=\max} A_{ij} M_c^{i,j}$$

Table 3. Coefficients of the Tunnel 16T Calibration for Specific Mach Numbers at Various Reynolds Numbers with $\theta = \theta^*$ and $P_t \geq 1,000$ psfa

M_∞	A_0	A_1	A_2
0.55	8.7460-03	5.0951-07	7.8679-11
0.60	9.2460-03	5.0951-07	7.8679-11
0.70	1.0891-02	-5.9953-07	4.0951-10
0.80	1.1013-02	4.4467-08	2.2746-10
0.85	1.1469-02	-1.0949-07	2.5992-10
0.90	1.2732-02	-7.3111-07	3.5683-10
0.95	1.3678-02	-1.3392-06	5.4923-10
1.10	-3.4748-03	6.6287-06	-1.4913-09
1.20	1.5141-02	-2.0910-06	7.2069-10
1.40	2.3794-02	-5.5939-06	1.3398-09
1.50	2.4811-02	-4.5656-06	5.7399-10
1.60	2.4107-02	-3.9998-06	0

Where the curve is of the form

$$M_\infty - M_c = A_0 + A_1(P_t) + A_2(P_t)^2$$

Table 4. Coefficients of the Tunnel 16T Calibration for Specific Mach Numbers at Various Reynolds Numbers with $\theta = \theta^*$ and $P_t < 1,000$ psfa

M_∞	B_0	B_1
0.55	1.1010-02	-1.4999-06
0.60	1.1584-02	-1.6897-06
0.70	1.1945-02	-1.3858-06
0.80	1.3591-02	-2.3189-06
0.85	1.3361-02	-1.5984-06
0.90	1.3799-02	-1.4797-06
0.95	1.5064-02	-2.3730-06
1.10	-4.3726-03	6.0099-06
1.20	1.3319-02	4.6779-07
1.40	2.2432-02	-2.8903-06
1.50	2.6332-02	-5.5066-06
1.60	2.4107-02	-3.9998-06

Where the curve is of the form

$$M_\infty - M_c = B_0 + B_1(P_t)$$

Table 5. Coefficients of the Slopes for the Tunnel 16T Reynolds Number Corrections with $\theta = 0$

	$0.2 \leq M_\infty \leq 1.6$	$M_\infty \leq 1.0$	$M_\infty > 1.0$
i	A_i	A_i	A_i
0	3.4800-07	-2.4990-06	2.1456-04
1	-1.2728-05	2.1238-05	-7.5143-04
2	5.7660-05	-8.8056-05	1.0222-03
3	-8.5927-05	1.9601-04	-6.6843-04
4	5.3462-05	-1.9624-04	2.0810-04
5	-1.2117-05	7.0117-05	-2.4410-05
Maximum Residual	0.17-06	0.05-06	0.06-06

When the curve is of the form

$$\frac{\Delta(M_\infty - M_c)}{\text{psf}} = \sum_{i=0}^{i=5} A_i \left[M_\infty (P_t = 1600) \right]^i$$

and the corrected Mach number from $P_t = 1,600$ psfa is

$$M_\infty = M_\infty(P_t = 1,600) + \frac{\Delta(M_\infty - M_c)}{\text{psf}} (P_t - 1,600)$$

Table 6. Coefficients of the Slopes for the Tunnel 16T Reynolds Number Corrections for Variable Test Section Wall Angle

	$0.2 \leq M_\infty \leq 1.6$	$M_\infty \geq 1.05$	$M_\infty \geq 1.05$
i	A_i^*	A_i^*	B_i^{**}
0	-1.1303-06	-1.0694-03	1.9263-07
1	9.2080-07	4.3281-03	4.8322-07
2	1.5197-05	-6.8906-03	9.2006-06
3	-2.8526-05	5.4168-03	-4.7083-05
4	1.8995-05	-2.1071-03	-1.3345-04
5	-4.6210-06	3.2466-04	-7.9457-05
Maximum Residual	0.32-06	0.05-06	0.13-06

*
$$\frac{\Delta(M_\infty - M_c)}{\text{psf}} = \sum_{i=0}^{i=5} A_i \left[M_\infty(P_t=1,600) \right]^i$$

**
$$\frac{\Delta(M_\infty - M_c)}{\text{psf}} = \sum_{i=0}^{i=5} B_i(\theta)^i$$

APPENDIX A TYPICAL DATA CORRECTIONS

The primary test pressure for the Ref. 1 calibration was 1,600 psfa; however, some data were obtained at 800 and 3,200 psf. The effect of Reynolds number variation on the tunnel calibration at $M_\infty = 0.6$ and 0.8 for $\theta = 0$ is illustrated in Fig. A-1. The data indicate that the free-stream Mach number increases slightly with increasing Reynolds number. With the exception of data at $Re > 4.5 \times 10^6/\text{ft}$ for $M_\infty = 0.6$, the Ref. 1 Reynolds number calibration data agree with Ref. 2 within ± 0.002 . Such agreement was considered satisfactory especially since such an increment is about the same order of magnitude as the Tunnel 16T Mach number uncertainty.

Considering the small effects of Reynolds number and in lieu of a complete calibration with Reynolds number, the Ref. 2 calibration was used to conduct the AEDC NAB test program. Following the conduct of the AEDC tests, data analysis revealed that some trends in model afterbody drag with Reynolds number could be attributed to the tunnel calibration. The errors in stream parameters (M_∞ , P_∞ , and Q_∞) attributed to use of the Ref. 2 calibration, neglecting the effects of Reynolds number, are presented in Fig. A-2. These data indicate errors less than 0.4, 0.2, and 0.6 percent for M_∞ , P_∞ , and Q_∞ , respectively. For many test programs in the AEDC-PWT wind tunnels such errors, which are the same order of magnitude as instrumentation uncertainty errors, are not significant. For testing of models which have a substantial base area, such as those used for the AEDC NAB test programs, the error in static pressure can induce significant error in model drag. For example, for the AGARD NAB test, the error in afterbody drag at $M_\infty = 0.6$ and $Re = 5.0 \times 10^6$ was found to be about 70 drag counts (based on model maximum cross-sectional area).

The results of the Tunnel 16T Reynolds number calibration were utilized to correct the AEDC NAB test data. In spite of the small errors associated with neglecting Reynolds number effects, the fact that the data trends were definable allows Reynolds number effects to be considered. Typical effects of these corrections upon nozzle afterbody integrated pressure drag are presented in Fig. A-3. The data indicate that the corrections are significant at $M_\infty = 0.6$, marginally significant at $M_\infty = 0.8$, but insignificant at $M_\infty \geq 0.9$. It is interesting to note that the largest data correction occurred at $M_\infty = 0.6$ which had been the Mach number for which NAB data were analyzed to justify the need for the Reynolds number calibration.

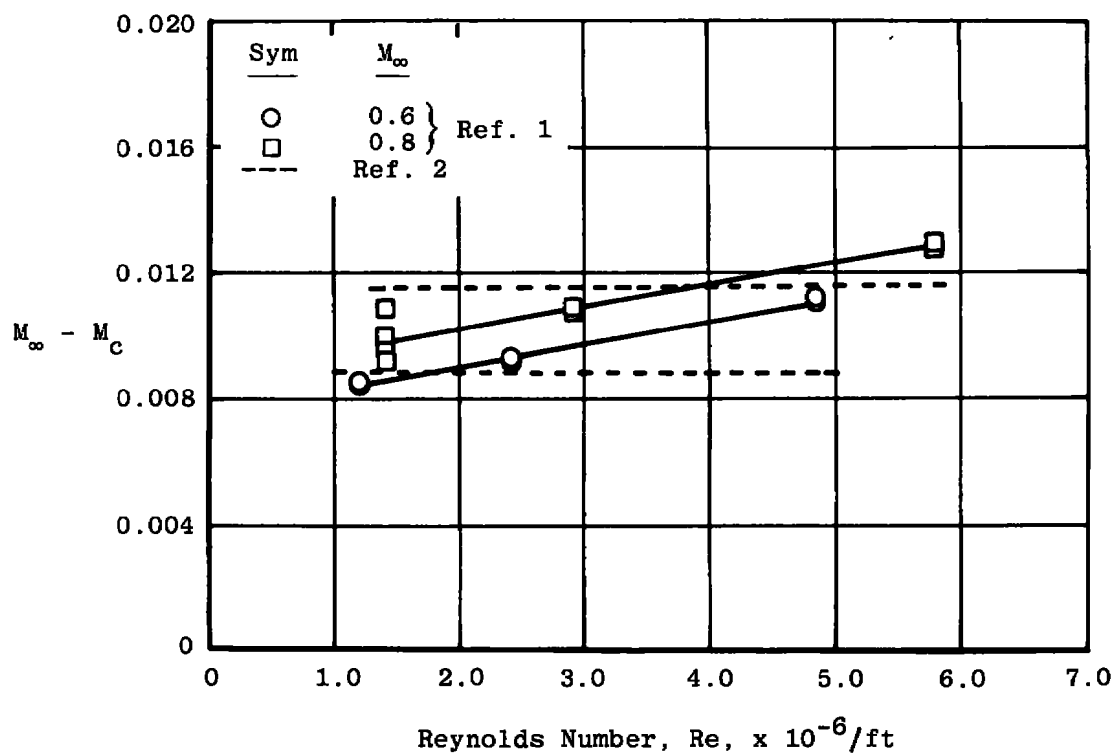


Figure A-1. Effects of Reynolds number on the Tunnel 16T calibration at $M_\infty = 0.6$ and 0.8 for $\theta = 0$.

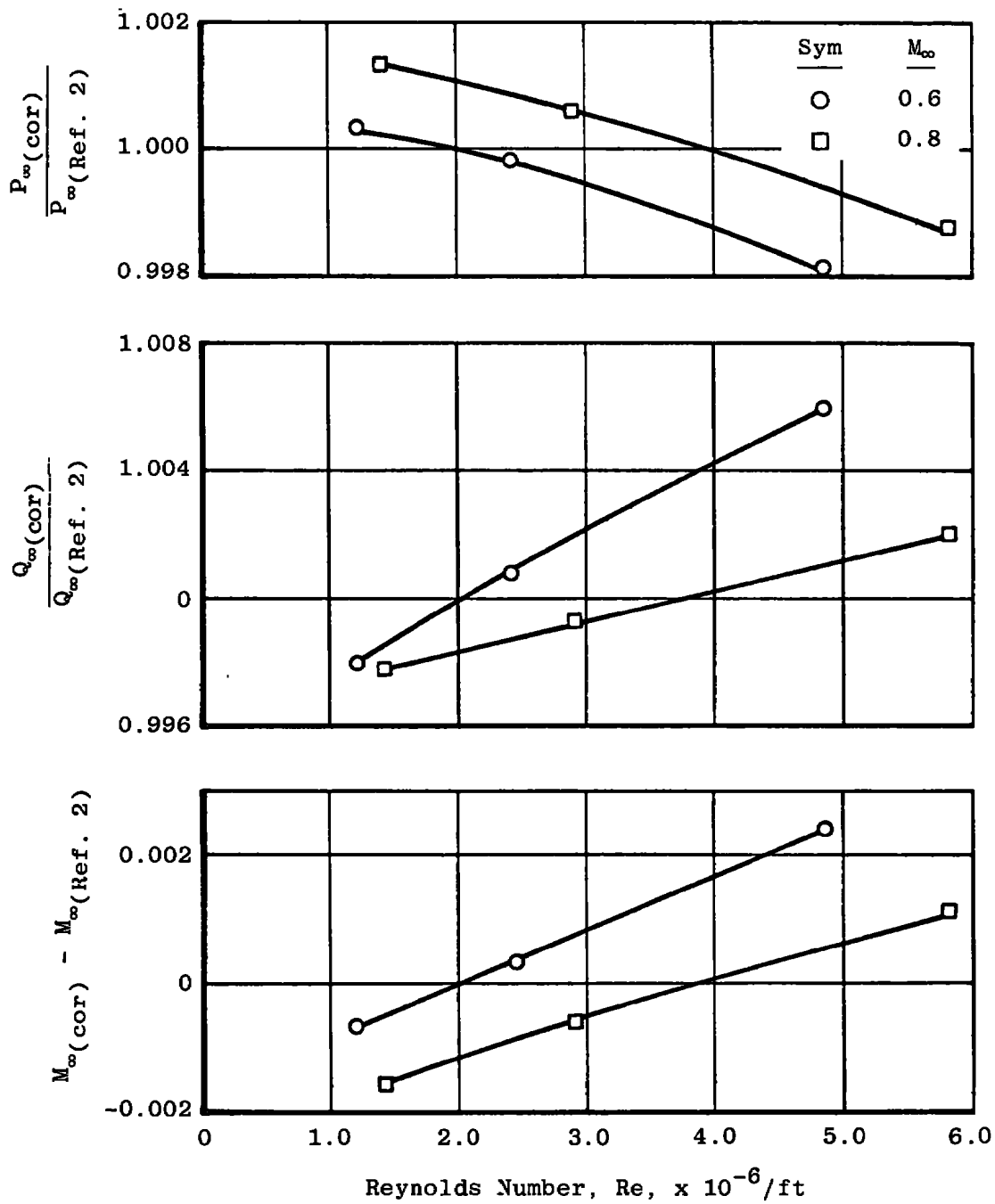
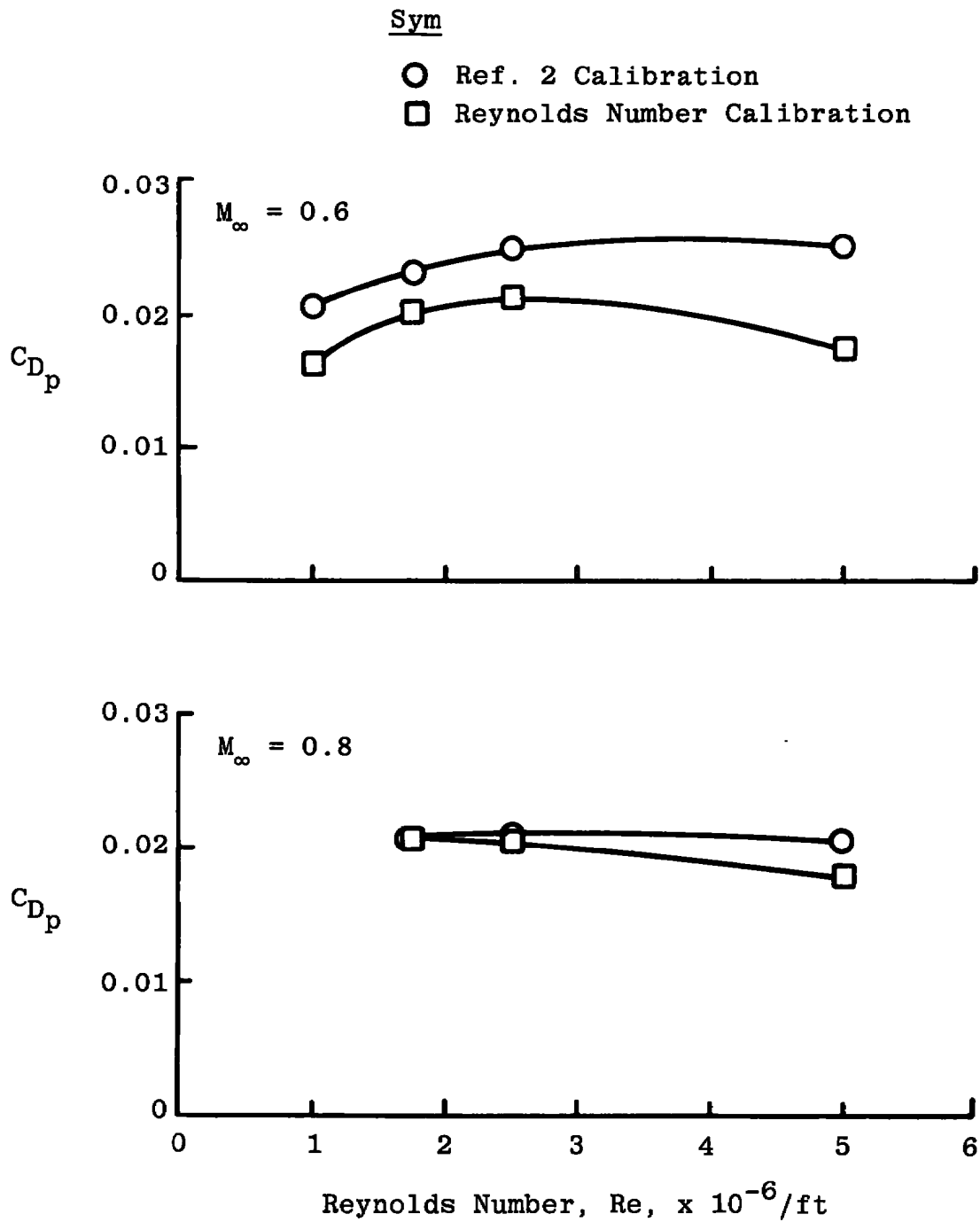
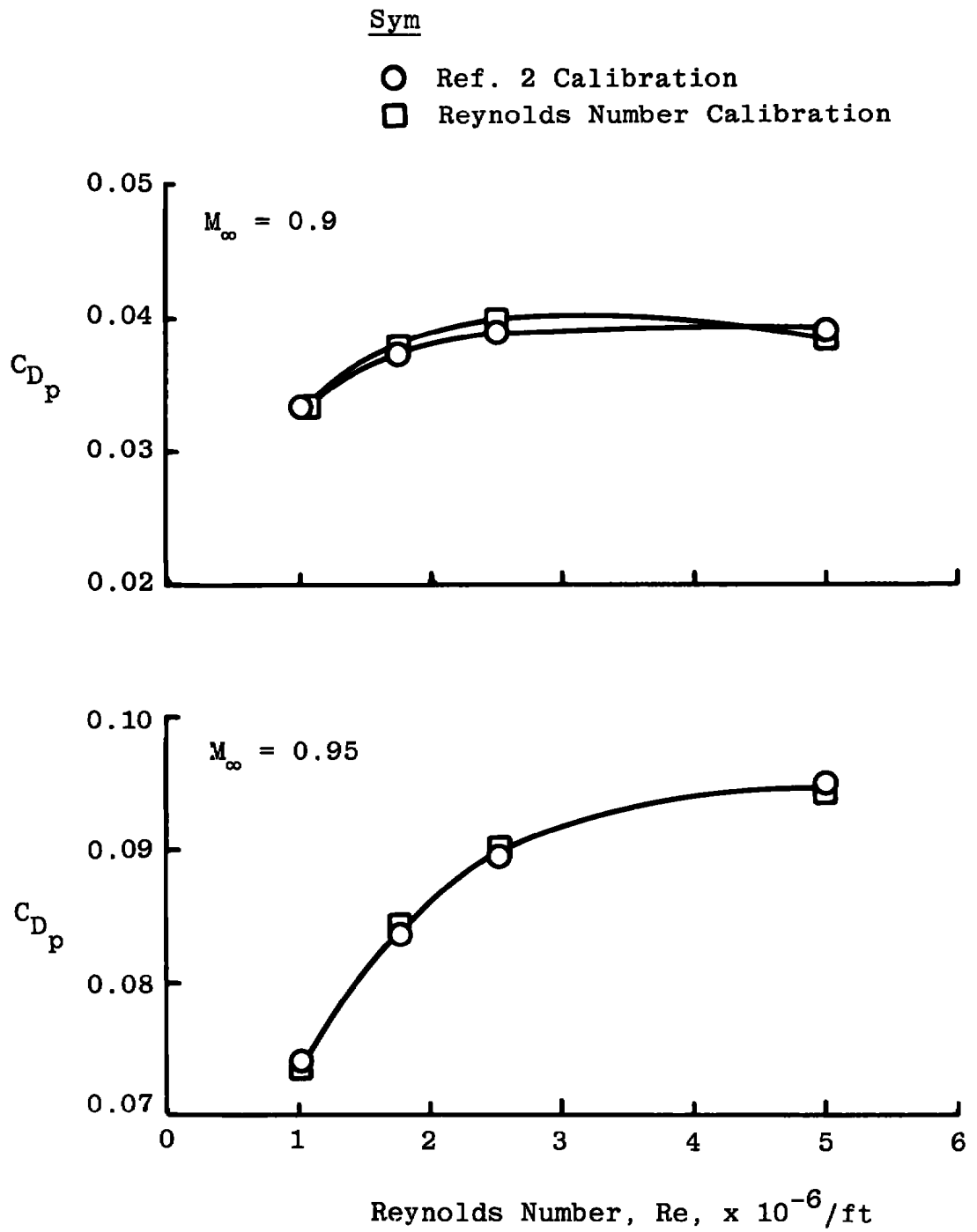


Figure A-2. Effects of Reynolds number upon the Tunnel 16T flow parameters.

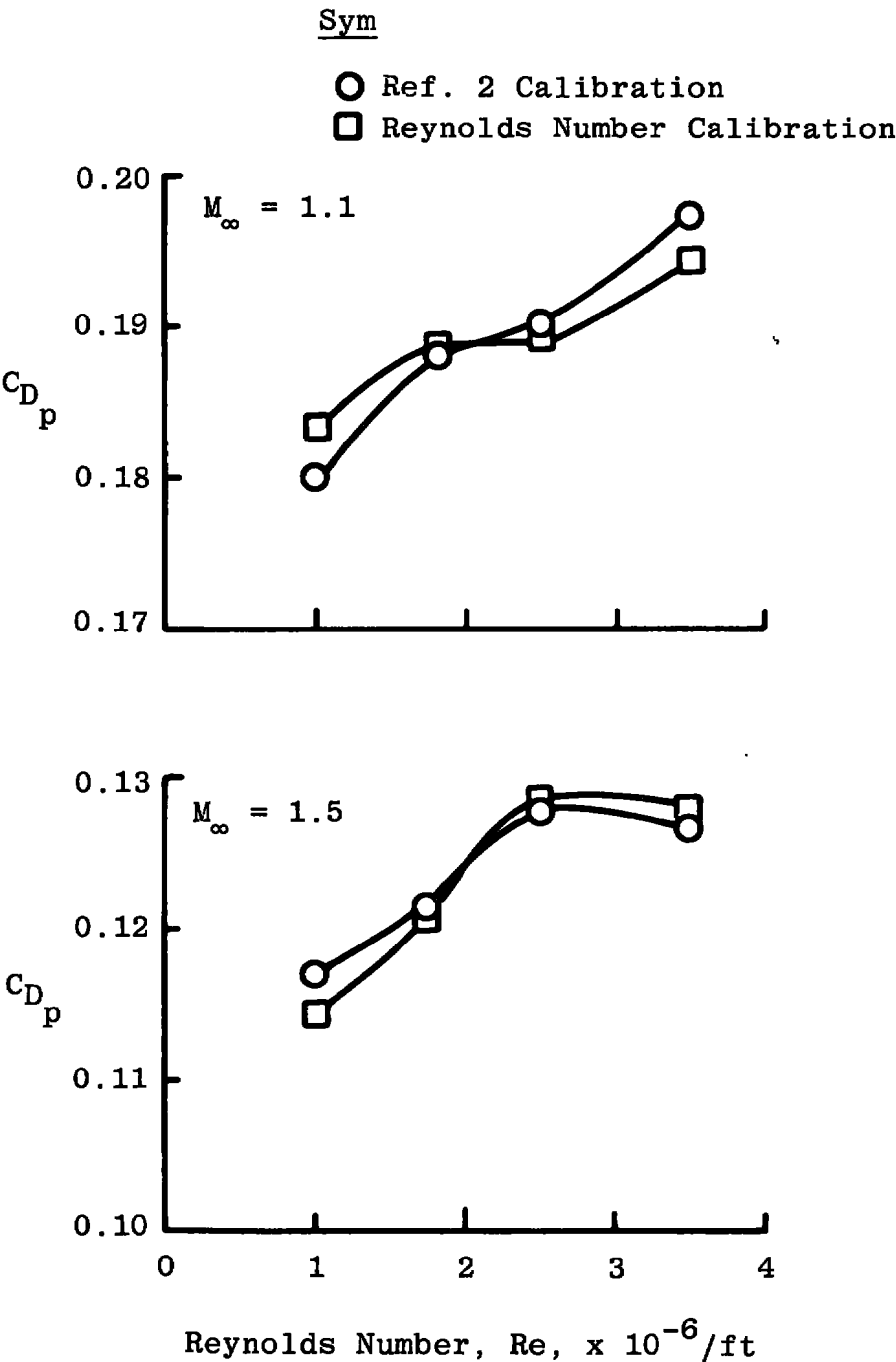


a. $M_\infty = 0.6$ and 0.8

Figure A-3. Typical data corrections for AGARD NAB integrated pressure drag.



b. $M_\infty = 0.9$ and 0.95
Figure A-3. Continued.



c. $M_\infty = 1.1$ and 1.5
Figure A-3. Concluded.

NOMENCLATURE

C_{D_p}	NAB integrated pressure drag
$\overline{C_p}$	Average of local pressure coefficients from tunnel stations 8 to 28
E_t	Tunnel total power factor, (total power)/ P_t
M_c	Equivalent plenum Mach number
M_∞	Free-stream Mach number, determined from the average of local Mach numbers from tunnel stations 8 to 28
P	Local static pressure, psfa
P_t	Tunnel stagnation pressure, psfa
P_∞	Free-stream static pressure, psfa
Q_∞	Free-stream dynamic pressure, psfa
Re	Unit Reynolds number, 1/ft
θ	Test section wall angle, deg (positive when walls are diverged)
θ^*	Optimum wall angle, deg (Fig. 3)
λ	Tunnel pressure ratio, ratio of P_t to the compressor inlet pressure
λ^*	Nominal tunnel pressure ratio (Fig. 2)
σ	Standard deviation (conventional statistical parameter)
ω	Auxiliary weight flow ratio; auxiliary flow requirements divided by tunnel weight flow